Microscopic insights into the partial oxidation of methanol on gold using Au(332) as a model system

Inaugural-Dissertation

to obtain the academic degree

Doctor rerum naturalium (Dr. rer nat.)

submitted to the Department of Biology, Chemistry, Pharmacy
of Freie Universität Berlin

by

Christoph D. Feldt
from Illertissen, Germany

Berlin, 2021

This dissertation has been prepared between September 2017 and November 2021 in the group of Prof. Dr. Thomas Risse in the department of Physical and Theoretical Chemistry, Freie Universität Berlin, Arnimallee 22, 14195 Berlin.

1st reviewer:	Prof. Dr. Thomas Risse
2nd reviewer:	Prof. Dr. Beate Paulus
Date of defense:	05.04.2022

The most dangerous phrase in the language is,
"We've always done it this way."
Grace Hopper

Acknowledgments

As I started this project, I knew almost nothing about working in the UHV. Now, after four years, I can proudly say that this changed quite a bit! I am glad, that I had a lot of people along my way helping me to make my life as a PhD student easier.

First, I want to thank Prof. Thomas Risse for the opportunity to work on this interesting topic, for sharing his knowledge and also for his scientific input and for giving me the opportunity of teaching. My gratitude goes to Prof. Beate Paulus for being the second referee for my thesis.

A person who deserves special acknowledgement is Dr. Wiebke Riedel. She was my mentor during my time in the working group and most of the things about the work with UHV machines I learned from her. Moreover, I am grateful for her scientific input, for ordering stuff and for proofreading of my thesis. Dr. Raphaell Moreira, Dr. Peter Clawin and Dr. Eric Meyer are acknowledged for setting up the molecular beam apparatus and Rudolf Cames for technical support. A special thank goes to Horst Binkowski, Frank Totzauer and the team of the machine shop as well as Peter Schwartze. I thank my students Jian Liang Low, Paul Albrecht, Henrik Wiedenhaupt, Yiran Zhang and Carolina Lopez who did a great job during their internships and bachelor theses and Thorren Kirschbaum for his important data on the methanol oxidation from his bachelor thesis. Furthermore, I thank Salma Eltayeb and Keyun Tang for their technical support. My special thank goes to Hendrik Ronneburg who helped me out with various technical problems and, together with Nina Richter, Sarah Schmerbeck and Marlon Winter for the nice and realxing coffee breaks and off times on long working days. Of course, I also want to thank all other current and former members of the AG Risse Tomislav Kremer, Zoreh Asadi, Dr. Krzystof Tadyshak, Dr. Yuri Dedkov and Sabine Köppe. Furthermore I thank Julija Djordjevic for her help with administrative tasks.

I am grateful for financial support by the DFG (in the framework of research project FOR2213 "Nagocat"). I thank Prof. Lyudmila Moskaleva and Prof. Thorsten Klüner as well as Dr. Wilke Dononelli and Dr. Gabriele Tomaschun for their important theoretical calculations and Prof. Markus Bäumer, Dr. Arne Wittstock and Adrian Tapia Burgos for sharing and discussing scientific results. Prof. Gunther Wittstock and Bastian Krueger are acknowledged for the well organized scientific meetings. Of course I also thank all other present and former members of the "Nagocat" research group. Working with you was always fun and I learned a lot!

I thank the IMPRS “Functional Interfaces in Physics and Chemistry" and its successor "Elementary Processes in Physical Chemistry" for finacial support, valuable soft skill seminars and the insight into other topics in surface science. Especially I want to mention Dr. Alexander Paarmann, Bettina Menzel and Ines Bressel for the awesome organisation and the warm and helpful interaction with the students. I further thank the student members of the IMPRS for the great time!

Sometimes your progress becomes slow and things won’t work out. I am very grateful to my friends for always supporting and looking out for me! I am very lucky to have you on my side! I also thank my extended family, especially Katrin and Karsten for being always great support and motivation for me!

With my whole heart, I thank Anne who always stood by my side, encouraged and supported me! Thank you for always being there for me!

Finally, I want to thank my family, my brother Michael and my parents Elisabeth and Christian! Thank you for your encouragement, your support and for always believing in me!

Eidesstattliche Erklärung

Hiermit erkläre ich, die Dissertation selbstständig und nur unter Verwendung der angebenen Hilfsmittel und Literatur angefertigt zu haben. Ich versichere, dass diese Arbeit bei keinem früheren Promotionsverfahren eingereicht wurde. Die Promotionsordnung des Fachbereichs Biologie, Chemie, Pharmazie basierend auf den Mitteilungen im Amtsblatt der Freien Universität Berlin Nr. 21/2018 vom 31.05.2018 habe ich zur Kenntnis genommen und akzeptiere diese.

Berlin, 14.12.2021 Christoph Feldt

Abstract

Nanoporous gold (np-Au) is a pure metal-based catalyst, which forms methyl formate very selectively in the partial oxidation of methanol. Although several model studies under ultrahigh vacuum as well as quantum mechanical calculations attempted to provide insight into the structural and catalytic properties of np-Au, the understanding of the factors leading to the high activity and selectivity remain incomplete. In this work, a single crystalline Au(332) surface was used to model structural properties like low index (111) facets as well as low coordinated Au atoms. The experiments were conducted under well-defined UHV conditions by pulsed, isothermal molecular beam (MB) experiments combined with *in situ* infrared reflection adsorption spectroscopy (IRAS) as well as temperature programmed reaction (TPR) experiments. Using CO as a probe molecule applying isotopically diluted gas mixtures to prevent dipolar coupling between CO molecules, the several adsorption sites on Au(332) were spectroscopically evidenced and assigned by a combination with DFT calculations. In isothermal MB experiments on the partial methanol oxidation to methyl formate, varying the surface temperature as well as the methanol and oxygen fluxes revealed two distinct surface deactivation processes for methyl formate formation due to the formation of formate and due to impurities in the used methanol. Low coordinated sites were found to form methyl formate at a higher rate compared to other sites on the Au(332), while other reaction steps, *e.g.* formation of methoxy proceed also effectively on terrace sites and with gold-oxygen (AuO_x) phases. TPR results demonstrated unwanted oxidation of methyl formate, the desired partial oxidation product in methanol oxidation, to occur on Au(332) already at low temperatures and even for low oxygen coverages, as expected for typical reaction conditions on np-Au. Three different reaction mechanisms for CO_2 formation from methyl formate were identified by isotopic labeling experiments, which were connected to specific oxygen species on minority sites. Due to its dependence on oxygen at special sites, the methyl formate oxidation is slow under isothermal conditions compared to the oxidation of methanol which provides a microscopic understanding of the high selectivity of np-Au on the formation of methyl formate.

Kurzzusammenfassung

Nanoporöses Gold (np-Au) ist ein rein metallbasierter Katalysator, der Methanol sehr selektiv zu Methylformiat partialoxidiert. Experimente im Ultrahochvakuum (UHV) sowie quantenmechanische Rechnungen wurden zur Modellierung struktureller und katalytischer Eigenschaften von np-Au durchgeführt, dennoch bleibt das Verständnis der hohen Aktivität und Selektivität von np-Au unvollständig. In dieser Arbeit wurden wesentliche strukturelle Eigenschaften von np-Au durch eine einkristalline Au(332)-Oberfläche nachgebildet, die neben niedrig indizierten (111)-Facetten auch niedrig koordinierte Au-Atome aufweist. Die Experimente wurden unter wohldefinierten UHV-Bedingungen mit gepulsten, isothermen Molekularstrahl-Experimenten (MB) zusammen mit *in situ* Infrarot-Reflektions-Absorptionsspektroskopie (IRAS) und temperaturprogrammierter Reaktionsspektroskopie (TPR) durchgeführt. Isotopenverdünnte CO-Mischungen, zur Vermeidung dipolarer Kopplung, wurden verwendet um Adsorptionsplätze auf der Au(332) spektroskopisch zu untersuchen und mithilfe von DFT Rechnungen zuzuordnen. In isothermen MB-Experimenten zur selektiven Methanoloxidation zu Methylformiat zeigten sich durch Variation der Oberflächentemperatur und der Methanol- und Sauerstoffflüsse zwei verschiedene Deaktivierungsprozesse der Methylformiatbildung durch Formiatbildung und Verunreinigungen des Methanols. Niedrig koordinierte Plätze zeigten eine höhere Methylformiatbildungsrate im Vergleich zu anderen Plätzen auf der Au(332), wohingegen andere Reaktionsschritte wie die Methoxybildung auch auf Terrassenplätzen und mit Gold-Sauerstoff-Phasen (AuO_x) stattfinden. TPR Experimente zeigten unerwünschte Oxidation des gewünschten Partialoxidationsprodukts Methylformiat, bereits bei niedrigen Temperaturen und sogar für niedrige Sauerstoffbedeckungen, wie sie unter typischen Reaktionsbedingungen auf np-Au erwartet werden. Drei verschiedene CO_2-Bildungsmechanismen aus Methylformiat wurden in Isotopenmarkierungsexperimenten identifiziert, die aus Sauerstoffspezies auf speziellen Minoritätsplätzen resultieren. Durch ihre Abhängigkeit von speziellen Reaktionsplätzen ist die Methylformiatoxidation unter isothermen Bedingungen im Vergleich zur Methanoloxidation langsam, was zu einem mikroskopischen Verständnis der hohen Selektivität zur Methylformiatbildung auf np-Au beiträgt.

List of Publications

Paper I

CO Adsorption on Au(332): Combined Infrared Spectroscopy and Density Functional Theory Study

Christoph D. Feldt*, Raphaell Moreira*, Eric Meyer, Peter Clawin, Wiebke Riedel, Thomas Risse, Lyudmila Moskaleva, Wilke Dononelli* and Thorsten Klüner, The Journal of Physical Chemistry C, **2019**, 123, 8187 - 8197. DOI: https://doi.org/10.1021/acs.jpcc.8b08406

*equally contributed

Paper II

Methanol oxidation on Au(332): an isothermal pulsed molecular beam study

Christoph D. Feldt, Thorren Gimm, Raphaell Moreira, Wiebke Riedel and Thomas Risse, Physical Chemistry Chemical Physics, **2021**, 23, 21599-21605. DOI: https://doi.org/10.1039/D1CP03436G

Paper III

Methanol oxidation on Au(332): Methyl formate selectivity and surface deactivation under isothermal conditions

Christoph D. Feldt, Thorren Kirschbaum Jian Liang Low, Wiebke Riedel and Thomas Risse, submitted to Catalysis Science & Technology.

Paper IV

Low Temperature Oxidation of Methyl Formate on Au(332)

Christoph D. Feldt, Jian Liang Low, Paul Albrecht, Keyun Tang, Wiebke Riedel and Thomas Risse, The Journal of Physical Chemistry C, **2021**, 125, 26522-26529. DOI: https://doi.org/10.1021/acs.jpcc.1c08531

Paper V

Heterogeneity of oxygen reactivity is crucial for selectivity of partial oxidation of methanol on gold surfaces

Christoph D. Feldt, Paul A. Albrecht, Salma Eltayeb, Wiebke Riedel and Thomas Risse, submitted to Chemical Communications.

Contents

1 Introduction

Our modern industry and society strongly depend on the use and the development of modern catalysts for a variety of different applications. As today, more than 75 % of industrially produced chemical products are made by processes involving catalysts.[1] Among the most important industrial processes is the ammonia synthesis according to the *Haber-Bosch process* on iron catalysts with a worldwide production over 140 megatons.[2] In 2008 it was estimated, that about 100 Tg (*i.e.* 10^6 tons) of fertilizer nitrogen was necessary to maintain the food production for the worlds growing population, while approximately 1% of the global energy consumption was used for the ammonia synthesis.[3] In connection to the growing demand for harvesting and storing energy from renewable energy sources, ammonia was also proposed as a hydrogen storage medium for the use in fuel cells.[4] Another power-to-X approach is the production of green methanol from CO_2 and water which is subsequently coupled to larger molecules like methyl formate, which is an important C_1-building block and a promising candidate for alternative fuels(additives).[5,6]

A catalyst is a material, that speeds up a chemical reaction by reducing the activation barrier of a reaction which is associated with a change of the reaction pathway. Importantly, catalysts themselves are not consumed in the reactions and they do not change the chemical equilibrium. By tuning of specific properties like morphology or chemical composition, unwanted side reactions or consecutive reactions of products can be minimized, pushing the selectivity of a reaction towards a desired product. In general, catalytic processes can be classified in homogeneous (*i.e.* catalyst and educts are in the same phase), enzyme catalyzed processes and heterogeneous processes, where the mostly solid catalyst is in contact with a liquid or gas phase containing the educts. A major advantage of heterogeneous catalysis is, that the catalyst can be easily separated from the product phase which minimizes costs for product purification as well as reduced discharge of catalyst material. Ideally, catalysts are not consumed or changed during the catalytic cycle. However, side reaction, catalyst aging or changes in surface morphology result in a finite lifetime of catalysts.

Transition metals and -oxides exhibit excellent catalytic properties and are widely used in several processes like oxidation[7] or hydrogenation reactions.[8,9] A well-known application of metals catalyzing oxidation reactions is the *tree-way-catalyst* in automobiles with gasoline engines, where Pt and Pd promote the conversion of CO and hydrocarbons.[1,10] The efficiency of oxidation catalysis on metals is a complex interplay of various effects and depends for example on the binding strength of adsorbates (*e.g.* oxygen atoms or oxidation products) to the metal. The *Sabatier principle* denotes a correlation between the binding strength and the catalytic activity of a metal. Plotting the activity for a given metal in dependence of the binding strength results in a so-called *volcano plot* as shown in Figure 1.1.

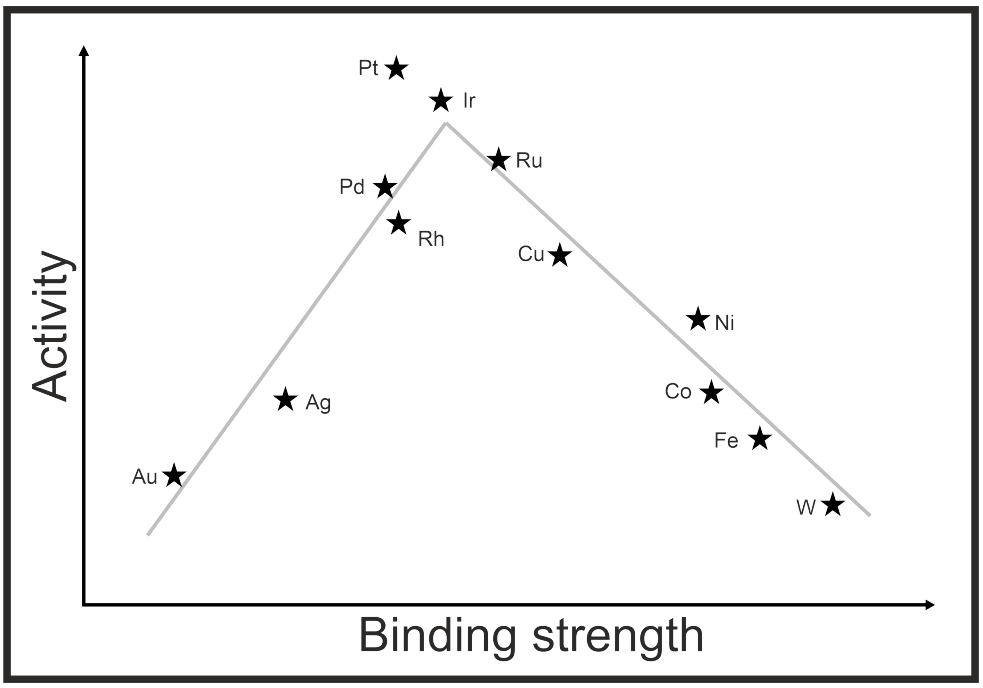

Figure 1.1: Simplified representation of the *Sabatier principle*, depicted as a so-called *volcano plot*, shown for the example of the decomposition of formic acid into formate, adapted from reference [11]. The figure describes the dependence of the activity of formate production from the binding strength of the formate on the transition metal surface. The binding strength on d-block metals increases with increasing group number. The values for the activity and binding strength are arbitrary and shall only qualitatively demonstrate the principle.

Generally, the early d block elements like Ti or Zr bind stronger to oxygen whereas the binding is weaker for late transition metals like Ag and Au and the binding strength de-

creases with increasing period number. Especially group 8 - 10 elements (*e.g.* Ru, Ir or Pt) exhibit optimal binding strengths which makes them suitable (oxidation)catalysts.[12] Gold is the noblest metal[13] and has a low affinity to oxygen[14] which makes it suitable for the production of jewelry or electrical contacts, as it is neither oxidized under ambient conditions[15] nor does it chemisorb oxygen in form of O atoms under ultrahigh vacuum conditions.[16,17] However, in the 1980s, Haruta and co-workers observed catalytic activity of metal oxide supported Au nanoparticles in CO oxidation, even at low temperatures.[18] Further studies revealed, that beside the particle size (below 5 nm), the metal oxide support and the contact between support system and particle play a crucial role for the catalytic activity.[19,20] In the last decades, gold mediated catalytic reactions advanced to a "hot topic" and were thoroughly studied.[21–26]

Recently, pure metal based nano-structured, sponge-like gold materials, so-called nanoporous gold (np-Au), was found to exhibit significant activity in the oxidation of CO[27] even at - 30 °C[28] and in oxidation and hydrogenation reactions of organic molecules[29], although it comprises structures significantly larger than 5 nm and has no oxidic support.[30] Among other reactions, the selective oxidation of methanol to its self-coupling product methyl formate was observed on np-Au to occur with selectivities close to 100 % at high conversions and at low temperatures[31], which hence makes np-Au a promising candidate as non-toxic, green catalyst for the transformation of methanol using atmospheric oxygen.[32] The starting material for the production of np-Au are gold alloys with an excess of a less noble metal (*e.g.* Ag or Cu). The latter is subsequently leached out, either by a corrosive acid (*e.g.* HNO_3[34]) or by electrochemical dealloying.[35–37] The structural properties of the resulting material are shown in Figure 1.2. It exhibits a highly porous structure of gold ligaments (see the inset in Figure 1.2 (I)) whose surfaces are composed of low index planes and low coordinated gold atoms at steps or kinks[33] (see Figure 1.2 (II), right panel). It is assumed, that these low coordinated atoms play an important role for the catalytic activity of np-Au.[38,39] After dealloying, np-Au always contains residuals of the less noble metal, which are able to activate molecular oxygen[40–42] and are thus assumed to be involved in oxygen activation.[35,36] Moskaleva and coworkers demonstrated a lowering of the O_2 dissociation barrier on Au adsorption sites when neighboring Ag atoms are present.[43]

In many works, ultrahigh vacuum (UHV) model studies were employed to address the adsorption behavior (*e.g.* CO[44–46], methanol[47–49] or formaldehyde and methyl formate[50])

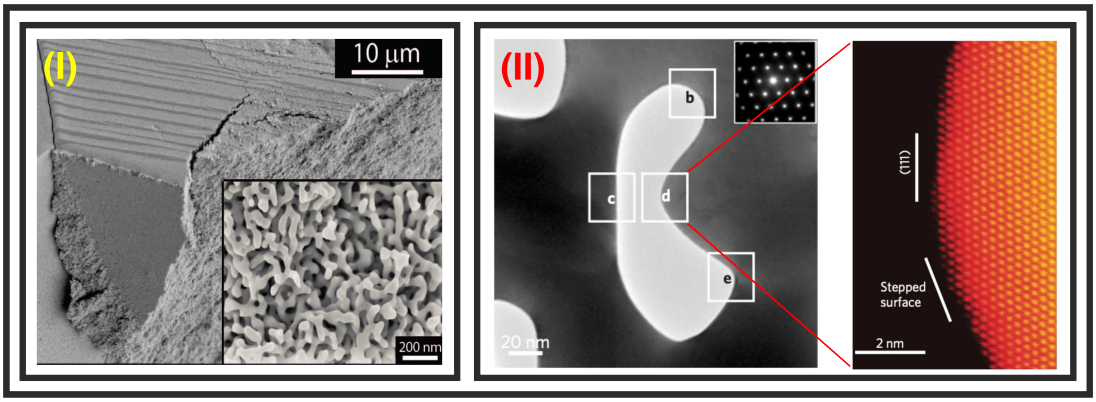

Figure 1.2: (I) SEM image of np-Au with different magnifications. The figure demonstrates the highly porous framework of Au ligaments. Adapted with permission from ref. [30], copyright 2009 American Chemical Society. (II)left: TEM image of a pore in np-Au. The figure on the right side is a close-up HAADF-STEM image of region d and shows a low index (111) surface plane as well as stepped surfaces with low coordinated Au atoms. Adapted from ref. [33], copyright 2012 Macmillan Publishers Limited.

on Au surfaces complemented by theoretical studies on activation and adsorption of oxygen[43,51,52] and other molecules.[53] Reactivity studies on CO oxidation[54–57] and methanol oxidation[47,48,58–60] were conducted by temperature programmed reaction spectroscopy (TPR) on differently oriented surfaces (*e.g.* (111), (110) etc.). The UHV approach enables well-defined conditions like low impurities form the residual gas phase, as the base pressure is in the range of $1 \cdot 10^{-10}$ mbar. This allows for obtaining absolute reaction probabilities and probing competing pathways, which would not be possible under ambient reaction conditions as the likelihood of multiple adsorption processes of the same molecule is very low. Nevertheless, there are limitations to this approach. Low pressures and in consequence low surface concentrations as well as the difficulty to obtain kinetic data of reactions by TPR experiments engrave the comparability to results from np-Au under ambient conditions. Moreover, model studies lack of the ability to activate molecular oxygen on the Au surfaces. For this reason different methods of providing activated oxygen under UHV conditions have been presented in the literature like O^+ sputtering[61], exposure to ozone[62], NO_2 dissociation[63] or direct splitting of oxygen molecules by radio frequency plasma[48] or by means of thermal cracking[64]. A more detailed description of a thermal effusive oxygen atom source, modified for this work, can be found in Chapter 3.1.1 and in ref. [64].

Among others, the adsorption of CO has been widely studied on both stepped and sputtered low index single crystalline Au surfaces under UHV conditions[38,46,65–70] and theoretical studies revealed an approximately linear correlation between the CO adsorption energy and the coordination number of the Au sites.[38,43,65,71] Many attempts were made to probe the CO adsorption properties on different Au sites by vibrational spectroscopy (*e.g.* infrared reflection adsorption spectroscopy (IRAS)), but mostly broad signals were observed which rendered limited insight *e.g.* into the nature of the involved adsorption sites.[38,66,72] Au surfaces reveal a dynamic nature in presence of some adsorbate molecules indicated by remarkable surface restructuring *e.g.* in the presence of CO adsorbates. In consequence to CO exposure at low temperatures to Au(111) surfaces with hexagonal shaped etch pits and subsequent thermal CO desorption, the edges of the pits adopted a more roundish shape and were decorated by Au particles.[73] Similar effects were also observed on Au(110) at near ambient pressures[74] and also in np-Au, where exposure to CO and O_2 lead to changes in the surface morphology of the pores.[75] This shows, that these surface modifications are observable in a large pressure range and the implication of the restructuring on the abundance of low coordinated surface sites and hence adsorption properties and reactivities can be probed under well-defined UHV conditions.

A very similar behavior of morphological modifications was observed due to oxygen adsorption on Au surfaces under the formation of oxidic phases on both single crystal surfaces and np-Au. On the Au(111), the formation of notched step edges and Au islands as a result of lifting Au atoms from the *herringbone reconstruction* was observed.[63,76] This dynamic behavior of the Au surfaces is corroborated by *ab initio* molecular dynamic simulations on the stepped Au(321) surface revealing the formation of Au-O chain structures preferentially at the step edges accompanied by a change of the surface structure.[77] Experimental evidence for such chain-like structures was found on Au(110)-(1×2) surfaces already at low oxygen coverages.[78] Importantly, also the treatment of np-Au with ozone resulted in a significant change of the surface morphology and the formation of oxidic AuO_x phases.[79] This points out that UHV studies can be used to model the implications of those oxidic phases and surface reconstructions on the catalytic performance of np-Au. In oxidation reactions, several oxidic phases on np-Au have been observed, where reaction conditions influence their size and structure.[79,80] This is further reflected in TPR studies, where increasing oxygen coverages result in larger two-dimensional AuO_x phases and eventually three-dimensional bulk oxides, which were linked to a diminished activity in CO oxidation due to a lower reactivity of those extended phases.[54,81] Similarly adverse effects of AuO_x phases on the methanol oxidation on Au(110) were observed in model

studies for oxygen coverages only slightly above 0.08 monolayers (ML).[60] Under reaction conditions typically used for active np-Au catalysts, the concentration of activated oxygen is assumed to be low as a result of low silver contents.[82,83] For low oxygen concentrations, the selectivity towards the formation of methyl formate is well above 90 %, whereas increasing oxygen concentrations or higher silver contents promoted total oxidation processes.[31,79,82,83] This could be interpreted as a shift of selectivity influenced by the nature of involved oxygen species, which is however still subject of research. TPR studies on Au(111) reveal a qualitatively similar behavior to np-Au as the relative selectivity towards methyl formate formation is increased for low oxygen coverages whereas total oxidation is favored for higher coverages.[58] It is important to point out, that it is difficult to deduce selectivities directly from these model studies, as desorption processes compete with reactions on the surface resulting in constantly changing concentrations during the TPR experiments. Nevertheless, a reaction mechanism for the methyl formate formation from the selective oxidation of methanol was concluded from these model studies, starting with the formation of methoxy due to the abstraction of the acidic proton of methanol by activated oxygen. Consecutively, rate limiting β-H elimination produces formaldehyde which subsequently couples to another methoxy and eventually forms methyl formate.[47,58,84] A schematic representation of the important steps in this reaction mechanism is given in Figure 1.3.

Depending on the reaction conditions like temperature or surface concentrations, side or total oxidation products (*e.g.* CO_2, formate and formaldehyde) were observed. A facile reversible reaction of formaldehyde with oxygen results in the formation of a dioxomethylene species, which acts as a reservoir for formaldehyde. Below 200 K, the overoxidation of dioxomethylene via formate species was calculated to significantly compete with the coupling reaction, in line with the observation of formate species below 200 K which consecutively reacts to total oxidation products.[47,48,58,84,85] This points out, that reaction conditions in surface studies significantly influence the selectivity of the overall reaction, which is most likely also the case for the methanol oxidation on np-Au. As described before, model studies on single crystalline Au surfaces enable the investigation of many aspects of np-Au catalysts under well-defined UHV conditions, although further experimental issues complicate direct comparability of the results. As an example, desorbing reaction products are unlikely to re-adsorb due to single collision conditions in UHV experiments, while multiple interactions of the products with the surface of np-Au are probable under ambient conditions, which might lead to consecutive reactions of those

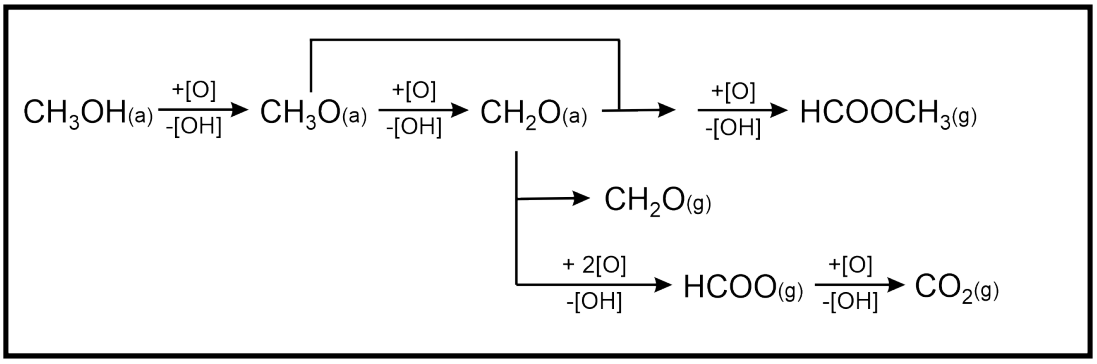

Figure 1.3: Schematic representation of the mechanism on gold as proposed in literature. Taken from Paper [**III**].

products. Furthermore, those studies on np-Au are usually conducted under isothermal conditions with a constant flux of educts at the entrance of the catalyst bed, which is not possible in TPR experiments and engraves qualitative and quantitative comparison of reaction probabilities, rates and selectivities.

The aim of this work

It has been pointed out, that several aspects of structural and catalytic properties of np-Au can be modeled under UHV conditions but, however, several questions still remain open as they have not or only incompletely been addressed in literature yet. For example, the role of low coordinated sites for the catalytic activity of np-Au as well as the influence of reaction conditions and the role of the AuO_x phases on the selectivity is still subject of further investigations. Moreover, the question of the importance of possible side reactions *e.g.* an unwanted overoxidation of methyl formate with low amounts of oxygen, as expected in np-Au under usual reaction conditions[31] is not clearly answered yet. In this work, model studies are conducted to add to an understanding for some of these open questions by giving additional insights to findings already reported in literature. On the one hand, detailed studies of the interactions between CO and different surface sites on the Au(332) sheds light into their adsorption properties. On the other hand structural modifications on the Au(332) due to CO exposure are investigated. Furthermore, reaction probabilities and selectivities are deduced from pulsed, isothermal molecular beam experiments that are used to close the gap between isothermal studies on np-Au under ambient conditions and TPR model studies as they enable constant transient concentrations at constant temperatures. Moreover, the significance of low coordinated surface sites for

the catalytic activities and selectivities in both methanol oxidation and methyl formate oxidation is addressed. In connection, the influence of different oxygen species on the selectivity in methanol oxidation is studied. In the end, also overoxidation processes of methyl formate with adsorbed oxygen are investigated in terms of the underlying mechanistic properties of the reaction as well as kinetic aspects. This shall contribute to an understanding of the high selectivity towards methyl formate in the selective oxidation of methanol.

This work employs an ultrahigh vacuum approach to address the open questions formulated above. To mimic structural properties of nanoporous gold, *i.e.* low index surfaces as well as low coordinated Au atoms, a stepped single crystalline Au(332) surface is used. It consists of six atom wide vicinal (111) terraces separated by close packed, monoatomic

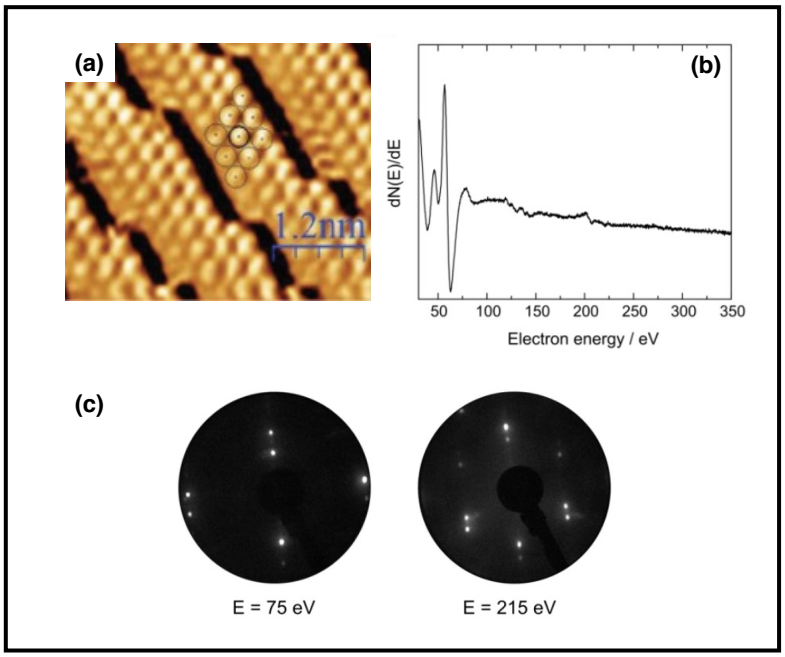

Figure 1.4: (a) STM image of an Au(332)surface, adapted from ref. [86] with permission from the Royal Society of Chemistry. (b) Auger spectrum of a cleaned Au(332) surface. (c) LEED patterns of a cleaned Au(332) surface at 75 eV and 215 eV electron energy. Taken from ref. [64].

steps which are aligned along the [110] crystallographic direction. Additionally, kink sites are present due to crystal miscut (see Figure 1.4 (a)).[86] According to expectations, the LEED image (see Figure 1.4 (c)) shows the pattern of hexagonal diffraction peaks re-

ferring to the (111) surface unit cell. Between the main reflections, five additional, less intensive diffraction peaks along the $q_\perp$ direction are observable, which correspond to the super structure of the monoatomic steps, separated by the six atom wide terraces. The Au atoms at the steps as well as kinks reveal a lower coordination number compared to the sites on the (111) planes and act therefore as a model for the low coordinated sites in np-Au.

This thesis is structured in six chapters, including this introductory section (**Chapter 1**).
Chapter 2 gives an overview about important theoretical concepts for surface reactivity and describes the theory of the used experimental and detection techniques.
Chapter 3 describes modifications to parts of the molecular beam apparatus that were made specifically for the studies within this thesis and are not previously presented in ref. [64]. Furthermore, a detailed description of data treatment like rescaling and evaluation protocols as well as descriptions of calibration measurements are given in this chapter.
Chapter 4 summarizes the results of the publications, which comprises the scientific body of this thesis:
In the first paper, adsorption sites on the Au(332) are characterized in terms of their adsorption strength and the lateral interactions of adsorbates. Furthermore, the stability of those sites is tested with respect to adsorbate induced restructuring processes. In specific, a mixture of ^{12}CO diluted in ^{13}CO was applied onto the Au(332) and studied in coverage dependent series as well as annealing experiments by IRAS. The observed IR modes were assigned to adsorption sites based on DFT calculations.
In the second paper, the reactivity and selectivity of the partial methanol oxidation to methyl formate on the Au(332) is tested under isothermal conditions by pulsed, molecular beam experiments for rather oxygen-rich conditions, following the methyl formate production rate by time resolved mass spectrometry. *In situ* IRAS measurements were used to detect surface species during the pulse sequence. A mechanism for the deactivation of methyl formate formation rate as well as the influence of different oxygen species on the selectivity of the reaction are discussed.
In the third paper, the dependence of the methyl formate formation rate on the applied surface temperature as well as the applied methanol and oxygen flux conditions was investigated in a similar approach as described in the second paper. A second, methanol dependent deactivation mechanism was identified and discussed. Furthermore, the dependence of the applied flux conditions on the selectivity of the methanol oxidation was tested and further insights into the reaction mechanism were obtained.

The fourth paper addresses the question, if methyl formate is further oxidized under conditions, that are comparable to conditions where methanol oxidation has the highest selectivity towards methyl formate formation (*i.e.* low oxygen concentrations). In a TPR study, combined with IRAS annealing experiments, three different oxidation channels were identified. By using ^{18}O, differences in the CO_2 isotopic ratio were observed which suggests different CO_2 formation pathways. For the oxidation channel with the highest temperature, the production of formate presumably on low coordinated kink sites was observed as intermediate for the subsequent CO_2 and H_2O production.
In the fifth paper, the methyl formate oxidation was investigated under isothermal conditions in pulsed, molecular beam experiments at 310 K. The question about the significance of methyl formate oxidation in terms of kinetics is attempted by comparing it with methanol oxidation under similar conditions. The experiments show that methyl formate oxidation is substantially slower than methanol oxidation but, however, contributes to the oxidation kinetics when applied in high excess in a co-feed experiment, similar to a situation on np-Au for high methanol conversions. In conclusion the origin of the high selectivity towards methyl formation was ascribed to structural aspects on Au surfaces.
Chapter 5 concludes the thesis and gives an outlook, how remaining open questions can be addressed in future experiments.
Chapter 6 contains the published and submitted papers that form the scientific backbone of this work. For each paper, my own contribution to the publications is stated.

2 Theoretical background

This chapter will give an overview about concepts and methods needed to understand the results presented in this thesis. First, dynamic and kinetic processes on surfaces namely the interactions of adsorbates with (metal)surfaces are explained and models for their electronic interaction are presented. The second part of this section briefly introduces into molecular beams, and the third part describes the theoretical background of the detection techniques that were used in this work.

2.1 Dynamic and kinetic processes on surfaces

Heterogeneous catalysis comprises a complex interplay of various processes like adsorption, desorption and usually a variety of reaction steps. In real catalysts, diffusion processes to and from the active sites are as important as the reaction at the catalyst surface and have to be considered in a rational catalyst design. However, within this thesis, planar surfaces were used exclusively and hence, this section is limited to the description of the main processes on catalyst surfaces.

2.1.1 Principles of adsorbate-surface interactions

This section describes the main principles of dynamic and kinetic processes that occur on surfaces, including scattering processes, adsorption, diffusion, reaction and desorption, which are schematically shown in Figure 2.1. A more detailed discussion can be found in references [12, 87, 88].

Scattering, trapping and sticking

Atoms or molecules in the gas phase exhibit at a certain amount of energy when colliding with a surface. As a result of such a collision event, the species can be scattered and repelled from the surface under conservation of their energy (elastic scattering) or with momentum transfer to the surface (inelastic scattering). If an inelastic scattering process

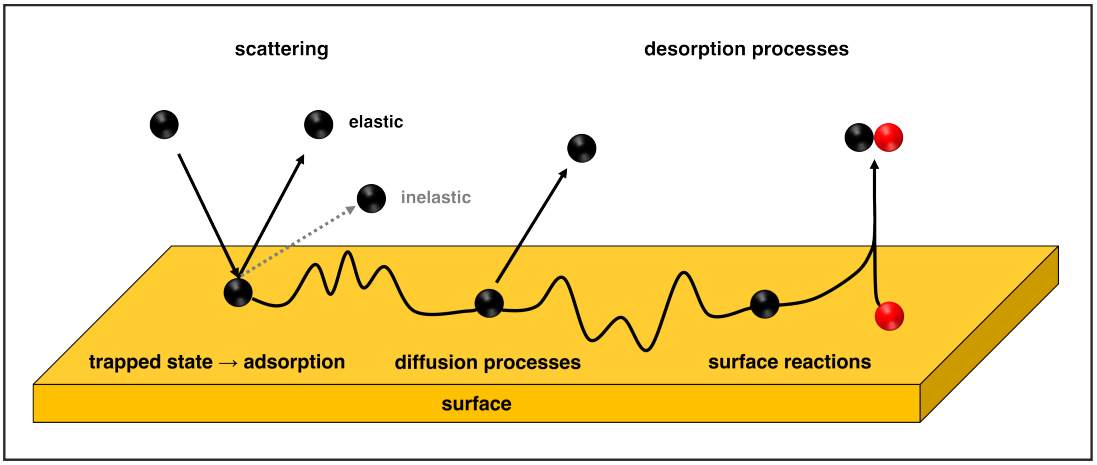

Figure 2.1: Schematic illustration of fundamental adsorbate-surface interaction occurring during catalytic processes.

transfers a sufficient amount of momentum perpendicular to the surface, the atom or molecule becomes trapped into a gas-surface potential well.[89] Trapped molecules are often associated with molecules in a weakly bound precursor state with low diffusion barriers. From this state, adsorbates can undergo oftentimes activated processes resulting in more strongly bound states. An example is the adsorption of oxygen in form of O atoms via a physisorbed state of O_2 on Ag, which transits in an activated O_2^- state and subsequently forms two O atoms.[90] A measure of the probability of an adsorption event is the sticking coefficient S which gives the ratio between adsorbates and the total number of collisions with the surface. The sticking probability depends on temperature as well as on steric factors like surface coverage.[87,89,90]

Adsorption

Trapped molecules can further interact with the surface in a process called adsorption, which describes the binding of an atom or a molecule to a surface, which is either physisorbed or chemisorbed. As described before, species can also adsorb in a weakly bound precursor state, which subsequently form more strongly bound adsorbates. A typical example for weak interactions leading to physisorption are dispersive interactions with typically low adsorption energies *e.g.* 14.5 kJ $\cdot$ mol^{-1} for methane on Au(111).[91] The term chemisorption is typically used in case adsorbates are bonded strongly with adsorption energies above 100 kJ $\cdot$ mol^{-1}. However, there are also examples for chemisorbed species with low adsorption enthalpies *e.g.* H_2 on a variety of metal surfaces[92] and hence desorb already at low temperatures.

The adsorption rate r_{ads} can be expressed as a function of surface coverage θ (with θ being the sum of all adsorbates) by a modified Langmuir isotherm, as shown in equation 2.1 (see e.g. ref. [93]).

$$r_{ads} = f \cdot s_0 \cdot (1 - \theta) \cdot exp(-\frac{E_{des}}{RT_s}) \tag{2.1}$$

where f denotes the flux of molecules, given by equation 2.2.

$$f = \frac{p}{\sqrt{2\pi \cdot m \cdot k_B \cdot T}} \tag{2.2}$$

Here, s_0 is the initial sticking coefficient, E_{des} denotes the activation barrier that must be exceeded for desorption, T_s and T the substrate temperature and gas temperature, respectively, p is the gas pressure, m is the mass of the adsorbed species and k_B is the Boltzmann factor. According to equation 2.1 the adsorption rate decreases with increasing coverage as the number of unoccupied surface sites is reduced.
The saturation of the surface by one layer of molecules is defined as one monolayer (ML), which differs in the amount of adsorbed species due to the size and steric interactions of the molecules. For small molecules or atoms (*e.g.* O atoms), the monolayer is often approximated by the number of surface atoms (*e.g.* $1.4 \cdot 10^{15}$ cm^{-2} for Au(111) or Au(332)).

Diffusion

Adsorbed atoms or molecules bind to the surface on specific sites, which are separated from each other by energetic barriers rendering diffusion an activated process. For the translation of the surface species in a diffusive process, excess energy is necessary to overcome the barrier. The temperature dependence of the diffusion coefficient for surface species $D_{surf.}$ (with units in $cm^2 \cdot s^{-1}$) can be expressed by an Arrhenius-type equation 2.3 (see ref. [12] for details):

$$D_{surf.} = k_0 \cdot exp(-\frac{E_{diff}}{RT}) \tag{2.3}$$

with k_0 and E_{diff} being the pre-exponential factor and the activation energy for diffusion, respectively.
Diffusion on surfaces can be understood in a random walk model, where adsorbed species move in a hopping motion. If $RT \gg E_{diff}$ the diffusion is observed as a kind of Brownian

motion. Especially on defective surfaces (*e.g.* stepped and kinked surfaces), diffusion processes can be anisotropic. Step sites exhibit a different binding energy and therefore diffusion barriers change. As an example, diffusion across a terrace reveals a lower diffusion barrier compared to the diffusion between two neighboring terraces, which is known as the *Ehrlich-Schwoebel barrier*.[94,95] Moreover, the *step-up* diffusion is energetically disfavored against the *step-down* diffusion.[12,94,95]

Reactions on surfaces

Surface reactions can be classified in two main types which are the Langmuir-Hinshelwood (LH) mechanism and the Eley-Rideal (ER) mechanism. In the ER mechanism one educt A is equilibrated with the surface while the second educt B reacts fast before equilibration. In contrast, both educts are equilibrated with the surface in the LH mechanism.[12] Figure 2.2 schematically shows the important steps in the LH mechanism. The majority of

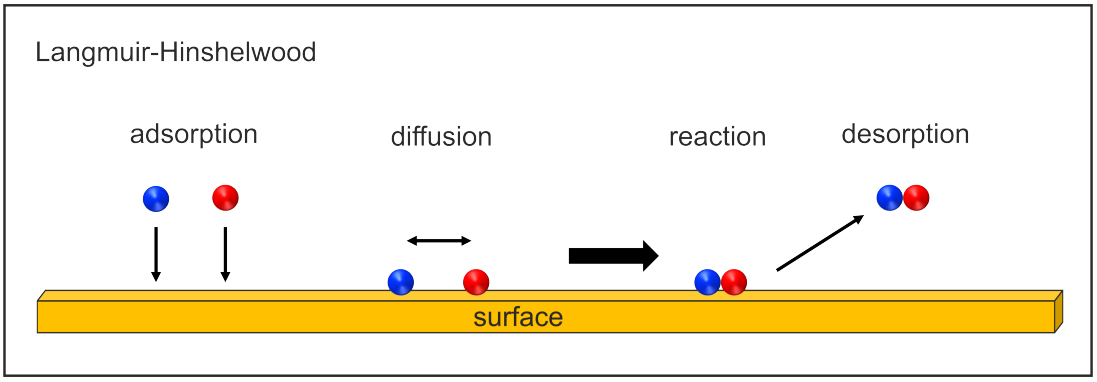

Figure 2.2: Schematic illustration of the main steps in the Langmuir-Hinshelwood mechanism.

reactions on surfaces proceed according to the LH mechanism, including the reactions studied in this work. The main steps in the mechanism can be expressed by following simplified model reaction of A and B on a surface:
Initially, species A and B adsorb at free sites $*$ on the surface.

$$A_{(g)} + *_{(A)} \rightleftharpoons A_{ads} \tag{2.4}$$

$$B_{(g)} + *_{(B)} \rightleftharpoons B_{ads} \tag{2.5}$$

By diffusion, A and B adsorb on neighboring sites and react to AB and a free surface site $*$.

$$A_{ads} + B_{ads} \rightleftharpoons AB_{ads} + * \tag{2.6}$$

Subsequently, the product desorbs into the gas phase and releases the second $*$.

$$AB_{ads} \rightarrow AB_g + * \tag{2.7}$$

Commonly, surface reactions exhibit more complex reaction mechanisms, which are significantly influenced by the applied reaction conditions. In general, a proper description of the rate law would require a detailed understanding of the underlying reaction mechanism. However, reaction kinetics are often dominated by the slowest process, known as the *rate-limiting step*, which may be one of the processes mentioned above, *e.g.* surface diffusion, adsorption, limited abundance of surface sites due to slow product desorption or a slow reaction due to a high activation barrier. However, it is important to mention, that reaction mechanisms are generally complex networks of competing processes like side reactions or desorption contributing to the overall reaction rate. The kinetics of a surface reaction between reactants A and B may be formally described by equation 2.8.

$$\frac{d\theta_{AB}}{dt} = \theta_A^a \cdot \theta_B^b \cdot k \cdot (-\frac{E_A}{RT}) \tag{2.8}$$

where a and b denote the reaction orders for species A and B, respectively.

Desorption

The desorption of an adsorbate requires energy and its kinetic can be described as an activated process. Therefore, the rate of desorption r_{des} of a species i can be expressed by following Arrhenius-type equation (2.9):[93]

$$r_{des} = -\frac{\mathrm{d}N_i}{\mathrm{d}t} = \nu \cdot N_i^n \cdot exp(\frac{-E_{des}}{RT}) \tag{2.9}$$

where N_i is the number of species, ν is the pre-exponential factor, n denotes the desorption order, E_{des} is the desorption energy, R is the molar gas constant and T is the temperature. The order of desorption is characterized by its rate limiting step. Thermally induced desorption is used as an analytical tool namely temperature programmed desorption/reaction (TPD/TPR) spectroscopy which is discussed in section 2.3.3.

2.1.2 Specific interactions between (transition) metals and adsorbates

In metals, atoms are connected by metallic bonds, where a fraction of valence electrons are delocalized and form a so-called *electron gas*. The simplest description of an electron in a metal is by a particle in a box. The energy states electrons can adapt in a metal are very close to each other and can be described by the band model. A chemical intuitive way to understand the band formation (in the one-dimensional case) is based on the molecular orbital theory. As a model, we assume a hypothetical chain of H atoms forming cyclic macro molecule (Figure 2.3 (a)). The overlap of the atomic orbitals (AOs) results in the formation of the equal amount of molecular orbitals (MOs) (*e.g.* $6.023 \cdot 10^{23}$ for one mol of H atoms). The molecular orbitals have slightly different energy values dependent

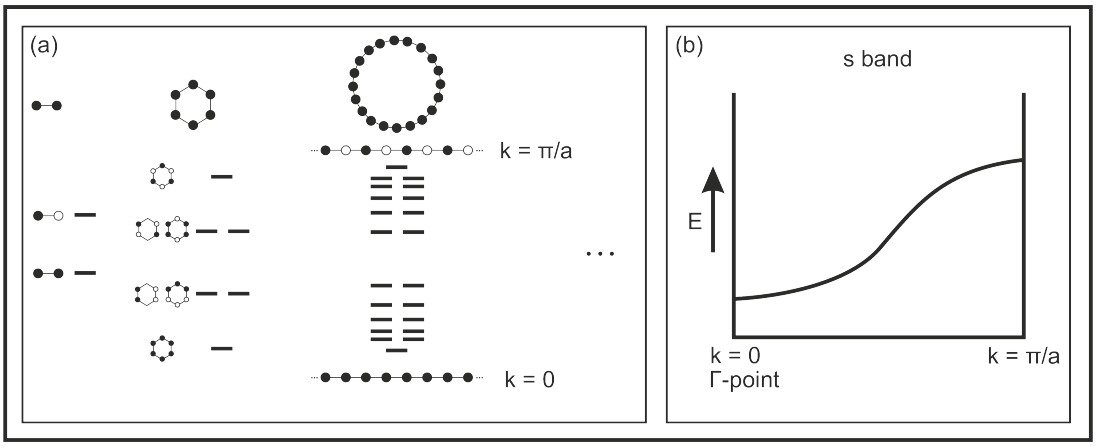

Figure 2.3: Schematic description of the band model using molecular orbital (MO) theory. For a hypothetical chain of n H atoms, cyclic macro molecules form with the amount of n MOs. As an example, Figure (a) shows the overlap of the s orbitals in (hypothetical) molecules with two, six and 20 H atoms. The energies of the MOs as a function of the k vector is depicted in (b) between the center and one edge of the Brillouin zone. Adapted from reference [96].

on the amount of nodal planes, which can be plotted as a function of the k vector as demonstrated in Figure 2.3. The molecular orbital without nodal planes has the lowest energy, referring to $k = 0$ (for the s orbitals) at the Γ point of the Brillouin zone, whereas the highest energy is found at the edge of the Brillouin zone with the highest number of nodal planes at $k = \frac{\pi}{a}$, where a denotes the overlap of the AOs. The amount of discrete k values is so dense for this high amount of atoms that they form a quasi-continuum,

which is referred to as a band. According to the angular momentum of the overlapping AOs, the resulting bands are called s, p or d bands which are energetically overlapping. The bandwidth is dependent on the degree of orbital overlap, which is strong for s and p orbitals resulting in wide s and p bands whereas the bandwidth of d bands is rather narrow. The electrons are now filled into these bands, starting from the lowest energy up to the point where all valence electrons are filled in. In metals, the corresponding energy is called the Fermi energy. In contrast, it is called the top of the valence band, if the Fermi energy is positioned in the middle of the band gap. In case of narrow low lying d bands such as in Au, the s band crosses the d band and the Fermi energy is located above the d bands (d^{10}) and in the absence of hybridization would be situated in the middle of the s band, which would then be half filled (s^1).[96–98] The interaction of adsorbates with metal surfaces results on one hand in the donation of electron density to the metal, on the other hand electron density is transferred in empty, *e.g.* anti-bonding orbitals of the adsorbate, which is the so-called back donation. Several models have been established to describe the interaction between adsorbates and metals (see e.g. ref. [99] for examples). Among those, the Blyholder model and the d band model will be discussed in more detail in this section.

The Blyholder model

The Blyholder model[100] was developed to describe the electronic structure of transition metal carbonyl complexes and can also be used to describe the interaction of CO molecules with surfaces of transition metals like Au. The adsorption of CO is influenced by the electronic structure of both CO and Au. For CO, mainly the frontier molecular orbitals are important, which are the non-bonding 5 σ (HOMO), which is localized at the carbon end of the molecule, and the anti-bonding 2 π^* (LUMO), symmetrically distributed along the molecule axis.[12] Figure 2.4 shows schematically the interaction between the CO frontier orbitals and the Au surface. The fully occupied 5 σ orbital donates electron density to empty, high lying Au states (*e.g.* 6 s states), since the d band is completely filled. Due to the non-bonding character, withdraw of electron density from the CO does not affect the binding strength of the CO molecule. However, the increase of electron density in the gold affects neighboring adsorption sites such, that the adsorption of another CO molecule becomes less favorable. Additionally, so-called π back-donation of electron density from the filled Au d band into the 2 π^* of the CO molecule reduces the binding strength of CO, which is for example observable as a red shift of the vibrational frequency.

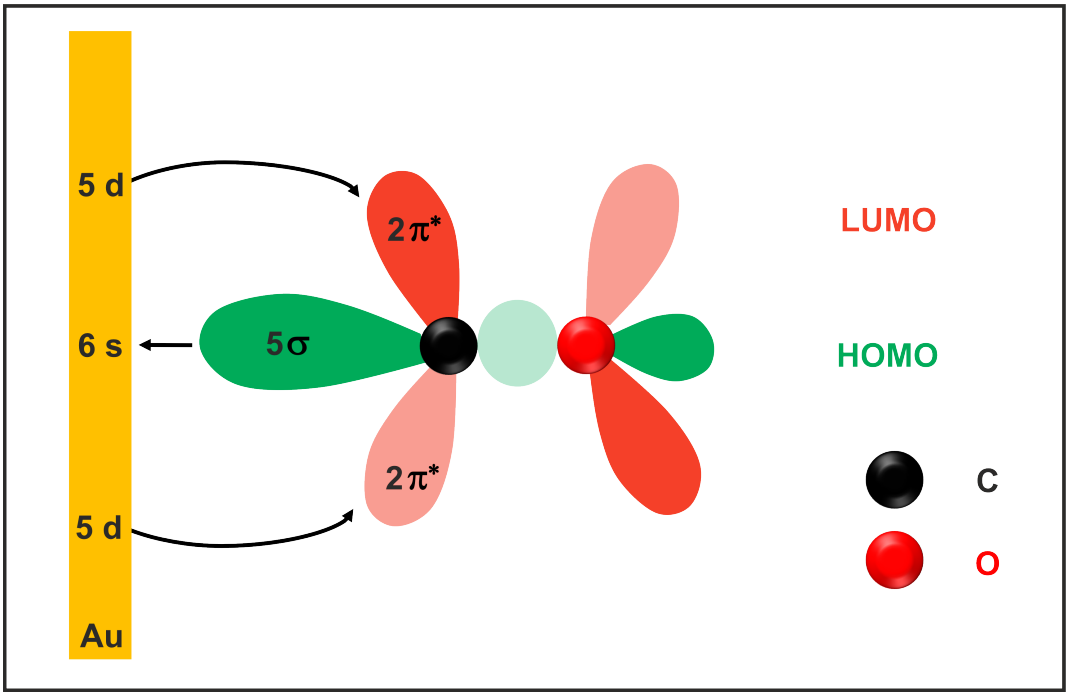

Figure 2.4: Simplified model of CO frontier orbitals, interacting with metal surfaces. The degeneracy of the $2\pi^*$ orbital is not depicted for the sake of clarity. The 5 σ orbitals interact with 6 s states of the Au and π back-donation takes place from the filled 5 d states into the $2\pi^*$ orbital.

Influence of the metal band structure (d band model)

The binding of an adsorbate on a metal surface can be described in a simple model where s or p orbitals of the adsorbate (*e.g.* 5 σ of CO) interact with the s band of the metal, which is broad especially for transition metals. Additionally, the adsorbate couples to the d band of the metal, resulting in the splitting into a bonding and an anti-bonding orbital.[12] The position of the anti-bonding orbital with respect to Fermi level E_F indicates, to which extend they interact with electron density of the d band. With increasing group number and especially for late transition metals like Cu, Ag and Au, the d band is below E_F and anti-bonding sates are occupied which disfavors adsorption.
The overlap between the orbitals requires re-hybridization and thus energy has to be expended. This re-hybridization energy increases with the magnitude of the coupling matrix element between the s (adsorbate) and the d (metal) orbital V_{sd}^2 which is larger for the 5 d orbital because it is spatially more extended than the 3 d orbital, which explains why Au is more noble than Cu.[13] Figure 2.5 demonstrates schematically the coupling process of the adsorbate to the metal. The band structure of the metal surface is affected

by the surface morphology of the metal. Both tensile strain and a decreasing coordination number of surface atoms result in a lower overlap of the d states and a narrowing and up-shifting of the d band towards E_F. As a result, more anti-bonding states of the metal interact with the adsorbate and enhance adsorption.[99]

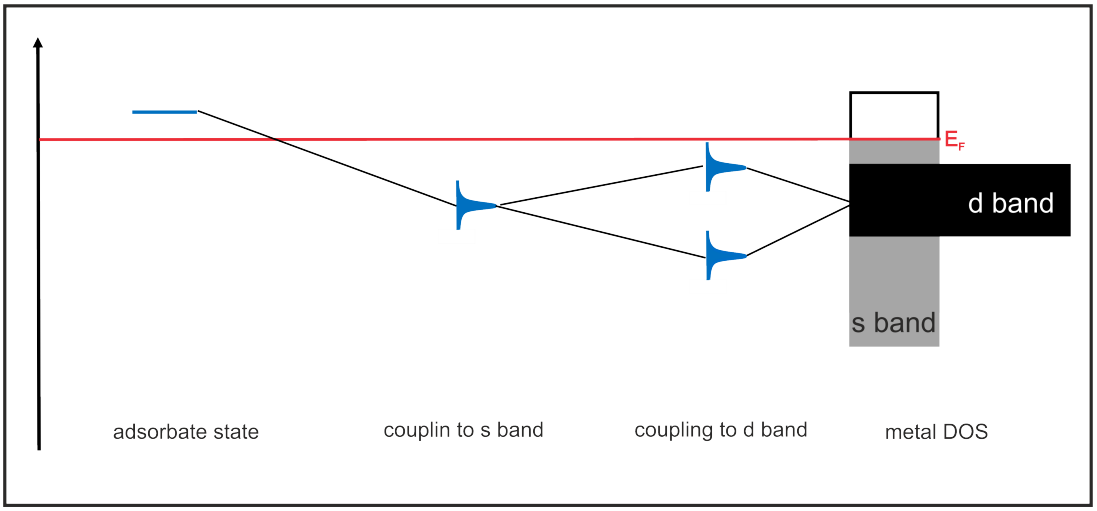

Figure 2.5: Schematic illustration of the interactions between the electronic state of adsorbates with the band structure of d block metals, adapted from ref. [101]. The values for energy levels and band widths in this figure are arbitrary.

2.2 Experimental methods

2.2.1 Effusive molecular beams

Effusive molecular beams are a powerful tool to study reaction kinetics under well-defined UHV conditions. Under these conditions, molecules provided by the molecular beam can adsorb on the surface or are scattered into the vacuum with a very low likelihood for re-adsorption. The latter holds, if the background pressure in the chamber is sufficiently low and the corresponding conditions are often referred to as single collision conditions. With this technique, it is possible to study reaction kinetics under isothermal conditions, which are typically used in catalytic experiments at ambient pressure *e.g.* in case of np-Au. As single collision conditions also apply for reaction products, it is possible to elucidate absolute reaction probabilities due to competing reaction and desorption processes, which wouldn't be possible under conditions at elevated pressures and ambient conditions. Molecular beams can be easily modulated which allows for studies of transient kinetics,

giving additional information to elucidate the reaction mechanism. A molecular beam is characterized by a directed, temporally constant and collision-free movement of atoms or molecules. The basic principle of effusive molecular beams is based on kinetic gas theory, where the effusion from an infinitely thin walled orifice is described by equation 2.10:[102]

$$f \cdot A_0 = \frac{p \cdot A_0 \cdot N_A}{\sqrt{2\pi \cdot M \cdot R \cdot T}} \tag{2.10}$$

where f is the molecular flux, A_0 is the orifice area, A is the Avogadro number, M and T are the molar mass and temperature of the effusing species and R is the universal gas constant. The spatial distribution of the effusing species follows a $\cos^2$ distribution.[103] A collision-free movement of atoms or molecules is possible, if the mean free path (λ) of the travelling species is large compared to the diameter d of the orifice, which is characterized by the Knudsen number K_n.

$$K_n = \frac{\lambda}{d} \tag{2.11}$$

Effusive molecular beams are typically generated with $K_n \gg 1$. To achieve a more forward focused and collimated beam, the aspect ratio $\frac{L}{R}$ of the orifice can be increased by increasing its length L and lowering its radius R resulting in narrow tubes. L and R need to be properly chosen, since the radius determines the pressure range that can be used to maintain $K_n \gg 1$. If the required pressure is too high, substances with a low vapor pressure *e.g.* liquids may not be used in molecular beams. On the other hand, significant diffusion from the surrounding atmosphere into the gas causes problems with purity for too low pressures. The forward focusing is given by the so-called *peaking factor* κ, which is the inverse transmission probability of species W^{-1} and can be approximated by equation 2.12.[102]

$$\kappa = W^{-1} = \frac{3L}{8R} \tag{2.12}$$

A highly forward focused molecular beam exhibits a high peaking factor but also a low transmission probability. This reduces the flux trough the tube, as species that are not translated parallel to the tube will be scattered at the tube wall. To circumvent low fluxes and still enable relatively high peaking factors, arrays of multiple, parallel tubes are used. In this work, this is achieved by *glass capillary arrays* (GCA) enabling a homogeneous distribution of the molecular flux across the sample surface.[104]

To further collimate the molecular beam, two apertures cut off molecules that do not move along the surface normal of the Au(332). To maintain low pressures and thus transparent flux conditions, the apertures are connected to differential pumping stages that remove

the repelled molecules by means of turbomolecular pumps.

2.3 Analytical methods

This section describes the theoretical background for the analytical methods in this thesis, which are infrared reflection adsorption spectroscopy (IRAS), time-resolved mass spectrometry and temperature programmed desorption (TPD). However, the description is limited to the most important aspects. For further information see references [105, 106] (IRAS), [107, 108] (MS) and [109, 110] (TPD). Within this thesis, also low energy electron diffraction (LEED) images have been recorded, which was however not the main focus of this work and therefore the theory of LEED will not be further discussed in this section. For detailed information see reference [111].

2.3.1 Infrared reflection adsorption spectroscopy (IRAS)

Working principle and instrumentation

In Figure 2.6 a typical IRAS setup is shown, which consists of an FTIR spectrometer, a reflecting sample in an UHV system and a detector, which was kept in a pumped detector box under high vacuum in the order of $1 \cdot 10^{-6}$ mbar in this work. Polychromatic IR light, mostly produced by thermal sources like globars, is directed onto the sample surface by means of mirrors. The infrared light irradiates the sample in a geometry of grazing reflection and hereby excites vibrations of adsorbates on the surfaces, where a part of the IR light gets adsorbed. The remaining part is reflected and directed onto a detector. The key part of an FTIR spectrometer is the Michaelson interferometer. A beam splitter divides the incoming light beam in two parts of equal intensity. One beam is reflected at a stationary mirror while the other is reflected at a movable mirror, which generates a difference in path length δ. By overlapping these two beams, interference occurs in dependence on δ. The modulation of the intensity will be subsequently explained for a monochromatic light source with the intensity $I(\tilde{\nu}_0)$, which can be expressed by equation 2.13:[105]

$$I(\delta) \propto I(\tilde{\nu}_0) cos(2\pi\tilde{\nu}_0\delta) \tag{2.13}$$

This describes an ideal scenario of perfectly monochromized light and no contributions from the instrument to the modulation of the intensity. In reality, processes like absorption or scattering contribute significantly to the measured intensity so the arriving IR intensity

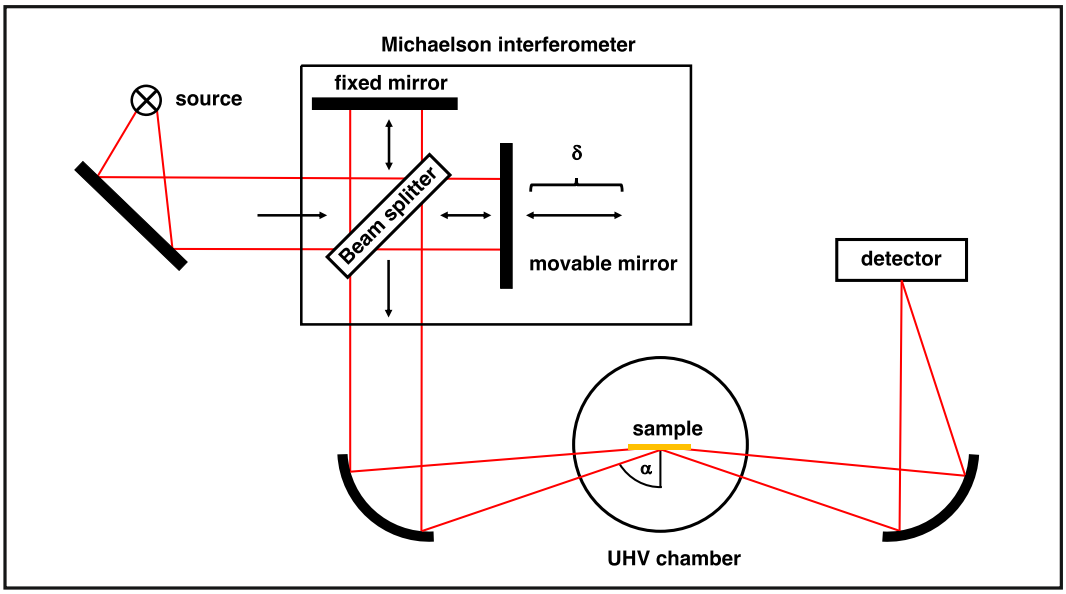

Figure 2.6: Schematic illustration of an IRAS setup indicating the important components. A representation of the working principle of the Michaelson interferometer is depicted in the inset.

at the detector is expressed as $B(\tilde{\nu}_0)$. The intensity of the detected IR light generates a signal in the detector. The detector output for the modulated intensity of all spectral components of polychromatic IR light, the so-called interferogram can be expressed as

$$S(\delta) = \int_{-\infty}^{\infty} B(\tilde{\nu}) cos(2\pi\tilde{\nu}\delta) d\tilde{\nu} \tag{2.14}$$

Fourier transformation decomposes the interferogram in each individual spectral component $B(\tilde{\nu})$ across an infinitely wide spectral range. By truncation of the interferogram by a so-called sinc function, artifacts in the spectra arising from the Fourier transformation are minimized.

The resulting spectrum of adsorbates on the surface is subsequently referenced to a spectrum of a bare surface by division, which is a simple way to remove all unwanted contributions of the instrument and molecules in the beam path. However, small changes in the contributions to the background strongly affect the baseline of the resulting spectra, which is especially problematic for series of measurements (*e.g.* coverage series). To minimize problems in the resulting spectra, the IR source intensity as well as the detector temperature need to be constant and the sample should not move (*e.g.* by vibrations of the manipulator) during the measurements.

Selection rules

The probability of the excitation of a molecular vibration is derived from the time-dependent perturbation theory and can be expressed by the *transition matrix element*.

$$P_{i\to f} \propto |\langle\psi_f(Q_k)|\vec{\mu}(Q_k)|\psi_i(Q_k)\rangle|^2 \tag{2.15}$$

$\psi_i(Q_k)$ and $\psi_f(Q_k)$ denote the nuclear wave functions of the initial state (i) and the excited state (f) in dependence on a normal coordinate (Q_k). For

$$\langle\psi_f(Q_k)|\psi_i(Q_n)\rangle = 0 \tag{2.16}$$

if $k \neq n$ because $\psi_i(Q_k)$ and $\psi_f(Q_n)$ are orthogonal wave functions. A necessary requirement for being IR active is, that the transition matrix element (see equation 2.15), which itself can be treated as a vector, may not disappear (*i.e.* $\neq 0$). This will only be the case if the dipole moment is not independent of the motion of the nuclei. The latter can be formally described by expanding the dipole moment into a Taylor series around the equilibrium geometry. Non-zero intensity is possible if the first derivative of the dipole moment, the so-called *dynamic dipole moment* $d\vec{\mu}$ along Q_k is unequal to zero. The IR light consists of components which are polarized perpendicular to the surface (p-polarized) and parallel to the surface (s-polarized). Near the metal surface, the s-polarized component undergoes a phase shift by approximately π, which leads to the cancellation of the resulting waves and hence, adsorbates cannot be probed by s-polarized light. On the other hand, p-polarized light undergoes a phase shift of approximately $\frac{\pi}{2}$ around the angle of total reflection, which enhances the amplitude due to constructive interference. For the same reasons, dipole moments that are oriented parallel to the surface plane cannot be probed because they induce an image dipole in the metal leading to cancellation of intensity. On the other hand, dipoles perpendicular to the surface face enhancement of the amplitude.[97,105,106] This so-called *metal surface selection rule* can give information on changing adsorption geometries of adsorbates.

Frequency shifts

The spectral position of a vibration can be approximated by the harmonic oscillator, its energy eigenvalues $E_v(Q_k)$ given as:

$$E_v(Q_k) = \hbar \cdot \omega_{Q_k}(v + \frac{1}{2}) \tag{2.17}$$

with the frequency ω_{Q_k} and the vibrational quantum number v. An approximation for the quantum mechanic harmonic oscillator is given by the classic description of two masses which are connected by a spring.

$$\omega_{Q_k} = \sqrt{\frac{k}{\mu}} \tag{2.18}$$

with k is the force constant of the bond and μ is the reduces mass, given as

$$\mu = \frac{m_1 \cdot m_2}{m_1 + m_2} \tag{2.19}$$

Equation 2.18 demonstrates, that the frequency is proportional to the square root of the inverse reduced mass. Furthermore, the frequency depends on the square root of the force constant. The nuclear mass does not contribute to the electronic Schrödinger equation and therefore has no effect on the properties of the potential energy curve of the ground state, which is approximated by the force constant in the classical model of the harmonic oscillator. This means, that the vibrational frequency for different isotopologues of the same molecule (*e.g.* ^{12}CO versus ^{13}CO) decreases for the heavier isotopologue.
Furthermore, the vibrational frequency of a species reveals coverage dependent frequency shifts. If oscillators with the same frequency interact, they form a system of N coupled oscillators, resulting in the same amount of vibrations. Here, only the total symmetric *in-phase* vibration, which has the highest frequency, reveals a significant intensity and can be probed by IR spectroscopy.[112] For this reason, dipolar coupling always results in a blue-shift with respect to the *singleton* frequency.
In addition, the frequency of a mode also depends on its adsorption site. Population of surface sites in vicinity to an adsorption site influences the electronic structure of the latter. This so-called *chemical shift* is material dependent an can result in both a red- or blue shift of the stretching frequency. For the group 12 metals Cu and Au, a red shift upon increasing surface population was found.[113,114] In case of CO on Au, this increases electron density in the Au and therefore increases the amount of π back-donation and hence weakens the CO bond, (*i.e.* the force constant k) resulting in a lower vibrational frequency according to equation 2.18.
For CO molecules, these counteracting shifts in total lead to a red shift which is strongly dependent on the adsorption site as well as the surface coverage. An experimental approach to deconvolute the individual contributions of chemical and dipolar shift is isotopic dilution (*e.g.* ^{12}CO in ^{13}CO).[67] This is possible, because dipolar coupling does not only depend on spacial but especially also on spectral proximity. The calculated difference in

vibrational frequencies (according to the harmonic oscillator) between ^{12}CO and ^{13}CO is around 48 cm^{-1} which is large enough do disable contributions of dipolar coupling on the position of the lines.[112]

Intensity effects

The intensity of IRAS spectra depends on several factors. Three of those are subsequently briefly described. The intensity of IR modes generally depends on the magnitude of the dynamic dipole moment, the so-called *oscillator strength*. This is high for *e.g.* C-O modes, whereas C-H modes have a lower oscillator strength and appear therefore weaker in the spectra. Additionally, the metal surface selection rule (see section 2.3.1) enhances vibrations with dipole moments oriented along the surface normal and reduces the intensity of modes with components of the dipole moments in the surface plane. On one hand, this complicates the interpretation of the observed intensities but on the other hand gives valuable insights into coverage and temperature induced changes of the adsorption geometries of adsorbates. As mentioned before, the dipolar coupling results in a blue shift of IRAS modes which is less pronounced if the oscillators have different frequencies, but still a significant intensity transfer from oscillators of lower frequencies to higher frequent oscillators is given, which is less strongly dependent on the spectral proximity. This so-called *intensity borrowing* can significantly affect the apparent intensity ratios of IRAS spectra.[112]

2.3.2 Mass spectrometry

In this work, mass spectrometry was used for the time-resolved analysis of the gaseous products in the pulsed isothermal molecular beam experiments as well as for the detection of desorbing species in TPD and TPR experiments (see section 2.3.3). This method is especially suitable for detection of gas phase products under UHV condition because the applied pressure conditions are usually too low for other techniques like gas chromatography. Among other mass filtering techniques like *time of flight*, mass spectrometers with quadrupole mass filters are widely used. The main working principle is based on the ionization of the gaseous analyte and the selection of the ions according to their *mass-to-charge* ratio (m/z), subsequently described in more detail. For further and more detailed information see also references [107, 108].

The oldest and widely used ionization technique is electron impact ionization.[107] Elec-

trons are emitted from a cathode (*e.g.* heated filaments) and accelerated to kinetic energies of 10 – 100 eV. When the electron undergoes a collision event with a molecule in the gas phase, ionization of the molecule may occur by ejecting an electron:

$$M + e^- \rightarrow M^{\cdot+} + 2e^- \tag{2.20}$$

If a large amount of energy was transferred, the primary formed cations can undergo further fragmentation.

$$M^{\cdot+} \rightarrow A^{\cdot+} + B \tag{2.21}$$

The ionized species are guided into a quadrupole mass filter which is composed by four parallel cylindrical or hyperbolic metal rods, which have a fixed distance r_0 from the central axis (z-direction). Opposing rods are connected, creating two sets of electrodes (I and II) of which each set is lying on the same potential according to equations 2.22 and 2.23

$$\Theta_I = +(U - Vcos\omega t) \tag{2.22}$$

$$\Theta_{II} = -(U - Vcos\omega t) \tag{2.23}$$

where U is a direct potential, whereas V denotes the amplitude of an alternating potential with a modulation frequency ω in the radio frequency range.
The resulting total potential is expressed by the potential difference of the two sets (see equation 2.24).[107]

$$\Theta_0 = \Theta_I - \Theta_{II} = 2(U - Vcos\omega t) \tag{2.24}$$

The ionized species propagate along the z-axis in an oscillating motion. The mass selection is realized by alternating U, V and ω where only ions with a fitting m/z ratio undergo a stable motion along the z-axis and are otherwise deflected out of the mass filter. The description of the oscillating motion follows Mathieu's differential equations, which are discussed in more details in.[107]

$$\frac{d^2x}{dt^2} + \frac{2ze}{mr_0^2}(U - Vcos\omega t)x = 0; \frac{d^2y}{dt^2} - \frac{2ze}{mr_0^2}(U - Vcos\omega t)y = 0 \tag{2.25}$$

After passing the quadrupole mass filter, the ions are accelerated onto a conversion dynode, which lies on a high potential of opposite polarity and electrons are emitted as a result of the impact of ions. As placing the conversion dynode outside the *line of sight*

of the quadrupole mass filter, unwanted creation of electrons can be suppressed. The emitted electrons are subsequently accelerated onto a channeltron detector, in which a cascade of electrons is generated by emitting secondary electrons from an emissive layer (*e.g.* SiO_2) which is evaporated onto a conducting layer of lead oxide on a highly lead doped glass tube. In curved channeltron detectors, amplification factors up to 10^8 can be achieved.[108] However, due to the high applied potentials around 2 kV, the detector has to be kept under high vacuum conditions to avoid electric arcs which would destroy the detector. Even under ultrahigh vacuum conditions, a channeltron detector has a finite lifetime, which is mainly determined by ion impurities or depletion due to electron impact. Ions with high kinetic energies can induce sputtering effects including changes of the morphology or oxidize parts of the emissive layer. Additionally, electron stimulated processes and electromigration can cause surface oxidation and the deposition of carbonaceous species, which significantly changes the work function and thus the gain of the detector. Furthermore, the detector gain degrades proportional to the number of electron impacts per surface area, which limits the total output of charge to a few coulombs.[115]

2.3.3 Temperature programmed desorption (TPD)

Temperature programmed desorption (TPD) spectroscopy is a widely used technique in surface science to probe desorption characteristics of atoms and molecules adsorbed on surfaces. In a TPD experiment, the substrate is heated with a constant rate and desorbing species are subsequently detected by a mass spectrometer (see 2.3.2). Typically, activation energies for desorption and their coverage dependence can be probed by TPD allowing for the determination of attractive or repulsive molecular interactions. An important quantity to access these information is the number of adsorbed molecules, which can be obtained by measuring the amount of desorbing species in relation to the saturation coverage. Desorption is, as described in 2.1.1, a kinetic phenomenon. The observed shape of the desorption peaks as a function of coverage strongly depends on the kinetics of the process *i.e.* the desorption order. The corresponding effects are exemplarily shown in Figure 2.7. Zeroth-order desorption (*e.g.* multilayer desorption like desorption of H_2O from metal surfaces) is characterized by an increasing desorption temperature with increasing coverage where the spectra reveal a common leading edge. Molecular desorption that is not connected to the collective desorption of multilayers (*e.g.* individual desorption of molecules from a monolayer) is described by first-order kinetics (*e.g.* CO from Pt(112)) and characterized by a constant temperature of the desorption peak. Associative or re-

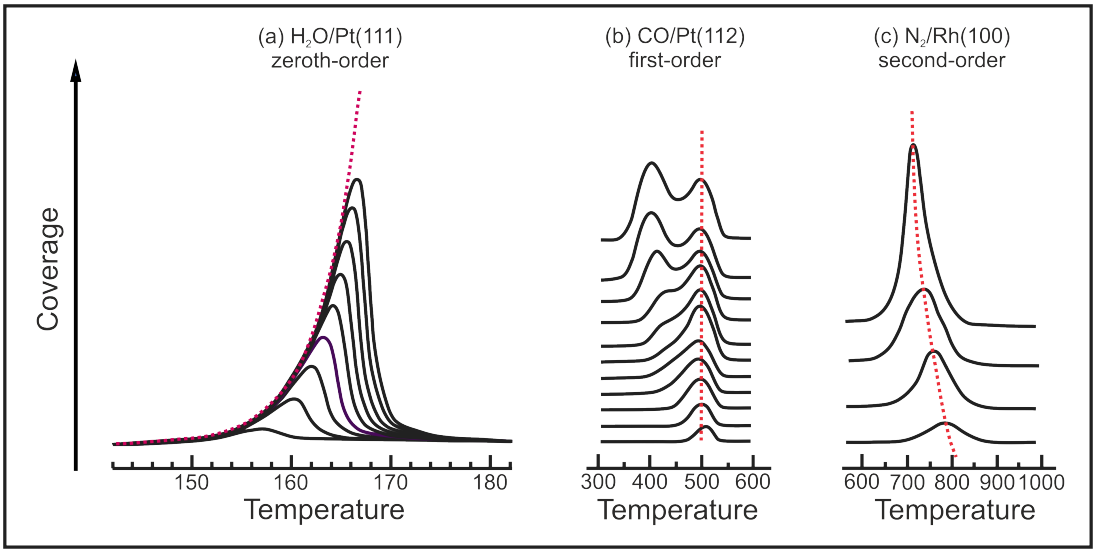

Figure 2.7: (a) Zeroth-order, (b) first-order and (c) second-order desorption, adapted from ref. [116] (a) and ref. [88] (b) and (c).

combinative desorption follows a second-order kinetic (see N_2 from Rh(100)) resulting in a decreasing desorption temperature for increasing coverage. Importantly, thermodynamic data like adsorption energy cannot directly be extracted from the spectra. Therefore, several techniques like the method of Readhead[117] have been developed to extract kinetic data like the activation energy for desorption from the TPD spectra.

In this thesis, TPD was used to quantify the amount of adsorbed oxygen atoms relative to the Au(332) surface saturated with oxygen (see more details in chapter 3.2.2). There are various technical details that have to be taken into account for an accurate TPD experiment. As the desorption characteristic from a surface also follows a $\cos^2$ spatial distribution, a reproducible distance between the mass spectrometer and the sample is crucial for quantitative and semi-quantitative measurements. The sensitivity of measurement can be increased by means of a so-called *Feulner cup*[118], which can increase the number of species being detected with the mass spectrometer. Although the sensitivity is significantly increased, the Feulner cup induces different experimental difficulties like extended tailing, which might hamper the analysis of the desorption peak. For this reason, a sufficient pumping power, either by a differential pumping stage or a sufficiently large pumping cross section on the exit side of the Feulner cup is important.

If the desorbing species is produced by the reaction of at least two adsorbates, a TPD experiment is often referred to as a temperature programmed reaction (TPR) experiment. Due to increasing temperatures, the concentrations of the adsorbates change with time

and in consequence, a simple analysis of reaction kinetics is not possible. In particular, changes in the surface concentrations may influence the selectivity of a reaction which is especially problematic for more complex reaction networks. As an example, a desorption process can compete with surface reactions if the activation barrier for the desorption is lower than for the surface reaction.

3 Experimental details

3.1 Experimental setup

3.1.1 UHV Apparatus

The model studies conducted in this work were performed in an ultrahigh vacuum setup that has been described in detail by Moreira[64] and is therefore only briefly summarized. The apparatus is set up by two main chambers, separated by a manual gate valve, which are subsequently denoted as preparation chamber and scattering chamber. The vacuum (around $1 \cdot 10^{-10}$ mbar) is measured by means of ion gauges (350 UHV Gauge, Granville Phillips) and maintained by turbo-molecular pumps (Turbovac 350i, Leybold and TMU 521 P, Pfeiffer) which are connected to rotary vane pumps (Duo 5 M, Pfeiffer). A vertical manipulator is used for the sample transfer between the chambers and the manipulation of the sample position along three additional axes. The preparation chamber is used for sample preparation and is furthermore equipped with instruments for low-energy electron diffraction (Omicron MCP LEED), Auger electron spectroscopy (PHI 11-010, PerkinElmer) and a TPD/TPR setup. The kinetic measurements were conducted in the scattering chamber which is equipped with two effusive molecular beams, an effusive thermal oxygen atom source (Dr. Eberl MBE-Komponenten GmbH) as well as *in situ* detection techniques like time-resolved mass spectrometry (MAX-500HT, Extrel) and IRAS (IFS 66v/S, Bruker).

Effusive thermal oxygen atom source (Oxygen cracker)

As gold does not activate molecular oxygen (see Chapter 1), oxygen has to be provided as activated species, *e.g.* as atomic oxygen onto the surface. The production of O atoms from O_2 molecules is achieved by a commercial thermal effusive source (subsequently called oxygen cracker). The O_2 collides with the surface of a hot Ir tube resulting in the cleavage of the oxygen molecule. The heater unit is embedded in a water-cooled Cu housing and input of thermal radiation into the scattering chamber is minimized by a Ta

shielding. The O atom flux strongly depends on the temperature of the Ir tube (1630 - 1730 °C) as well as the O_2 flow rate. For operating the oxygen cracker as an effusive source, transparent flux conditions have to be introduced, which is achieved by a 50 μm pinhole placed in front of the gas inlet of the oxygen cracker, allowing for operation up to 10 mbar backing pressure, while a forward focusing of approximately factor 2 is achieved. A combination of a baratron, a flow control valve and a PID controller (Type 250) (all MKS) is used to control the oxygen backing pressure and in turn control the flux of oxygen atoms. A pneumatically operable shutter, placed in front of the Ir tube is used to stop direct exposure of the sample and enables pulsing of O atoms. To increase forward focus, an additional quartz tube connected to a differential pumping stage can be mounted in front of the Ir tube.

Flag

To estimate the contributions of background reactivity, the Au(332) model surface can be blocked by a non-reactive flag from direct exposure. The flag consists of a quartz plate which is glued onto a stainless-steel lever with high vacuum proof glue (TorrSeal). A stepper motor is used for precise motion control. The flag is positioned in a distance to the crystal surface large enough to enable IRAS measurements but also as close as possible to the crystal surface to minimize the exposure to molecules and especially oxygen atoms.

TPD setup

The setup for the TPD and TPR experiments is schematically shown in Figure 3.1. A commercial quadrupole mass spectrometer (Pfeiffer, Prisma) with an electron ionization unit and a channeltron detector is used for the detection of the desorbing gas phase species. A home-made Feulner cup[118] is attached to the mass spectrometer and houses its entire ionization unit. The Feulner cup is made of a stainless steel tube with a cone on top that has an orifice of 7 mm diameter and can be placed at a close distance to the sample. This significantly increases the sensitivity of detection for desorbing species from the crystal surface while simultaneously minimizing contributions from the background. A reproducible positioning of the TPD setup with respect to the position of the Au(332) surface is crucial for reproducible quantification of the TPD results. This is enabled by a camera, mounted in 90° with respect to the alignment of the Feulner cup. Constant heating rates were achieved by a commercial PID controller (3508, Eurotherm). The analog output signal of the mass spectrometer (allowing for simultaneous recording of 4

masses) is converted by an AD converter (BNC-2110, National Instruments) and matched to the surface temperature by a home-written program.

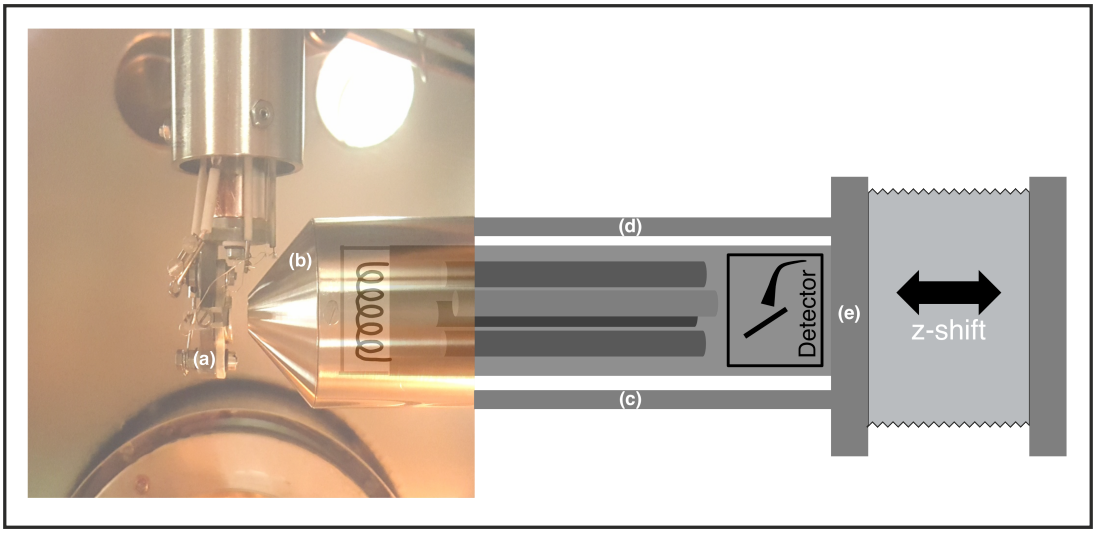

Figure 3.1: Schematic representation of the TPD setup. The Feulner cup (b) which is housing a quadrupole mass spectrometer (c) is brought close to the Au(332) (a). The Feulner cup is mounted by means of metal rods (d) onto a flange with a z-shift (e) to move the cup in horizontal direction.

3.2 Flux calibration and data treatment

3.2.1 Determination of a scaling factor for mass spectrometry

The gas phase products in the pulsed, isothermal molecular beam experiments are detected by time resolved mass spectrometry. In the detection unit, a channeltron detector with included conversion dynode (Detector Technology, Inc., 402A-H) is used. As described in section 2.3.2 aging effects in channeltron detectors lead to a decrease in their sensitivity and hence, the detected output signal decreases over time. In order to get comparable and reproducible data, a re-scaling protocol has been established. After each experiment involving MS measurements, the Au(332) sample was moved out of the scattering chamber and the non-reactive flag was placed at the sample position instead. A methanol pulse was applied via the molecular beam using a backing pressure of $2.5 \cdot 10^{-2}$ mbar while recording certain masses (*i.e.* m/z = 18, 20, 29, 30, 31, 45, 46, 47 each time). The intensity of $m/z = 29$ for methanol-^{12}C and $m/z = 30$ (methanol-^{13}C) for the first measurement of a series (R_0) is defined as 1. The intensity for all subsequent measurements is rescaled by

following equation:

$$I_{i,resc.} = \frac{R_i}{R_0} \cdot I_i \tag{3.1}$$

where $I_{i,resc.}$ is the rescaled intensity of any m/z ratio in experiment i, R_i the intensity of the reference pulse for experiment i (*e.g.* $m/z = 29$) and I_i the intensity of any mass trace of experiment i.

3.2.2 Calibration of the oxygen flux

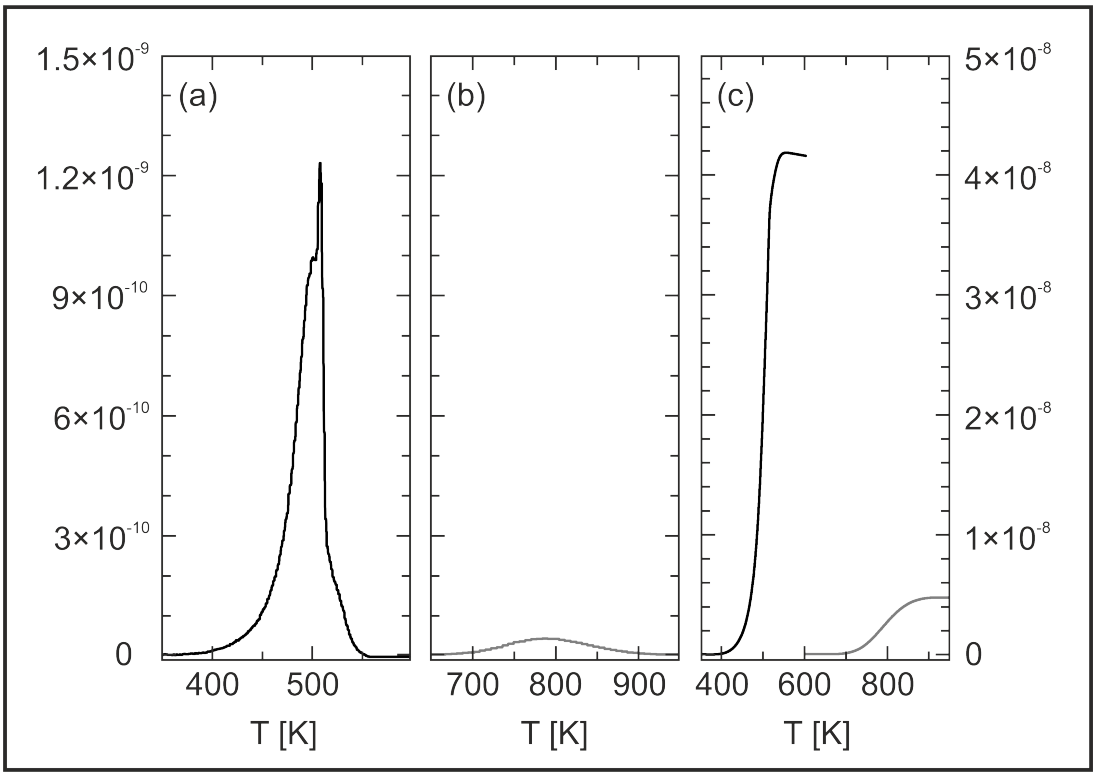

Figure 3.2: O_2 (m/z = 32) desorption from (a) Au(332) for saturation coverage, (b) Pt(111) with a p(2 × 2) O superstructure (0.25 ML) and (c) the integrated intensity of the desorption peaks. The coverage of oxygen on Au(332) is 8.4 times higher resulting into a saturation coverage of 2.1 ML O.

The oxygen flux from the oxygen cracker can be determined by referencing the amount of oxygen atoms, that adsorbs on the Au(332) within a certain time to the amount of oxygen on a fully covered Au(332). The amount of oxygen is determined by integration of the m/z = 32 (O_2) desorption peak in TPD experiments. As reference, the amount of a well known oxygen coverage was used as for a Pt(111) surface which was exposed to 400 L O_2 at 300 K, resulting in a p(2 × 2) oxygen superstructure on the Pt(111), evidenced by low energy

electron diffraction.[119] This amounts to a coverage of 0.25 ML O on the Pt(111).[120,121] On Au(332), saturation coverage was indicated by no further increase of TPD intensity for ongoing exposure. In Figure 3.2 the desorption peak of (a) O_2 from fully covered Au(332) is compared to the desorption from the p(2 × 2) O superstructure on Pt(111). From the differences of the integrated intensities depicted in (c) a factor of 8.4 is determined which amounts the saturation coverage of O on Au(332) to 2.1 ML. Note, that the amount of surface atoms and hence, the amount of O atoms in one monolayer differs for Au(332) ($1.4 \cdot 10^{15}\mathrm{cm}^{-2}$)[56] and Pt(111) ($1.5 \cdot 10^{15}\mathrm{cm}^{-2}$)[120] under the assumption of one O atom per surface atom. This difference is, however, within the experimental accuracy of the calibration.

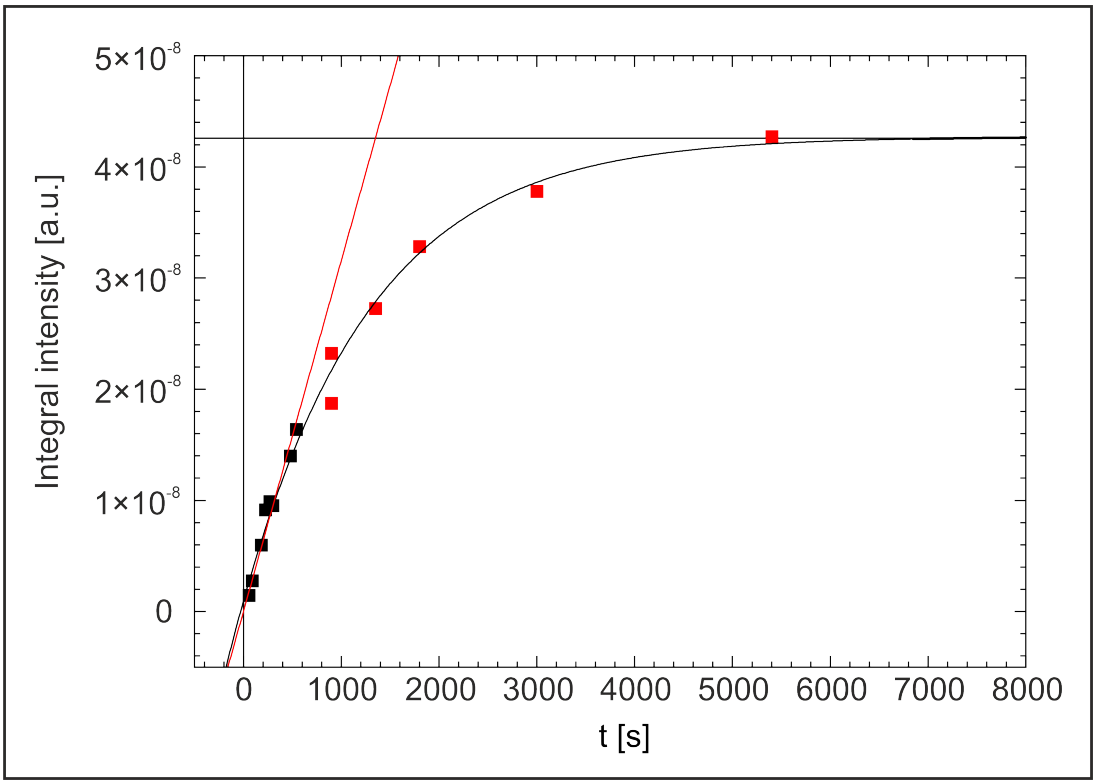

Figure 3.3: Determination of the oxygen atom flux. The linear fit through (x,y) = (0,0) and the data points at lower coverages (black) of the combined data set obtained for $T_{cracker} = 1700°C$, $p_{O_2} = 10$mbar and $p_{O_2} = 3$mbar intersect with the extrapolated saturation coverage. This was determined by a sigmoidal fit.

The flux determination is demonstrated exemplary for the oxygen cracker operated with an attached quartz tube and $T_{cracker} = 1700$ °C, $p_{O_2} = 10$ mbar and $p_{O_2} = 3$ mbar. The Au(332) was exposed to O atoms for a certain amount of time and the coverage was subsequently determined by TPD. Under the assumption of transparent flow conditions,

the backing pressure is directly proportional to the pressure inside the oxygen cracker. Therefore, the time axis of the 3 mbar measurement was divided by 0.3 to generate a common data set with the 10 mbar measurements for higher statistical significance. At low coverages, the sticking coefficient for oxygen is expected to be equal to one and the coverage increases linearly (see Figure 3.3). The saturation coverage was estimated by a sigmoidal fit of the data. The data points in the linear region (below 600 s) were fitted by a linear regression. According to the time ($t_{sat.}$) where the linear regression intersects the saturation coverage, the atomic flux per second can be calculated according to equation 3.2. The decreasing slope at higher coverage is attributed to a lower sticking probability. As described before, one monolayer of oxygen is defined by one O atom per Au atom giving $1.4 \cdot 10^{15}\mathrm{cm}^{-2}$ O atoms and thus, the saturation coverage on Au(332) amounts to $2.92 \cdot 10^{15}\mathrm{cm}^{-2}$ O atoms. The atomic flux for this example (1700 °C, 10 mbar) with $t_{sat.} = 1400s$ is given by:

$$f(O) = \frac{N_{O_2}}{t_{sat.}} = \frac{2.92 \cdot 10^{15} cm^{-2}}{1400s} = 2.08 \cdot 10^{11} cm^{-2} s^{-1} \tag{3.2}$$

3.2.3 Calibration of the methyl formate pressure

For TPD and TPR experiments, the methyl formate exposure is determined by the product of the background pressure as measured with an ion gauge and the time of exposure. The pressure measurement with ion gauges is proportional to the amount of ionized species detected at the collector electrode. Organic molecules have a higher ionization probability as noble gasses (*i.e.* Ar). This difference in ionization probability can cause significant errors, since the ion gauges are calibrated to N_2. This was corrected by comparing the pressures monitored at the ion gauge for argon and methyl formate, supplied by a molecular beam with the same backing pressure. The backing pressure is measured and maintained by a baratron, measuring a force which is independent on the nature of the molecule. From the resulting difference in the pressure measured by the ion gauges a correction factor between argon and methyl formate was concluded. The correction factor from N_2 to Ar is given by 0.775, according to the manufacturer.

$$p(MF) = \frac{p(Ar)}{0.775} \cdot 2.1 \tag{3.3}$$

3.2.4 Calibration of methyl formate formation rate

For the determination of the methyl formate formation rate, the $m/z = 60$ intensity was measured for methyl formate, which was dosed into the chamber by means of a molecular beam for different backing pressures. By linear extrapolation through (x,y) = (0,0), low production rates can be linked to corresponding backing pressures, under the assumption of transparent flow conditions.

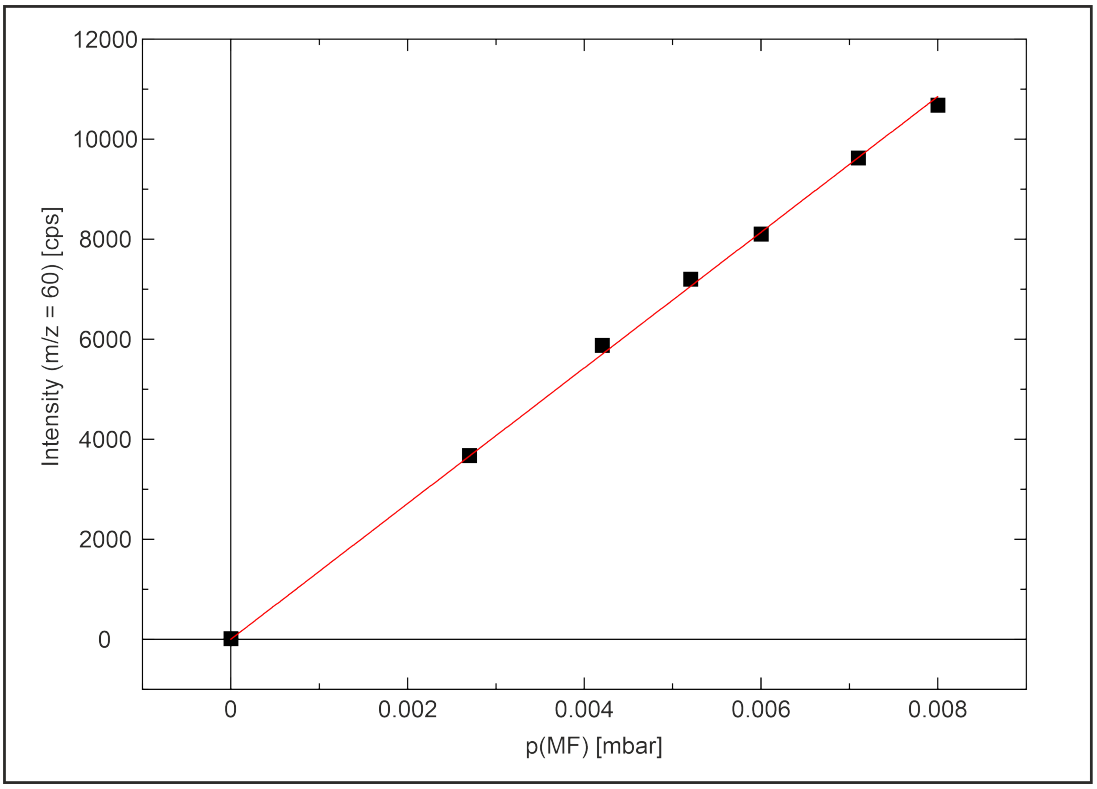

Figure 3.4: Methyl formate ($m/z = 60$) counting rate as a function of the methyl formate backing pressure $p_{(MF)}$[mbar]. By linear extrapolation through $(x|y) = (0|0)$, low methyl formate formation rates can be connected to a backing pressure and further attributed to a molecular flux

The flux from the molecular beams is calibrated for different backing pressures with argon $f_{(Ar)}$ (see ref. [64] for details) and can be directly calculated into flux of methyl formate $f_{(MF)}$ molecules by correcting for the square root dependence of the flux on the molecular mass $\sqrt{M_{(i)}}$:

$$\frac{f_{(Ar)}}{f_{(MF)}} = \frac{\sqrt{M_{(MF)}}}{\sqrt{M_{(Ar)}}} \tag{3.4}$$

4 Summary of the papers

The scientific discussion in this thesis is based on five papers (*i. e.* [**I - V**], see Chapter 6) which are summarized in this chapter in order to add to an understanding of the open questions concerning oxidation reactions on Au surfaces, as detailed in the introduction. As a starting point of the discussion, some previous results on the CO oxidation on Au(332) by Moreira[64] are briefly presented, as they also concern the understanding of oxidation reactions on np-Au and give complementary insights to the methanol oxidation on Au(332).

Previously, it was found that CO oxidation on Au(332) investigated by pulsed isothermal MB experiments at 200 K resulted in a strong deactivation of the CO_2 production rate, when a rather high oxygen flux was applied, whereas the deactivation was much less pronounced for a lower O atom flux. Although the CO_2 production rate was strongly depleted, residual activity clearly above the level of background CO oxidation was observed.[64] As AIMD simulations predicted the formation of gold-oxygen chains at step edges accompanied by significant modifications on the surface[77] and surface modifications were previously reported on Au(111) and in np-Au due to oxygen exposure[73–75], these observations were ascribed to oxygen diffusion along the step edges on the Au(332) forming less- or unreactive AuO_x phases at the step edges. Hence, the reduction of the CO_2 formation rate was ascribed to the blocking of step and kink sites which are conclusively assumed to oxidize CO at a higher rate than the remaining surface sites. Further insights into the reactivity of different oxygen species were gained from the transient CO_2 formation: While O atoms appeared to instantaneously oxidize CO to CO_2, larger AuO_x phases were found to be less reactive, in line with literature reports[54,81] and eventually poison the surface. In consequence to the accumulation of oxygen during the CO oxidation, the LEED pattern associated to the Au(332) was no longer observed, which is consistent with a more refaceted shape of the pores in np-Au after O_2 exposure.[75] An increase of the reaction temperature by merely 20 K was found to strongly affect the CO_2 formation exhibiting a pulse to pulse reproducibility, but a stronger reduction of the reaction rate during the oxygen pulses occurred. This behavior can be understood by two counteracting effects:

on the one hand, the reactivity of CO with the AuO_x increases due to higher temperatures and removes the AuO_x in the pulse delay times. On the other hand, a lower transient concentration of CO during the oxygen pulses results in the increased formation during the oxygen pulses. In conclusion, these previous results demonstrated that even a rather simple reaction like the oxidation of CO reveals a complex (kinetic) interplay between different surface sites and various types of oxygen species, including AuO_x phases.

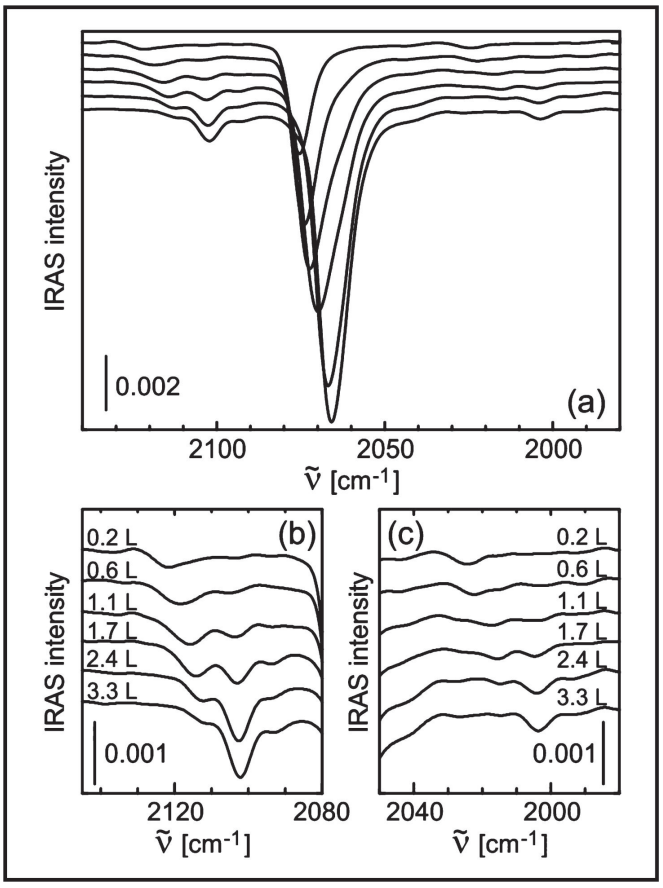

Figure 4.1: (a) IR spectra of a coverage dependent series of 5.4% $^{12}C^{16}O$ diluted in $^{13}C^{16}O$ adsorbed on the Au(332) at 320 K (exposure top to bottom 0.2 L, 0.6 L, 1.1 L, 1.7 L, 2.4 L and 3.3 L). Figure (b) and (c) show close-ups of the spectral range corresponding to $^{12}C^{16}O$ and $^{13}C^{18}O$, respectively. Taken from Paper [**I**], Copyright 2018 American Chemical Society.

In the present work (Paper [**I**]), the properties of adsorption sites on the Au(332) were further studied using CO as a probe molecule in a combined IRAS and DFT study. To separate the effect of the coverage dependent chemical shift from contributions of dipolar coupling, isotopically diluted gas mixtures (1.3 to 5.4 % $^{12}C^{16}O$ in ^{13}CO) were used. Fig-

ure 4.1 shows a series of coverage dependent IRAS measurements on the pristine Au(332). In the spectra of the $^{12}C^{16}O$ minority component (Figure 4.1 (b)) at least three different modes can be discerned that exhibit different intensity and frequency changes upon increasing coverages and correspond to sites with different adsorption energies as evidenced in a series of annealing experiments. Furthermore, the strong differences in the chemical shift suggest a non-isotropic distribution of the involved adsorption sites. DFT calculations (conducted by Wilke Dononelli) for CO adsorption on an ideal and a defective Au(332) with step atoms removed to form kink sites, as well as the Au(321) were used to provide further insight into the energetic properties of the sites. The DFT results on the adsorption energies and the coverage dependent frequency shifts are in qualitative agreement with the experimental spectroscopic data and allow for an assignment of the three observed modes: The mode at highest frequencies, present for low coverages and at high temperatures is assigned to both step and kink sites and a staggered configuration for CO on step sites at high coverages was found to minimize repulsive interactions. The mode at intermediate frequencies is assigned to an 8-fold site adjacent to a kink, while the lowest frequency mode is assigned to terrace sites next to a fully covered step edge.
Moreover, it was found that exposure to high CO pressures induces significant dynamic restructuring of the Au(332) resulting in a more heterogeneous set of adsorption sites in agreement to observations on other single crystalline Au surfaces (*e.g.* Au(111)[73] and Au(110)[74]) and on np-Au.[75] This leads to a depletion of CO adsorption sites especially of those with high adsorption energies, as indicated by the absence of CO signals already at 160 K. However, the LEED image of the restructured Au(332) shows a diffraction pattern according to the expectations for the Au(332) rendering the modification of the Au(332) without the loss of the long range ordered step structure as observed after CO oxidation.[64] In literature, structural modifications of Au surfaces due to CO were previously shown in theory, where CO lowers the barrier for Au diffusion along the step edges and enables the detachment of Au atoms from step edges.[65,73] This was also reflected in previous experiments as the perimeters of well-defined hexagonal shaped craters on etched Au(111) surfaces were rounded and decorated with Au particles after a TPD experiment with CO, which resulted in the depletion of the adsorbed amount of CO supporting the findings in our study.[73] Importantly, a similar rounding due to exposure of CO was observed in the pores of np-Au[75] which could be explained by the depletion of low coordinated sites with high adsorption energy. To this end, our results can be interpreted as a decoration of kink sites by Au particles, resulting in the preferential depletion of high energy adsorption sites and a more heterogeneous set of adsorption sites.

In summary, these results using CO as a probe molecule demonstrated a variety of sites on Au(332) differing in their adsorption properties for CO as well as the dynamic nature of the Au(332) surface exposed to CO. Hence, these findings provide further insights into the catalytic activity of np-Au exhibiting a large number of low-coordinated sites which are considered to play an important role not only in CO oxidation but may also exhibit a distinct reactivity in the (partial) methanol oxidation.[38,39]

The (partial) oxidation of methanol on Au was investigated in this work (Papers **[II]** and **[III]**) by pulsed, isothermal MB experiments combined with *in situ* IRAS using the stepped Au(332) surface as a model system for np-Au, while previous studies rather focused on low-index surfaces and TPR measurements. Based on these previous TPR experiments a reaction mechanism was proposed, already mentioned in the introduction (compare Figure 1.3), which is briefly described here as it is important to understand the results under isothermal conditions: According to literature, the reaction starts with the abstraction of the acidic proton of methanol by activated oxygen under the formation of methoxy. The latter is subsequently converted to formaldehyde by β-H elimination, which is reported to be the rate limiting step. Formaldehyde may either desorb, react with oxygen to formate and subsequently to CO_2 or couple to a neighboring methoxy species under formation of a hemiacetal. After another H abstraction the desired oxidation product methyl formate is released.[47,58,84] In the pulsed, isothermal MB experiments on Au(332) on the partial methanol oxidation to methyl formate conducted in this work, methanol was continuously applied at an excess in the gas phase, while atomic oxygen provided by the thermal cracker was pulsed onto the surface. For increasing the surface temperature from 220 K to 250 K, the methyl formate formation rate increases due to enhanced coupling of methoxy to formaldehyde at higher temperatures. However, at even higher temperatures, the desorption of formaldehyde (T_{des} = 160 K on Au(110)[50]) becomes significant and competes with the coupling reaction, resulting in a reduced methyl formate formation rate and no methyl formate production is observed above 280 K. Importantly, for all applied surface temperatures, a loss of the methyl formate formation rate is observed across the pulse sequence, while a quasi steady state rate is observed during the oxygen pulses. This behavior is in contrast to CO oxidation, where increased temperatures lifted the deactivation across the pulse sequence due to the higher reactivity of AuO_x phases, while the lowered transient CO concentration resulted in a rapid decrease of the CO_2 formation rate during the O pulses in consequence to the formation of AuO_x phases. This suggests that a different mechanism causes the deactivation for methanol as

compared to CO oxidation.

The origin of the surface deactivation for methyl formate formation was further investigated by pulsed MB experiment at 230 K varying the methanol to oxygen (MeOH:O) ratios (see Figure 4.2). For all scenarios, a decrease of methyl formate formation rate was observed across the pulse sequences. The reasons for the observed deactivation are discussed as following for the two extreme MeOH:O ratios *i.e.* the lowest (~10, Fig. 4.2 a) and the highest (~660, Fig. 4.2 d) MeOH:O ratio, respectively.

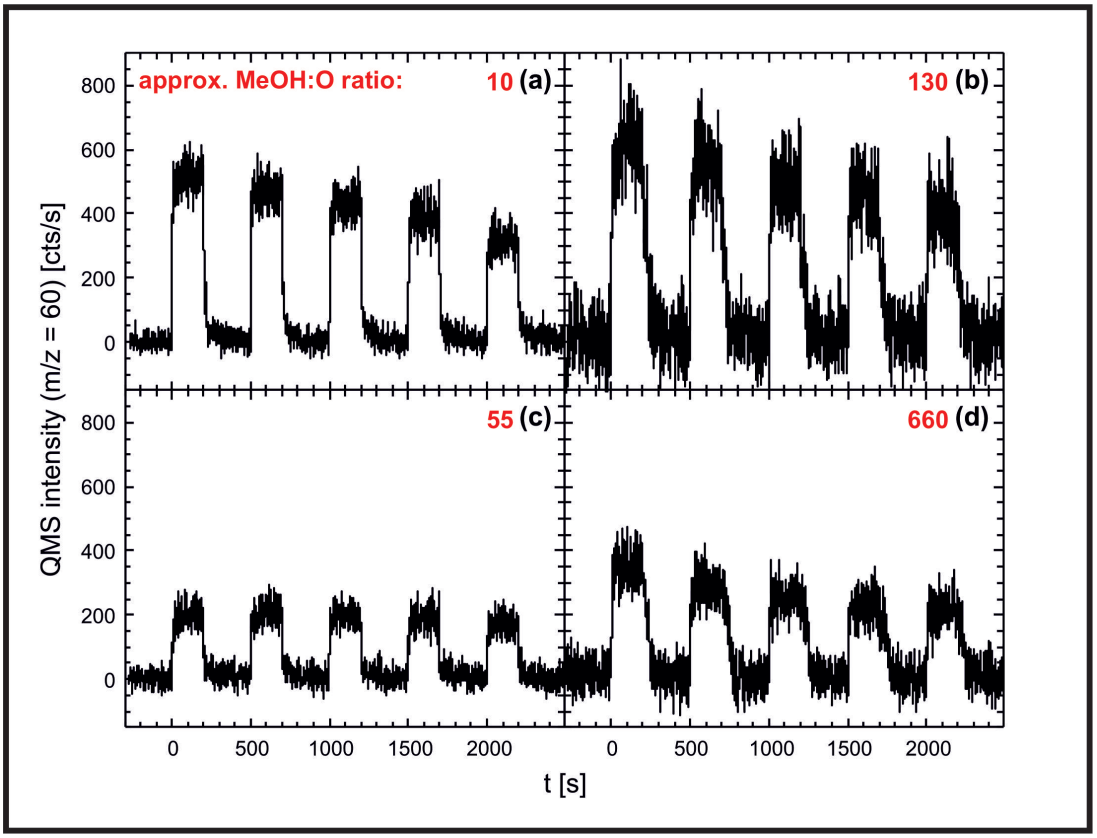

Figure 4.2: Pulsed molecular beam experiments on the methanol oxidation on the Au(332) at 230 K for different flux conditions. The methyl formate formation rate (m/z = 60) was recorded while methanol was constantly dosed and oxygen atoms (200s, delay 300s) were pulsed onto the Au(332). Adapted from Paper [**III**], Copyright 2021 Royal Society of Chemistry.

For a rather low excess of methanol and therefore rather oxygen rich conditions, the deactivation is directly correlated to an increasing amount of formate. Conclusively, the loss of the methyl formate formation rate is ascribed to the blocking of surface sites necessary for the coupling of formaldehyde with methoxy, which promotes the desorption of

formaldehyde and for even higher coverage total oxidation. The formate species mainly accumulate in the delay times which is initially surprising since rather oxygen deficient conditions between the pulses are not expected to favor overoxidation. This observation can be understood by the decomposition of formate due to atomic oxygen during the pulse which could be shown independently by IR spectroscopy. In contrast, incomplete oxygen consumption during the pulses presumably results in the formation of AuO_x phases which are able to form formate while the decomposition of formate and the methyl formate formation do not proceed effectively under these conditions. It is important to note that formate formation in the delay times also implies the formation of methoxy and formaldehyde in the presence of AuO_x phases being an intermediate for formate formation according to the expected reaction mechanism. Please note that methyl formate formation during the pulses, *i.e.* while AuO_x phases are formed, is not decreasing, showing that methyl formate formation is not reduced by AuO_x phases. To this end, these results under rather oxygen rich conditions further clarify the role of different oxygen species in (partial) methanol oxidation.

For rather methanol rich and oxygen deficient conditions (*i.e.* for an increasing MeOH:O ratio) a reduced overoxidation to formate was observed whereas the selectivity towards methyl formate was increased, in agreement with expectations.[31,58] However, the highest observed selectivity of 65% in the pulsed, isothermal MB experiments is clearly below the selectivities that are achieved for np-Au. In contrast to the single collision conditions on Au(332), formaldehyde can adsorb several times on the np-Au surface, which increases the probability of a coupling reaction and hence the apparent selectivity towards methyl formate. Although formate was absent for the highest MeOH:O ratio, a significant decrease of the methyl formate formation rate across the pulse sequence was detected, indicating a different deactivation mechanism which is dependent on the methanol exposure. Despite using high purity methanol, the experimental results point to a deactivation by an impurity in the methanol which can be removed by oxygen atoms or by heating the surface to 450 K *in vacuo*, resulting in a recovery of previously blocked CO adsorption sites as well as restoring the initial surface activity for methyl formate formation. A closer analysis of the deactivation as a function of methanol exposure reveals a fast initial rate decrease, followed by a more slowly deactivation, which is consistent with the preferential blocking of sites which are highly reactive for methyl formate formation, presumably low coordinated sites. In conclusion, similar to the CO oxidation, partial methanol oxidation to methyl formate occurs to be more facile on specific, presumably low coordinated sites on Au(332).

A preferential blocking of sites highly reactive for methyl formate formation is further evidenced by *in situ* IRAS measurements, which reveal (at least at the beginning of the pulse sequence) a high concentration of methoxy species in experiments using high methanol fluxes. This is in agreement with expectations for the steady state methoxy concentration $[H_3CO]_{stead.}$ in a simplified model (see equation 4.1) with the concentration of activated oxygen $[O_{act.}]$, where $[CH_3OH]$,$[CH_2O]$ denote the steady state surface concentrations of methanol and formaldehyde, respectively, while k_{H_3CO}, k_{CH_2O} and k_{H_3COOCH} are the rate constants for methoxy, formaldehyde and methyl formate formation, respectively.

$$[H_3CO]_{stead.} = \frac{k_{H_3CO}[CH_3OH][O_{act.}]}{k_{CH_2O}[O_{act.}] + k_{H_3COOCH}[CH_2O][O_{act.}]} \tag{4.1}$$

For only one kind of activated oxygen species, the steady state methoxy concentration should be independent from the concentration of $[O_{act.}]$ as it cancels out in equation 4.1. Furthermore, the model assumes the formaldehyde concentration to be constant. However, the experimental data reveal an increased methoxy formation at higher O fluxes, which can be understood as a suppression of the second methoxy consumption channel at higher O concentrations, *i.e.* the reduction of selectivity for methyl formate formation. Hence, the model differs from experimental data. This deviation can be explained, as the variety of different oxygen species differ in their reactivity for different steps in the reaction network, *e.g.* the overoxidation of formaldehyde. Moreover, for high oxygen flux, the methoxy concentration decreases across the pulse sequence while formate species accumulate, which is consistent with a blocking of surface sites. In contrast, for low oxygen flux conditions where the methanol related surface deactivation dominates, the methoxy concentration remains largely constant across the pulse sequence. This is consistent with a preferential blocking of a small number of highly reactive sites, while a large number of presumably terrace sites remain available for methoxy formation. Thus, the results show how the heterogeneity of sites and oxygen phases available on the Au(332) influence different steps in the reaction of methanol with oxygen. The blocking of active sites by impurities in the educt feed becomes even more important for increasing pressures as long as the temperature is low enough to allow for their accumulation on the surface. Hence, this observation is a possible explanation for the absence of steady state methyl formate formation on np-Au below 20 °C,[31] even though oxygen activation was shown to be feasible at already below 0 °C.[27,28]

In addition to the methanol oxidation, the unwanted oxidation of methyl formate on Au(332) was studied by TPR and pulsed, isothermal MB experiments in this thesis (Papers **[IV]** and **[V]**), since readsorption and subsequent oxidation of methyl formate may decrease the selectivity of the partial methanol oxidation in np-Au. As readsorption of desorbing products is negligible in UHV studies due to the applied single collision conditions, these effects, which may be important for np-Au catalysts, cannot be investigated by studies on methanol oxidation alone. Studies on Ag(110)[122] and Cu(110)[123] have shown that oxidation of methyl formate proceeds by the attack of active oxygen to the carbonyl carbon C_C (C_M stands for the methyl carbon) of methyl formate (see equation 4.2). The C-O bond cleavage results in the production of a formate and a methoxy species.

$$HC_COOC_MH_3 + O \rightarrow HC_COO + H_3C_MO \tag{4.2}$$

A similar study investigating the reaction of methyl formate with activated oxygen has not been reported on any Au surface. Therefore, the adsorption and reaction of methyl formate on oxygen pre-covered Au(332) was investigated by TPR and IRAS measurements (see Paper **[IV]**). Compared to the bare Au(332), low amounts of pre-adsorbed activated oxygen which are expected to preferentially decorate step sites have significant impact on the adsorption properties of methyl formate. On the one hand, the adsorption geometry is altered due to the oxygen, indicated by significant changes in the relative intensities of modes associated to methyl formate in the IR spectra. On the other hand, methyl formate is bound more strongly on the oxygen pre-covered Au(332) leading to an increased desorption temperature and a broadening of the methyl formate desorption peak on the high temperature side. Moreover, TPR experiments clearly reveal three different CO_2 desorption signals at 135 K, 185 K and 320 K due to methyl formate oxidation, occurring in particular at low oxygen coverage. In TPR experiments using isotopically labeled ^{18}O, different ratios of CO_2 isotopologues were observed which demonstrates different formation pathways due to different oxygen species with different nucleophilicity (see Figure 4.3): At 135 K, reactive oxygen attacks the carbonyl carbon of methyl formate, assuming a reaction mechanism similar to Ag(110)[122] and Cu(110)[123] (see eq. 4.2). The low reaction temperature points to a small reaction barrier on highly reactive sites. The formed water remains at the surface and desorbs together with water formed in other oxidation processes around 185 K. This renders an analysis of individual contributions of different reaction processes to the amount of formed water difficult and is therefore not further discussed. The oxidation channel at 185 K results solely in the production of

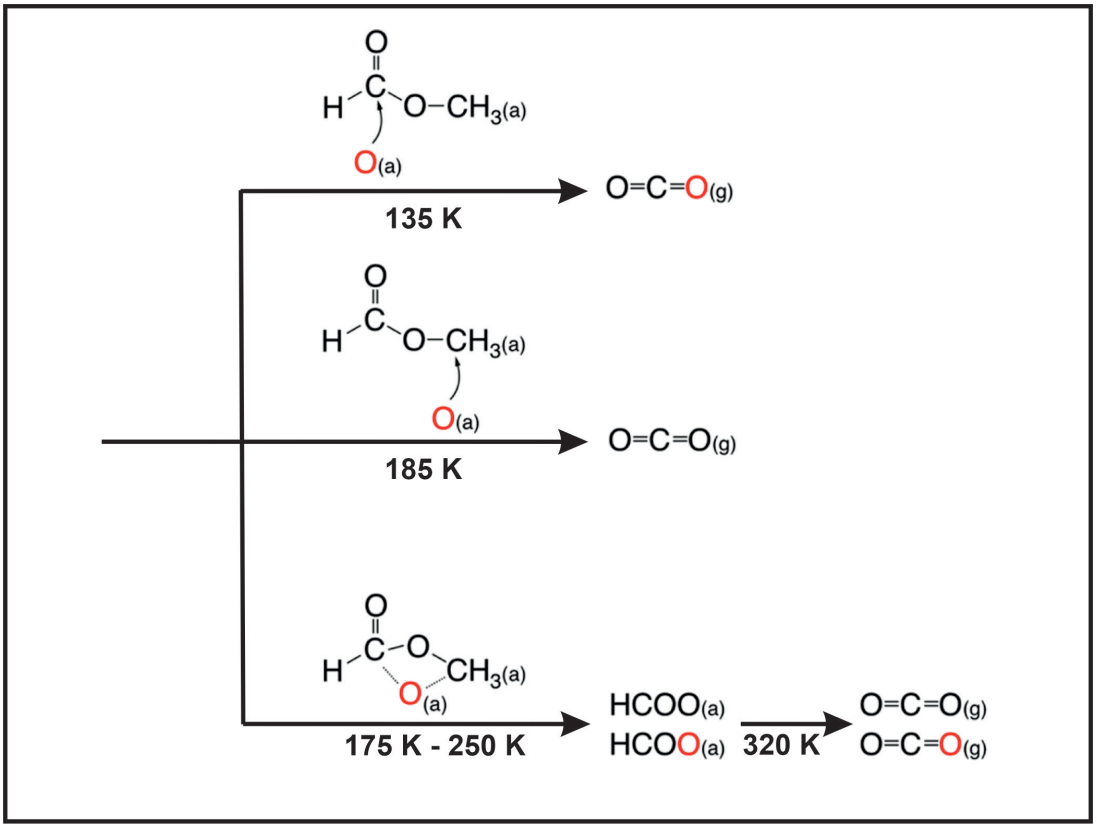

Figure 4.3: Overview on the three methyl formate oxidation channels at 135 K, 185 K and 320 K. The pathways of incorporation of surface oxygen is highlighted by the red O atoms. Adapted from Paper [**IV**], Copyright 2021 American Chemical Society.

$C^{16}O_2$. Assuming a similar reaction mechanism as in eq. 4.2 this can be explained by an attack of oxygen to the methyl carbon presumably resulting in the formation of formate containing both oxygen atoms of the methyl formate, whereas the methoxy species is formed due to the surface ^{18}O. However, both species are not spectroscopically evidenced by IRAS measurements. The formate is further oxidized to CO_2 and water, while not enough information could be obtained to determine the consecutive reactions of the assumed methoxy, where only overoxidation to CO_2 and desorption in form of methanol can be excluded. The oxidation channel at the highest temperature results in the formation of $C^{16}O_2$ and $C^{16}O^{18}O$ in approximately equal amounts, consistent with a cyclic transition state with a similar likelihood for the oxygen to attack the methyl or carbonyl carbon, respectively. Furthermore, IRAS measurements clearly show the formation of a bidentate formate species as reaction intermediate between 175 K and 250 K, which is subsequently overoxidized to CO_2 and water. It should be noted, that the fate of the methoxy species,

expected to be formed according to eq. 4.2 remains unclear. However, a total oxidation of the methoxy can be excluded, as the ratio of the desorbing CO_2 isotopologues is inconsistent with total oxidation of methyl formate. The amount of CO_2 evolution at 320 K is in very reproducible, irrespective of fluctuations in the amount of pre-adsorbed oxygen which points to the formation of formate species on specific sites. Moreover, for an increasing oxygen coverage, the CO_2 desorption at 135 K and 320 K was clearly reduced, consistent with a blocking of the sites involved in those reaction paths (see Paper [**V**]). For the lowest applied oxygen pre-coverage, which is lower than the number of step sites on the Au(332), the highest amount of CO_2 produced by the oxidation of methyl formate was evidenced, which was estimated to be less than 0.01 ML. This corresponds to the formation of approximately one CO_2 molecule per reacted methyl formate, in agreement with its incomplete oxidation. Furthermore, it suggests, that less than 10 % of the pre-covered activated oxygen is consumed by CO_2 formation. These results strongly indicate, that minority species like kink sites are responsible for the formate formation, which are blocked due to the formation of AuO_x phases preferentially along the step edges.[77] The obtained results show, that methyl formate oxidation is feasible on Au(332) already at low temperatures and even at very low oxygen coverages, as they are expected for np-Au catalysts under typical reaction conditions.

To evaluate the kinetic importance of these reaction channels for the methyl formate oxidation under isothermal conditions, pulsed MB experiments were conducted at a surface temperature of 310 K as presented in Paper [**V**]. This temperature is sufficiently high to prevent surface deactivation by formate and similar to those applied during np-Au studies.[31] Here, the $H_2^{18}O$ evolution at 310 K as a result of exposure to methanol an ^{18}O pulses was followed for the oxidation of methyl formate, methanol and a co-feed of methyl formate (MeFo) and methanol (see Figure 4.4). The water formation demonstrates a methyl formate oxidation under isothermal conditions. However, the methyl formate oxidation is slow which is evidenced by a slow transient rate increase during the pulse and significantly ongoing water production after the end of the oxygen pulse (see Fig. 4.4 (a)). In contrast, the methanol oxidation is much faster as indicated by a higher count rate and fast transient kinetics (Fig. 4.4 (b)). In the co-feeding experiment with a large excess of methyl formate as compared to methanol (factor of 30) the water formation kinetic is still dominated by the methanol but methyl formate oxidation clearly contributes to the water formation (Fig. 4.4 (c)). The reaction probability of oxygen towards methyl formate is estimated from these results to be approximately 60 times lower as compared

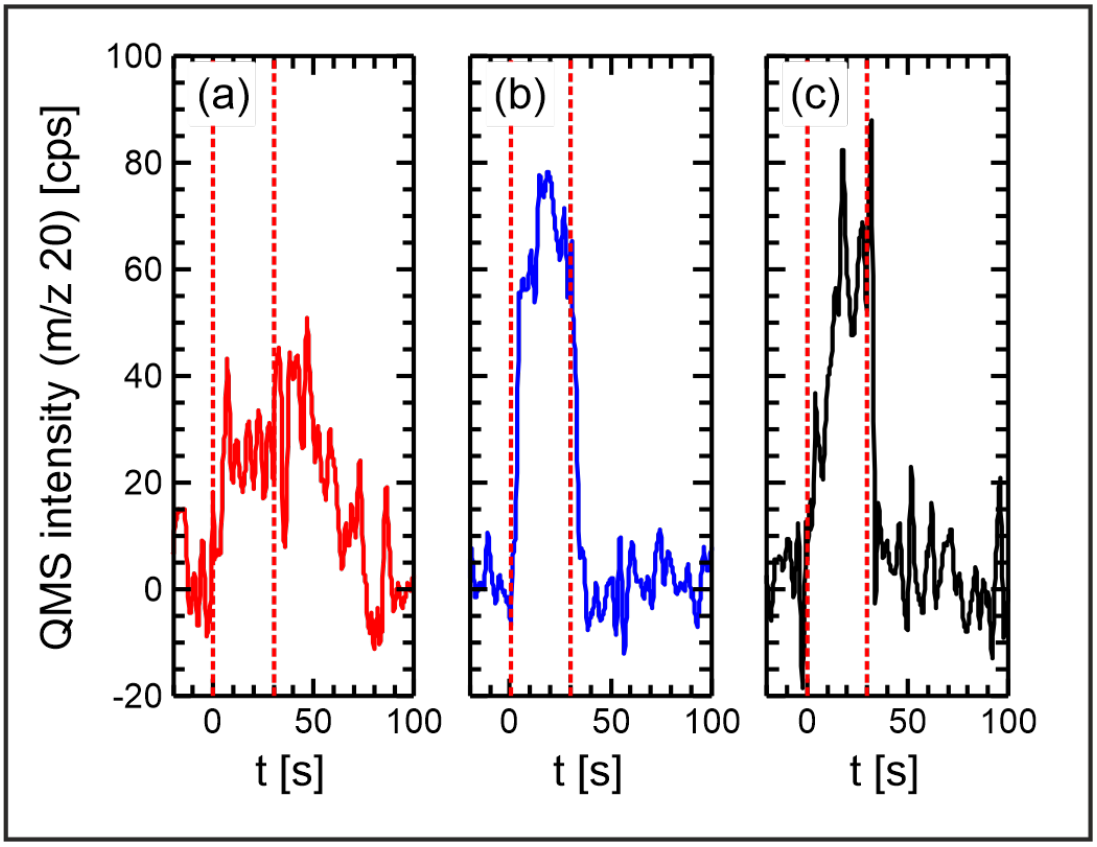

Figure 4.4: $H_2^{18}O$ evolution (m/z = 20) during ^{18}O pulses (30 s on, 100 s off, 31 pulses averaged) for the oxidation of (a) methyl formate (MeFo:O ratio ~1700), (b) methanol (MeOH:O ratio ~60) and (c) a co-feed of methanol and methyl formate at an excess of factor 30 in the gas phase. The figures show the difference of the $H_2^{18}O$ formation rate obtained for exposed Au(332) and a background measurement blocking the Au(332) by the flag. The length of one oxygen pulse is indicated by the red dashed lines. Taken from Paper [**V**].

to the methanol oxidation. This finding cannot be explained by a significantly lower methyl formate surface concentration, since the desorption temperatures of methanol and methyl formate are similar and methyl formate is provided in large excess in the gas phase. Moreover, methyl formate oxidation takes place at specific low coordinated minority sites with low activation barriers on the Au(332). The arriving activated oxygen atoms adsorb statistically at the surface and hence, the initial population of sites highly reactive for methyl formate oxidation is low. However, if methyl formate encounters an oxygen atom on a reactive minority site, fast reaction occurs resulting in the kinetic contribution to water formation in the co-feeding experiment. In contrast, the formation of methoxy and formaldehyde from methanol proceeds with different types of oxygen species on a variety

of surface sites as evidenced by the formation of formate and methoxy during methanol oxidation, respectively (see Paper **[II]** and **[III]**). Hence, the reaction of oxygen with methanol is expected to be favored, explaining the high selectivity of oxygen towards the reaction with methanol. These results are in agreement with the high selectivity in the partial methanol oxidation towards methyl formate on Au(332) and allow for an understanding of the high selectivity in np-Au. On np-Au, a large number of low coordinated sites in combination with low-index surfaces are present. Under usually applied reaction conditions, the concentration of activated oxygen is low and thus, the probability for the abundance of oxygen on sites reactive for the methyl formate oxidation is also low. In consequence, methanol oxidation on np-Au could possibly be conducted even for very high methanol conversions which reveals the potential of np-Au as an ideal partial oxidation catalyst for the selective oxidation of methanol to methyl formate.

In summary, the results have shown the importance of the heterogeneity of oxygen species and adsorption sites for different steps in the reaction network of the (partial) methanol oxidation on Au(332). Hence, the findings provide an improved understanding for processes on np-Au exhibiting also a variety of adsorption sites as well as different oxidic phases under reaction conditions.

5 Conclusions and outlook

In this work, the reactivity of the stepped Au(332) surface used as a model for np-Au catalysts was investigated under well-defined ultrahigh vacuum conditions. Adsorption sites on the Au(332) were probed by IRAS measurements of an isotopically diluted CO mixture containing less than 6 % of ^{12}CO allowing for the observation of the coverage dependent chemical shift without contributions of dipolar coupling. CO on three individual adsorption sites was identified differing significantly in adsorption energy and the lateral interactions between the adsorbed CO molecules, resulting in a non-isotropic chemical shift. Supported by DFT calculations, the observed modes were assigned to adsorption on step and kink sites (highest frequency), 8-fold coordinated sites adjacent to kink sites (intermediate frequency) as well as terrace sites next to fully covered step edges on the Au(332) (lowest frequency). In consequence to prolonged CO exposure at rather high CO pressures, a dynamic restructuring of the Au(332) was observed with depletion of sites with high adsorption energies, in line with literature reports of restructuring on other single crystalline Au surfaces as well as in np-Au. On the Au(332), a decoration of kink sites with small gold particles was concluded, resulting in a lower saturation coverage with CO and a lowering of the CO desorption temperature. Conclusively, a reduced number of low coordinated sites with high adsorption energy is expected to affect the catalytic properties of np-Au.

The partial methanol oxidation to methyl formate on Au(332) investigated by isothermal MB experiments was found to proceed also isothermally under UHV conditions exhibiting a maximum rate at 250 K under the applied single collision conditions. The selectivity of the methyl formate formation was found to overall increase with an increasing MeOH:O ratio, in qualitative agreement with literature. Two different deactivation mechanisms were observed depending on the educt ratio. Under oxygen rich conditions, formaldehyde is overoxidized to formate blocking adsorption sites on the Au(332) surface. This blocking reduces coupling of formaldehyde and methoxy to methyl formate, resulting in a shift of selectivity to the desorption of formaldehyde. Under methanol rich conditions,

the preferential deactivation of highly reactive sites was connected to the exposure of methanol containing small amounts of impurities, which effectively lowers the selectivity to methyl formate. The faster methyl formate formation on a small number of presumably low coordinated sites which are preferentially blocked under methanol rich conditions is further supported by the observation of methoxy species, revealing available surface sites for their formation. Furthermore, the results point to the formation of formate and thus also its precursors methoxy and formaldehyde, which is also feasible with AuO_x phases. In contrast, the oxidative composition of formate and the formation of methyl formate proceeds effectively in the presence of atomic oxygen. This highlights the importance of different oxygen species on Au catalysts for the selectivity of the methanol oxidation.

To study the unwanted oxidation of the partial oxidation product methyl formate, TPR, IRAS and isothermal MB experiments were conducted. Small amounts of activated oxygen change the adsorption geometry and enhance the adsorption strength of methyl formate. TPR studies show, that methyl formate is oxidized in three discernible channels, already at low temperatures pointing to low activation barriers. In experiments using ^{18}O, different ratios of CO_2 isotopologues for the three oxidation channels reveal differences in the underlying CO_2 formation mechanisms, which are all connected to specific oxygen species on minority sites. However, methyl formate is not totally oxidized, indicated by the ratio of the CO_2 isotopologues as well as estimated by the amount of produced CO_2 compared to reacted methyl formate. A bidentate formate species as reaction intermediate was clearly identified for the highest oxidation channel, which is formed on special surface sites, presumably kink sites. Increasing oxygen pre-coverage results in the occupation of these sites and lowers the CO_2 production in the channels at 135 K and 320 K. Under isothermal conditions, the reaction probability of the methyl formate oxidation is around 60 times lower compared to the methanol oxidation. This is attributed to the requirement of oxygen at special, low coordinated sites for the methyl formate oxidation while the activation of methanol proceeds with a variety of oxygen species and also on other sites (*e.g.* terrace sites). In summary, the obtained results in this thesis provide not only a microscopic understanding of the high selectivity of np-Au towards methyl formate, but also demonstrate the importance of the heterogeneity of oxygen species and adsorption sites on Au surfaces for the observed selectivity in oxidation reactions.

While this work enhanced the understanding of oxidation reactions on Au surfaces, a number of questions remain still open, which are beyond the scope of this thesis. To

directly test the role of the low coordinated sites for the selective methanol oxidation as well as the consecutive, unwanted oxidation of methyl formate, the results in this thesis should be compared to experiments conducted on flat model surfaces such as Au(111) or Au(110) which ideally exhibit no low coordinated sites. Furthermore, the influence of other reaction products, in specific, water was not systematically investigated in this thesis. However, first experiments pointed to an engraved deactivation of the methyl formate formation rate due to increasing water concentrations. Moreover, low amounts of residual silver play a central role in the activation of oxygen in np-Au, whereas an increasing amount of silver was found to decrease the selectivity towards methyl formate.[31] Furthermore, methoxy adsorbed on Ag(111) was found to yield formaldehyde in TPR experiments on Ag(111).[124] Therefore, silver should be implemented into the model system by evaporating small amounts of silver onto the Au(332) to test its influence on the reaction, especially on other reaction steps *e.g.* formaldehyde and formate formation.

Bibliography

[1] J. Hagen, *Industrial catalysis : A Practical Approach*, Third edition, Wiley-VCH, Weinheim, Germany, **2015**.

[2] A. Behr, D. W. Agar, J. Jörissen, A. J. Vorholt, *Einführung in die Technische Chemie*, 2. Auflage, Springer Spektrum, Berlin, Heidelberg, **2016**.

[3] J. W. Erisman, M. A. Sutton, J. Galloway, Z. Klimont, W. Winiwarter, How a century of ammonia synthesis changed the world, *Nat. Geosci.* **2008**, *1*, 636–639.

[4] I. I. Cheema, U. Krewer, Operating envelope of Haber–Bosch process design for power-to-ammonia, *RSC Adv.* **2018**, *8*, 34926–34936.

[5] M. Bertau, K. Räuchle, H. Offermanns, Methanol–die Basischemikalie, *Chem. Unserer Zeit* **2015**, *49*, 312–329.

[6] D. Kaiser, L. Beckmann, J. Walter, M. Bertau, Conversion of Green Methanol to Methyl Formate, *Catalysts* **2021**, *11*, 869.

[7] J. C. Védrine, Heterogeneous Catalysis on Metal Oxides, *Catalysts* **2017**, *7*, 341.

[8] L. Zhang, M. Zhou, A. Wang, T. Zhang, Selective Hydrogenation over Supported Metal Catalysts: From Nanoparticles to Single Atoms, *Chem. Rev.* **2020**, *120*, 683–733.

[9] X. Lan, T. Wang, Highly Selective Catalysts for the Hydrogenation of Unsaturated Aldehydes: A Review, *ACS Catal.* **2020**, *10*, 2764–2790.

[10] S. Rood, S. Eslava, A. Manigrasso, C. Bannister, Recent advances in gasoline three-way catalyst formulation: A review, *Proc. IMechE Part D: J. Automobile Engineering* **2020**, *234*, 936–949.

[11] E. Roduner, Understanding catalysis, *Chem. Soc. Rev.* **2014**, *43*, 8226–8239.

[12] K. W. Kolasinski, *Surface science : Foundations of Catalysis and Nanoscience*, John Wiley & Sons, LTD, Chichester, West Sussex, England, **2002**.

[13] B. Hammer, J. K. Nørskov, Why gold is the noblest of all the metals, *Nature* **1995**, *376*, 238–240.

[14] A. F. Holleman, E. Wiberg, N. Wiberg, *Anorganische Chemie. Band 2, Nebengruppenelemente, Lanthanoide, Actinoide, Transactinoide*, 103. Auflage, de Gruyter, Berlin/Boston, **2016**.

[15] P. Jiang, S. Porsgaard, F. Borondics, M. Köber, A. Caballero, H. Bluhm, F. Besenbacher, M. Salmeron, Room-Temperature Reaction of Oxygen with Gold: An In Situ Ambient-Pressure X-ray Photoelectron Spectroscopy Investigation, *J. Am. Chem. Soc.* **2010**, *132*, 2858–2859.

[16] J.-J. Pireaux, M. Chtaïb, J.-P. Delrue, P. Thiry, M. Liehr, R. Caudano, Electron spectroscopic characterization of oxygen adsorption on gold surfaces: I. Substrate impurity effects on molecular oxygen adsorption in ultra high vacuum, *Surf. Sci.* **1984**, *141*, 211–220.

[17] A. G. Sault, R. J. Madix, C. T. Campbell, ADSORPTION OF OXYGEN AND HYDROGEN ON Au(110)-(1x2), *Surf. Sci.* **1986**, *169*, 347–356.

[18] M. Haruta, T. Kobayashi, H. Sano, N. Yamada, Novel Gold Catalysts for the Oxidation of Carbon Monoxide at a Temperature far Below 0 C, *Chem. Lett.* **1987**, *16*, 405–408.

[19] M. Haruta, When Gold Is Not Noble: Catalysis by Nanoparticles, *Chem. Rec.* **2003**, *3*, 75–87.

[20] M. Valden, X. Lai, D. W. Goodman, Onset of Catalytic Activity of Gold Clusters on Titania with the Appearance of Nonmetallic Properties, *Science* **1998**, *281*, 1647–1650.

[21] G. C. Bond, D. T. Thompson, Catalysis by Gold, *Catal. Rev.* **1999**, *41*, 319–388.

[22] R. Meyer, C. Lemire, S. K. Shaikhutdinov, H.-J. Freund, Surface chemistry of catalysis by gold, *Gold Bull.* **2004**, *37*, 72–124.

[23] A. S. Hashmi, G. J. Hutchings, Gold catalysis, *Angew. Chem. Int. Ed.* **2006**, *45*, 7896–936.

[24] A. Villa, N. Dimitratos, C. E. Chan-Thaw, C. Hammond, G. M. Veith, D. Wang, M. Manzoli, L. Prati, G. J. Hutchings, Characterisation of gold catalysts, *Chem. Soc. Rev.* **2016**, *45*, 4953–4994.

[25] M. Sankar, Q. He, R. V. Engel, M. A. Sainna, A. J. Logsdail, A. Roldan, D. J. Willock, N. Agarwal, C. J. Kiely, G. J. Hutchings, Role of the Support in Gold-Containing Nanoparticles as Heterogeneous Catalysts, *Chem. Rev.* **2020**, *120*, 3890–3938.

[26] M. Haruta, Catalysis of Gold Nanoparticles Deposited on Metal Oxides, *Cattech* **2002**, *6*, 102–115.

[27] V. Zielasek, B. Jurgens, C. Schulz, J. Biener, M. M. Biener, A. V. Hamza, M. Bäumer, Gold catalysts: Nanoporous Gold Foams, *Angew. Chem. Int. Ed.* **2006**, *45*, 8241–4.

[28] C. Xu, J. Su, X. Xu, P. Liu, H. Zhao, F. Tian, Y. Ding, Low Temperature CO Oxidation over Unsupported Nanoporous Gold, *J. Am. Chem. Soc.* **2007**, *129*, 42–43.

[29] B. S. Takale, X. Feng, Y. Lu, M. Bao, T. Jin, T. Minato, Y. Yamamoto, Unsupported Nanoporous Gold Catalyst for Chemoselective Hydrogenation Reactions under Low Pressure: Effect of Residual Silver on the Reaction, *J. Am. Chem. Soc.* **2016**, *138*, 10356–64.

[30] A. Wittstock, B. Neumann, A. Schaefer, K. Dumbuya, C. Kübel, M. M. Biener, V. Zielasek, H.-P. Steinrück, J. M. Gottfried, J. Biener, A. Hamza, M. Bäumer, Nanoporous Au: An Unsupported Pure Gold Catalyst? *J. Phys. Chem. C* **2009**, *113*, 5593–5600.

[31] A. Wittstock, V. Zielasek, J. Biener, C. Friend, M. Bäumer, Nanoporous Gold Catalysts for Selective Gas-Phase Oxidative Coupling of Methanol at Low Temperature, *Science* **2010**, *327*, 319–322.

[32] C. H. Christensen, J. K. Nørskov, Green Gold Catalysis, *Science* **2010**, *327*, 278–279.

[33] T. Fujita, P. Guan, K. McKenna, X. Lang, A. Hirata, L. Zhang, T. Tokunaga, S. Arai, Y. Yamamoto, N. Tanaka, et al., Atomic origins of the high catalytic activity of nanoporous gold, *Nat. Mater.* **2012**, *11*, 775–780.

[34] J. Erlebacher, M. J. Aziz, A. Karma, N. Dimitrov, K. Sieradzki, Evolution of nanoporosity in dealloying, *Nature* **2001**, *410*, 450–453.

[35] L. C. Wang, Y. Zhong, D. Widmann, J. Weissmüller, R. J. Behm, On the Role of Residual Ag in Nanoporous Au Catalysts for CO Oxidation: A Combined Microreactor and TAP Reactor Study, *ChemCatChem* **2012**, *4*, 251–259.

[36] L. C. Wang, Y. Zhong, H. Jin, D. Widmann, J. Weissmüller, R. J. Behm, Catalytic activity of nanostructured Au: Scale effects versus bimetallic/bifunctional effects in low-temperature CO oxidation on nanoporous Au, *Beilstein J. Nanotechnol.* **2013**, *4*, 111–28.

[37] S. Parida, D. Kramer, C. A. Volkert, H. Rosner, J. Erlebacher, J. Weissmüller, Volume Change during the Formation of Nanoporous Gold by Dealloying, *Phys. Rev. Lett.* **2006**, *97*, 035504.

[38] W.-L. Yim, T. Nowitzki, M. Necke, H. Schnars, P. Nickut, J. Biener, M. Biener, V. Zielasek, K. Al-Shamery, T. Klüner, M. Bäumer, Universal Phenomena of CO Adsorption on Gold Surfaces with Low-Coordinated Sites, *J. Phys. Chem. C* **2007**, *111*, 445–451.

[39] G. Tomaschun, W. Dononelli, Y. Li, M. Bäumer, T. Klüner, L. V. Moskaleva, Methanol oxidation on the Au(310) surface: A theoretical study, *J. Catal.* **2018**, *364*, 216–227.

[40] A. Hodgson, A. Lewin, A. Nesbitt, Dissociative chemisorption of O_2 on Cu(110), *Surf. Sci.* **1993**, *293*, 211–226.

[41] P. Van Den Hoek, E. Baerends, Chemisorption and dissociation of O_2 on Ag(110), *Surf. Sci. Lett.* **1989**, *221*, L791–L799.

[42] A. Kleyn, D. Butler, A. Raukema, Dynamics of the interaction of O_2 with silver surfaces, *Surf. Sci.* **1996**, *363*, 29–41.

[43] L. V. Moskaleva, S. Röhe, A. Wittstock, V. Zielasek, T. Klüner, K. M. Neyman, M. Bäumer, Silver residues as a possible key to a remarkable oxidative catalytic activity of nanoporous gold, *Phys. Chem. Chem. Phys.* **2011**, *13*, 4529–39.

[44] A. M. Bradshaw, J. Pritchard, Infrared spectra of carbon monoxide chemisorbed on metal films: a comparative study of copper, silver, gold, iron, cobalt and nickel, *Proc. Math. Phys. Eng. Sci.* **1970**, *316*, 169–183.

[45] C. Ruggiero, P. Hollins, Interaction of CO molecules with the Au(332) surface, *Surf. Sci.* **1997**, *377*, 583–586.

[46] J. M. Gottfried, K. J. Schmidt, S. L. M. Schroeder, K. Christmann, Adsorption of carbon monoxide on Au(110)-(1×2), *Surf. Sci.* **2003**, *536*, 206–224.

[47] D. A. Outka, R. J. Madix, Brøensted Basicity of Atomic Oxygen on the Au(110) Surface: Reactions with Methanol, Acetylene, Water, and Ethylene, *J. Am. Chem. Soc.* **1987**, *109*, 1708–1714.

[48] J. Gong, D. W. Flaherty, R. A. Ojifinni, J. M. White, C. B. Mullins, Surface Chemistry of Methanol on Clean and Atomic Oxygen Pre-Covered Au(111), *J. Phys. Chem. C* **2008**, *112*, 5501–5509.

[49] M. A. Lazaga, D. T. Wickham, D. H. Parker, G. N. Kastanas, B. E. Koel, Reactivity of Oxygen Adatoms on the Au(111) Surface, In: Catalytic Selective Oxidation, *ACS Symp. Ser.* **1993**, *523*, 90–109.

[50] D. A. Outka, R. Madix, Acid-base and nucleophilic chemistry of atomic oxygen on the Au(110) surface: Reactions with formic acid and formaldehyde, *Surf. Sci.* **1987**, *179*, 361–376.

[51] W. Dononelli, G. Tomaschun, T. Klüner, L. V. Moskaleva, Understanding Oxygen Activation on Nanoporous Gold, *ACS Catal.* **2019**, *9*, 5204–5216.

[52] Y. Xu, M. Mavrikakis, Adsorption and Dissociation of O_2 on Gold Surfaces: Effect of Steps and Strain, *J. Phys. Chem. B* **2003**, *107*, 9298–9307.

[53] Y. Santiago-Rodriguez, J. A. Herron, M. C. Curet-Arana, M. Mavrikakis, Atomic and molecular adsorption on Au (111), *Surf. Sci.* **2014**, *627*, 57–69.

[54] B. K. Min, A. Alemozafar, D. Pinnaduwage, X. Deng, C. Friend, Efficient CO Oxidation at Low Temperature on Au(111), *J. Phys. Chem. B* **2006**, *110*, 19833–19838.

[55] T. A. Baker, B. Xu, X. Liu, E. Kaxiras, C. M. Friend, Nature of Oxidation of the Au(111) Surface: Experimental and Theoretical Investigation, *J. Phys. Chem. C* **2009**, *113*, 16561–16564.

[56] R. A. Ojifinni, J. Gong, D. W. Flaherty, T. S. Kim, C. B. Mullins, Annealing Effect on Reactivity of Oxygen-Covered Au(111), *J. Phys. Chem. C* **2009**, *113*, 9820–9825.

[57] D. A. Outka, R. Madix, The oxidation of carbon monoxide on the Au(110) surface, *Surf. Sci.* **1987**, *179*, 351–360.

[58] B. Xu, X. Liu, J. Haubrich, R. J. Madix, C. M. Friend, Selectivity Control in Gold-Mediated Esterification of Methanol, *Angew. Chem.* **2009**, *121*, 4270–4273.

[59] B. Xu, C. G. Siler, R. J. Madix, C. M. Friend, Ag/Au Mixed Sites Promote Oxidative Coupling of Methanol on the Alloy Surface, *Chem. Eur. J.* **2014**, *20*, 4646–52.

[60] F. Hiebel, S. Karakalos, Y. Xu, C. M. Friend, R. J. Madix, Structural Differentiation of the Reactivity of Alcohols with Active Oxygen on Au(110), *Top. Catal.* **2018**, *61*, 299–307.

[61] J. Gottfried, N. Elghobashi, S. Schroeder, K. Christmann, Oxidation of gold by oxygen-ion sputtering, *Surf. Sci.* **2003**, *523*, 89–102.

[62] N. Saliba, D. Parker, B. E. Koel, Adsorption of oxygen on Au(111) by exposure to ozone, *Surf. Sci.* **1998**, *410*, 270–282.

[63] B. K. Min, X. Deng, D. Pinnaduwage, R. Schalek, C. Friend, Oxygen-induced restructuring with release of gold atoms from Au(111), *Phys. Rev. B* **2005**, *72*, 121410.

[64] R. J. Moreira Silva, Setup of a Molecular Beam Apparatus to study the reactivity of single crystal surfaces and its application to CO oxidation on Au(332), PhD Thesis, Freie Universität Berlin, **2018**.

[65] J. Wang, M. McEntee, W. Tang, M. Neurock, A. P. Baddorf, P. Maksymovych, J. Yates, J. T., Formation, Migration, and Reactivity of Au-CO Complexes on Gold Surfaces, *J. Am. Chem. Soc.* **2016**, *138*, 1518–26.

[66] J. Kim, E. Samano, B. E. Koel, Oxygen adsorption and oxidation reactions on Au(211) surfaces: Exposures using O_2 at high pressures and ozone (O_3) in UHV, *Surf. Sci.* **2006**, *600*, 4622–4632.

[67] C. Ruggiero, P. Hollins, Adsorption of carbon monoxide on the gold (332) surface, *J. Chem. Soc. Faraday Trans.* **1996**, *92*, 4829–4834.

[68] I. Nakamura, A. Takahashi, T. Fujitani, Selective Dissociation of O_3 and Adsorption of CO on Various Au Single Crystal Surfaces, *Catal. Lett.* **2009**, *129*, 400–403.

[69] C. J. Weststrate, E. Lundgren, J. N. Andersen, E. D. L. Rienks, A. C. Gluhoi, J. W. Bakker, I. M. N. Groot, B. E. Nieuwenhuys, CO adsorption on Au(310) and Au(321): 6-Fold coordinated gold atoms, *Surf. Sci.* **2009**, *603*, 2152–2157.

[70] L. Piccolo, D. Loffreda, F. J. Cadete Santos Aires, C. Deranlot, Y. Jugnet, P. Sautet, J. C. Bertolini, The adsorption of CO on Au(111) at elevated pressures studied by STM, RAIRS and DFT calculations, *Surf. Sci.* **2004**, *566-568*, 995–1000.

[71] J. L. Fajín, M. N. D. Cordeiro, J. R. Gomes, DFT Study of the CO Oxidation on the Au(321) Surface, *J. Phys. Chem. C* **2008**, *112*, 17291–17302.

[72] F. Hoffmann, J. Hrbek, S. Ma, J. Park, J. Rodriguez, D. Stacchiola, S. Senanayake, Enhancing the reactivity of gold: Nanostructured Au(111) adsorbs CO, *Surf. Sci.* **2016**, *650*, 17–23.

[73] J. Hrbek, F. M. Hoffmann, J. B. Park, P. Liu, D. Stacchiola, Y. S. Hoo, S. Ma, A. Nambu, J. A. Rodriguez, M. G. White, Adsorbate-driven morphological changes of a gold surface at low temperatures, *J. Am. Chem. Soc.* **2008**, *130*, 17272–17273.

[74] Y. Jugnet, F. C. S. Aires, C. Deranlot, L. Piccolo, J. Bertolini, CO chemisorption on Au(110) investigated under elevated pressures by polarized reflection absorption infrared spectroscopy and scanning tunneling microscopy, *Surf. Sci.* **2002**, *521*, L639–L644.

[75] N. Kamiuchi, K. Sun, R. Aso, M. Tane, T. Tamaoka, H. Yoshida, S. Takeda, Self-activated surface dynamics in gold catalysts under reaction environments, *Nat. Commun.* **2018**, *9*, 2060.

[76] B. K. Min, A. R. Alemozafar, M. M. Biener, J. Biener, C. M. Friend, Reaction of Au(111) with Sulfur and Oxygen: Scanning Tunneling Microscopic Study, *Top. Catal.* **2005**, *36*, 77–90.

[77] Y. Li, W. Dononelli, R. Moreira, T. Risse, M. Bäumer, T. Klüner, L. V. Moskaleva, Oxygen-Driven Surface Evolution of Nanoporous Gold: Insights from Ab Initio Molecular Dynamics and Auger Electron Spectroscopy, *J.Phys.Chem.C* **2018**, *122*, 5349–5357.

[78] F. Hiebel, M. Montemore, E. Kaxiras, C. M. Friend, Direct visualization of quasi-ordered oxygen chain structures on Au(110)-(1× 2), *Surf. Sci.* **2016**, *650*, 5–10.

[79] B. Zugic, L. Wang, C. Heine, D. N. Zakharov, B. A. J. Lechner, E. A. Stach, J. Biener, M. Salmeron, R. J. Madix, C. M. Friend, Dynamic restructuring drives catalytic activity on nanoporous gold–silver alloy catalysts, *Nat. Mater.* **2017**, *16*, 558–564.

[80] B. Zugic, M. A. van Spronsen, C. Heine, M. M. Montemore, Y. Li, D. N. Zakharov, S. Karakalos, B. A. J. Lechner, E. Crumlin, M. M. Biener, A. I. Frenkel, J. Biener, E. A. Stach, M. B. Salmeron, E. Kaxiras, R. J. Madix, C. M. Friend, Evolution of steady-state material properties during catalysis: Oxidative coupling of methanol over nanoporous $Ag_{0.03}Au_{0.97}$, *J. Catal.* **2019**, *380*, 366–374.

[81] B. K. Min, C. M. Friend, Heterogeneous Gold-Based Catalysis for Green Chemistry: Low-Temperature CO Oxidation and Propene Oxidation, *Chem. Rev.* **2007**, *107*, 2709–2724.

[82] L.-C. Wang, M. L. Personick, S. Karakalos, R. Fushimi, C. M. Friend, R. J. Madix, Active sites for methanol partial oxidation on nanoporous gold catalysts, *J. Catal.* **2016**, *344*, 778–783.

[83] L. C. Wang, C. M. Friend, R. Fushimi, R. J. Madix, Active site densities, oxygen activation and adsorbed reactive oxygen in alcohol activation on npAu catalysts, *Faraday Discuss.* **2016**, *188*, 57–67.

[84] B. Xu, J. Haubrich, T. A. Baker, E. Kaxiras, C. M. Friend, Theoretical Study of O-Assisted Selective Coupling of Methanol on Au(111), *J. Phys. Chem. C* **2011**, *115*, 3703–3708.

[85] S. Liu, P. Jin, D. Zhang, C. Hao, X. Yang, Reaction mechanism for methanol oxidation on Au(111): A density functional theory study, *Appl. Surf. Sci.* **2013**, *265*, 443–451.

[86] M. J. Prieto, E. A. Carbonio, S. Fatayer, R. Landers, A. de Siervo, Electronic and structural study of Pt-modified Au vicinal surfaces: a model system for Pt-Au catalysts, *Phys. Chem. Chem. Phys.* **2014**, *16*, 13329–39.

[87] J. Bénard, *Adsorption on Metal Surfaces : An Integrated Approach*, Elsevier Scientific Pub. Co., Amsterdam, Oxford, New York, **1983**.

[88] I. Chorkendorff, J. W. Niemantsverdriet, *Concepts of Modern Catalysis and Kinetics*, Wiley-VCH, Weinheim, **2003**.

[89] C. Rettner, D. Auerbach, J. Tully, A. Kleyn, Chemical Dynamics at the Gas-Surface Interface, *J. Phys. Chem.* **1996**, *100*, 13021–13033.

[90] A. W. Kleyn, Molecular beams and chemical dynamics at surfaces, *Chem. Soc. Rev.* **2003**, *32*, 87–95.

[91] S. M. Wetterer, D. J. Lavrich, T. Cummings, S. L. Bernasek, G. Scoles, Energetics and Kinetics of the Physisorption of Hydrocarbons on Au(111), *J. Phys. Chem. B* **1998**, *102*, 9266–9275.

[92] I. Toyoshima, G. Somorjai, Heats of Chemisorption of O_2, H_2, CO, CO_2, and N_2 on Polycrystalline and Single Crystal Transition Metal Surfaces, *Catal. Rev. – Sci. Eng.* **1979**, *19*, 105–159.

[93] D. P. Woodruff, *Modern techniques of surface science*, Third edition, Cambridge University Press, Cambridge, **2016**.

[94] G. Ehrlich, F. G. Hudda, Atomic View of Surface Self-Diffusion: Tungsten on Tungsten, *J. Chem. Phys.* **1966**, *44*, 1039–1049.

[95] R. L. Schwoebel, E. J. Shipsey, Step Motion on Crystal Surfaces, *J. Appl. Phys.* **1966**, *37*, 3682–3686.

[96] R. Hoffmann, How Chemistry and Physics Meet in the Solid State, *Angew. Chem. Int. Ed.* **1987**, *26*, 846–878.

[97] G. Wedler, H.-J. Freund, *Lehr- und Arbeitsbuch Physikalische Chemie*, 7. Auflage, John Wiley & Sons, Newark, **2018**.

[98] A. Kitai, *Principles of Solar Cells, LEDs and Diodes: The role of the PN junction*, John Wiley & Sons, **2011**.

[99] B. Li, W. Gao, Q. Jiang, Electronic and geometric determinants of adsorption: fundamentals and applications, *J. Phys. Energy* **2021**, *3*, DOI 10.1088/2515-7655/abd295.

[100] G. Blyholder, Molecular Orbital View of Chemisorbed Carbon Monoxide, *J. Phys. Chem.* **1964**, *68*, 2772–2777.

[101] L. G. M. Pettersson, A. Nilsson, A Molecular Perspective on the d-Band Model: Synergy Between Experiment and Theory, *Top. Catal.* **2013**, *57*, 2–13.

[102] G. Scoles, *Atomic and molecular beam methods. 1*, Oxford University Press Inc., **1988**.

[103] P. Clausing, Über die Strahlformung bei der Molekularströmung, *Z. Phys.* **1930**, *66*, 471–476.

[104] J. Libuda, I. Meusel, J. Hartmann, H.-J. Freund, A molecular beam/surface spectroscopy apparatus for the study of reactions on complex model catalysts, *Rev. Sci. Instrum.* **2000**, *71*, 4395–4408.

[105] P. R. Griffiths, *Fourier transform infrared spectrometry, Peter R. Griffiths, James A. de Haseth.* Second edition, Wiley-Interscience, Hoboken, N.J, **2007**.

[106] J. M. Hollas, *Modern Spectroscopy*, Fourth edition, John Wiley & Sons, Chichester, West Sussex, England, **2004**.

[107] P. Urban, Y.-C. Chen, Y.-S. Wang, *Time-Resolved Mass Spectrometry: From Concept to Applications*, John Wiley & Sons, Inc., Chichester, West Sussex, **2016**.

[108] J. H. Gross, *Massenspektrometrie : Ein Lehrbuch*, Springer Spektrum, Berlin, Heidelberg, **2013**.

[109] A. de Jong, J. Niemantsverdriet, Thermal desorption analysis: Comparative test of ten commonly applied procedures, *Surf. Sci.* **1990**, *233*, 355–365.

[110] D. A. King, Thermal desorption from metal surfaces: A review, *Surf. Sci.* **1975**, *47*, 384–402.

[111] M. A. Van Hove, W. H. Weinberg, C.-M. Chan, *Low-energy electron diffraction : experiment, theory and surface structure determination*, First edition, Springer Verlag, Berlin,Heidelberg, **1986**.

[112] P. Hollins, J. Pritchard, Infrared studies of chemisorbed layers on single crystals, *Prog. Surf. Sci.* **1985**, *19*, 275–349.

[113] D. Woodruff, B. Hayden, K. Prince, A. Bradshaw, Dipole coupling and chemical shifts in IRAS of CO adsorbed on Cu(110), *Surf. Sci.* **1982**, *123*, 397–412.

[114] P. Dumas, R. Tobin, P. Richards, Study of adsorption states and interactions of CO on evaporated noble metal surfaces by infrared absorption spectroscopy: II. Gold and copper, *Surf. Sci.* **1986**, *171*, 579–599.

[115] Website, http://www.detechinc.com/technotes.html, **13.08.2021**.

[116] J. L. Daschbach, B. M. Peden, R. S. Smith, B. D. Kay, Adsorption, desorption, and clustering of H_2O on Pt(111), *J. Chem. Phys.* **2004**, *120*, 1516–23.

[117] P. Redhead, Thermal desorption of gases, *Vacuum* **1962**, *12*, 203–211.

[118] P. Feulner, D. Menzel, Simple ways to improve "flash desorption" measurements from single crystal surfaces, *J. Vac. Sci. Technol.* **1980**, *17*, 662–663.

[119] D. L. Bashlakov, L. B. Juurlink, M. T. Koper, A. I. Yanson, Subsurface Oxygen on Pt(111) and Its Reactivity for CO Oxidation, *Catal. Lett.* **2012**, *142*, 1–6.

[120] P. Norton, J. Davies, T. Jackman, Absolute coverages of CO and O on Pt(111); comparison of saturation CO coverages on Pt(100),(110) and (111) surfaces, *Surf. Sci. Lett.* **1982**, *122*, L593–L600.

[121] K. Mortensen, C. Klink, F. Jensen, F. Besenbacher, I. Stensgaard, Adsorption position of oxygen on the Pt(111) surface, *Surf. Sci. Lett.* **1989**, *220*, L701–L708.

[122] M. Barteau, M. Bowker, R. Madix, Acid-base reactions on solid surfaces: The reactions of HCOOH, H_2CO, and $HCOOCH_3$ with oxygen on Ag(110), *Surf. Sci.* **1980**, *94*, 303–322.

[123] B. Sexton, A. Hughes, N. Avery, A spectroscopic study of the adsorption and reactions of methanol, formaldehyde and methyl formate on clean and oxygenated Cu(110) surfaces, *Surf. Sci.* **1985**, *155*, 366–386.

[124] W. Sim, P. Gardner, D. King, Structure and Reactivity of the Surface Methoxy Species on Ag {111}, *J. Phys. Chem.* **1995**, *99*, 16002–16010.

6 Papers

Paper I

CO Adsorption on Au(332): Combined Infrared Spectroscopy and Density Functional Theory Study

Christoph D. Feldt*, Raphaell Moreira*, Eric Meyer, Peter Clawin, Wiebke Riedel, Thomas Risse, Lyudmila Moskaleva, Wilke Dononelli* and Thorsten Klüner, The Journal of Physical Chemistry C, **2019**, 123, 8187 - 8197. DOI: https://doi.org/10.1021/acs.jpcc.8b08406

*equally contributed

Contributions

I conducted all experiments and evaluated the experimental data. The theoretical calculations were carried out by Wilke Dononelli. The paper was written by Thomas Risse. Wilke Dononelli, Raphaell Moreira and I contributed equally and share the first autohrship.

Page 68 - 87 are not displayed due to copyright protection of the article

Paper II

Methanol oxidation on Au(332): an isothermal pulsed molecular beam study

Christoph D. Feldt, Thorren Gimm, Raphaell Moreira, Wiebke Riedel and Thomas Risse, Physical Chemistry Chemical Physics, **2021**, 23, 21599-21605. DOI: https://doi.org/10.1039/D1CP03436G

Contributions

I conducted all experiments in this work and most of the data evaluation. I analyzed the data and developed the model together with Wiebke Riedel and Thomas Risse. The writing of the paper was coordinated by Wiebke Riedel with contributions by all co-authors.

PCCP

ROYAL SOCIETY OF CHEMISTRY

PAPER

View Article Online
View Journal | View Issue

Cite this: *Phys. Chem. Chem. Phys.*, 2021, **23**, 21599

Methanol oxidation on Au(332): an isothermal pulsed molecular beam study†

Christoph D. Feldt,[a] Thorren Gimm,[ab] Raphaell Moreira,[a] Wiebke Riedel *[a] and Thomas Risse *[a]

Received 27th July 2021,
Accepted 14th September 2021

DOI: 10.1039/d1cp03436g

rsc.li/pccp

Isothermal molecular beam experiments on the methanol oxidation over the stepped Au(332) surface were conducted under well-defined ultra-high vacuum conditions. In the measurements, a continuous flux of methanol at excess in the gas phase and pulses of atomic oxygen were provided to the surface kept at 230 K. The formation of the partial oxidation product methyl formate under the applied conditions was evidenced by time-resolved mass spectrometry, and accumulation of formate species, which resulted in a deactivation of the surface for methyl formate formation, was followed by *in situ* Infrared Reflection Absorption Spectroscopy measurements. The results suggest a different reactivity of oxygen accumulated during the oxygen pulses and atomic oxygen for the competing reaction pathways in the oxidation of methanol to the desired partial and the unwanted overoxidation products.

Introduction

Gold catalysis has received much attention since the first report by Haruta and co-workers.[1–3] In recent years, a renewed interest emerged due to the unusual reactivity of nanoporous gold (np-Au) catalysts:[4–7] While it was reported that only very small Au nanoparticles (<5–7 nm) on oxide supports are catalytically active,[1,2,8,9] np-Au catalysts exhibit a high activity at low temperatures without an oxidic support and despite relatively large ligament sizes. Np-Au is formed by etching a less noble metal from an alloy with Au resulting in the formation of a porous structure. The resulting material contains mostly Au, but also residuals of the less noble metal, most often Ag, and consists of ligaments exhibiting both a number of low-coordinated sites as well as close-packed surfaces.[10] In specific, these np-Au catalysts have shown a high selectivity at high conversion for the partial oxidation of methanol to methyl formate.[6] Residual Ag is suggested to play an important role in the activation of molecular oxygen on these catalysts which is typically the rate limiting step for oxidation reactions on gold.[6,11] While a variety of oxygen species, including also ordered and disordered oxidic phases, with different reactivities have been reported depending on the applied reaction conditions,[12,13] the concentration of activated oxygen under typical reaction conditions is believed to be rather low due to a small number of active sites.[11,14] In methanol oxidation, short contact times were reported to favor formation of formaldehyde over the coupling reaction to methyl formate,[11] while an increase in oxygen or residual Ag content was connected to an enhancement in total oxidation products.[6,11,12,14]

As the microscopic understanding of the processes on these catalysts remains incomplete, a number of studies on simplified model systems, such as Au single crystal surfaces, under well-defined ultra-high vacuum (UHV) conditions have been conducted.[15–17] In agreement with results for np-Au, Temperature Programmed Reaction (TPR) measurements on Au(111) showed an enhanced selectivity to total oxidation for increased oxygen coverages as well as a lower methyl formate production.[15] Moreover, TPR measurements indicated a lowered methanol reactivity in the presence of extended oxidic gold (AuO_x) phases for Au(110).[17] Besides CO_2 and methyl formate, also formaldehyde and formic acid were reported as products, their ratio depending on the applied reaction conditions and surface coverages.[15,16,18,19] Based on TPR measurements, a reaction mechanism for methyl formate formation by partial methanol oxidation in the presence of activated oxygen was proposed proceeding *via* a methoxy intermediate and a subsequent β-elimination to formaldehyde as rate-limiting step.[15,18,20] Moreover, the formation of a dioxymethylene intermediate and formate species, which are formed at temperatures ≤200 K and stable up to at least 255 K, were reported as precursors for total oxidation products as well as for formic acid.[15,18–21] However, the model studies are mainly focused on

[a] *Institut für Chemie und Biochemie, Freie Universität Berlin, Arnimallee 22, 14195 Berlin, Germany. E-mail: wiebke.riedel@fu-berlin.de, risse@chemie.fu-berlin.de*
[b] *Helmholtz-Zentrum Berlin für Materialien und Energie, Hahn-Meitner-Platz 1, 14109 Berlin, Germany*

† Electronic supplementary information (ESI) available: Temperature Programmed Desorption measurements of oxygen from bare and formate precovered Au(332). Methyl formate formation rate as measured in a pulsed isothermal MB experiment with a prolonged pulse sequence. See DOI: 10.1039/d1cp03436g

low-index surfaces and reactivity has been mostly studied by TPR measurements on surfaces pre-covered with activated oxygen species whereas catalytic activity of np-Au was studied under isothermal conditions using molecular oxygen as the oxidizing agent. Residual metals such as Ag or Cu present in np-Au catalysts were shown to play an important role in oxygen activation.[6,11,12,14] In addition, low-coordinated sites present in large number on the ligaments of np-Au are considered to influence the catalytic properties as well, however, experimental evidence for this is scarce.[22,23]

In this study, an Au(332) surface exhibiting densely packed [110]-oriented steps separated by 6 atom wide (111) terraces is used as a model system. Previous structural investigations have shown that the steps may contain kinks depending on the crystal miscut.[24] On this surface, pulsed molecular beam (MB) experiments under well-defined single collision conditions are conducted to investigate the kinetics of the methanol oxidation under isothermal conditions. As gold single crystal surfaces cannot activate molecular oxygen under ultra-high vacuum conditions, pulses of atomic oxygen supplied by a thermal cracker were used to allow for the oxidation reactions. The evolution of the gas phase products is monitored by time-resolved mass spectrometry, and *in situ* Infrared Reflection Absorption Spectroscopy (IRAS) is used for the detection of adsorbed surface species.

Experimental details

All experiments were conducted in an UHV setup consisting of two chambers previously described in detail.[25] One chamber contains a sputter gun (IQE 11/35, SPECS), a low-energy electron diffraction (LEED) system (Omicron MCP LEED), an Auger spectrometer (PHI 11-010, PerkinElmer), and a quadrupole mass spectrometer (QMS, Prisma, Pfeiffer) with a Feulner cup for temperature programmed desorption (TPD) measurements. The second chamber is equipped with two effusive molecular beams[26] and a thermal atomic oxygen source (Dr Eberl MBE-Komponenten GmbH), that can be modulated by automated valves and shutters, as well as with a stagnation flow monitor with a high precision ion gauge (360 Stabil-Ion, Granville-Phillips) to measure the pressure at and its distribution over the sample. A quadrupole mass spectrometer (MAX-500HT, Extrel) is used to monitor the evolution of gas phase species (CH_2O^+ fragment at m/z = 30; H_3COCHO^+ at m/z = 60; CO_2^+ at m/z = 44) over time in the pulsed isothermal molecular beam experiments. For *in situ* IRAS measurements in grazing reflection geometry, an IR spectrometer (IFS 66v, Bruker) is used (256 scans, nominal resolution of 4 cm^{-1}, zero filling factor of 16). The Au(332) single crystal (10 mm diameter, 2 mm thick, Mateck) is mounted by Mo-clamps onto a boron nitride heater (HT-01, Momentive) which is attached to a home-made Mo-holder connected to a liquid nitrogen cooled Cu block allowing for sample cooling down to 100 K. The crystal temperature is measured by a type K thermocouple fixed in a 0.2 mm hole in the edge of the Au crystal. The thermocouple voltage is monitored by a commercial PID controller (3508, Eurotherm) allowing also for control of the sample temperature in TPD and isothermal experiments.

The Au(332) surface was cleaned by repeated cycles of Ar^+ ion sputtering (1000 V, 5–7 μA, 15 min) and subsequent annealing to 1000 K i. vac. for 10 min until no impurities could be detected by Auger spectroscopy and a sharp LEED image as expected for the (332) surface[27] was observed (see Fig. S1, ESI†). Before use, methanol (Roth, ≥99.98%; dried over molecular sieve, 3 Å) and methyl formate (Sigma Aldrich, ≥99.8%) were cleaned by repeated freeze–pump–thaw cycles and applied to the sample surface through an effusive molecular beam. Oxygen (Air Liquide, 99.998%) was used as received. The pressure on the sample as function of the inlet-pressure of the beam was calibrated by a beam monitor at the sample position using Ar gas. Atomic oxygen was supplied by means of a thermal cracker (T = 1615 °C, 12.45 V, 12.60 A). The flux of atomic oxygen was calibrated by TPD measurements in the same UHV apparatus comparing the integrated signal intensities of O_2 desorption from an Au(332) surface with respect to O_2 desorption from Pt(111) after O_2 exposure at 300 K resulting in $p(2 \times 2)$ structure with a coverage of 0.25 ML.[28,29] A saturation coverage of 2.1 ML (1 ML corresponding to 1.4×10^{15} cm^{-2}, thus, to one O atom per Au surface atom) was obtained on the Au(332) surface by exposure to atomic oxygen from the thermal cracker. The QMS signal intensity for methyl formate formation was quantified by calibration measurements with varying methyl formate fluxes dosed into the chamber using a well-defined effusive molecular beam source applying a non-reactive flag at the sample position to ensure comparable scattering conditions.

Results and discussion

Fig. 1 displays the results of a pulsed isothermal molecular beam experiment on the partial oxidation of methanol to methyl formate on the Au(332) surface. The reaction is conducted at 230 K by applying a constant flux of methanol (1.6×10^{-7} mbar, 4.2×10^{13} s^{-1} cm^{-2}) and pulsing (200 s on, 300 s off) atomic oxygen (2.6×10^{-3} ML s^{-1}, 0.4×10^{13} s^{-1} cm^{-2}, approx. 0.5 ML per pulse) onto the surface. In these experiments, the methanol flux onto the surface is about one order of magnitude higher than that of atomic oxygen. The surface temperature of 230 K was chosen above the desorption temperature of methanol, formaldehyde and methyl formate from Au surfaces to allow for gas phase detection and prevent build-up of ice layers, but low compared to temperatures used in np-Au studies to ensure sufficiently long residence times of methanol or formaldehyde to allow for the coupling reaction to methyl formate under the applied single collision conditions. The methyl formate formation rate is followed by time-resolved QMS, while surface adsorbed species are investigated by *in situ* IRAS measurements. It can be seen in Fig. 1a that methyl formate is produced on Au(332) at 230 K under the applied isothermal, single collision conditions. Based on the quantitative calibrations for the oxygen atom flux and the methyl

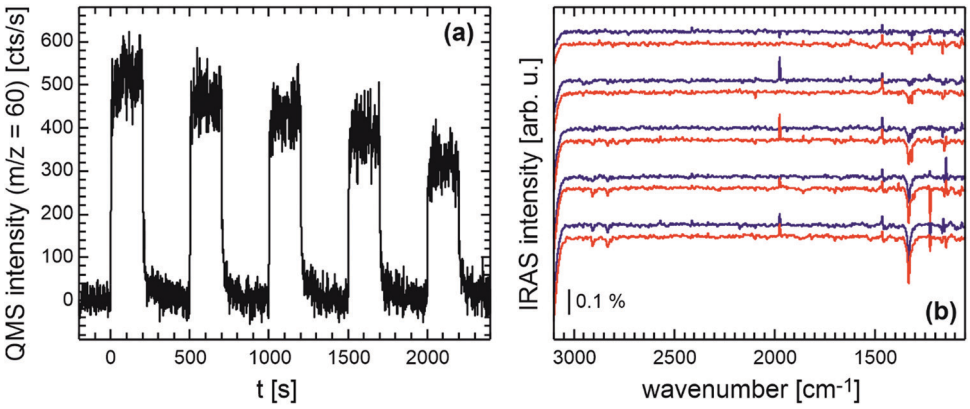

Fig. 1 Pulsed isothermal molecular beam experiment on the methanol oxidation on Au(332) at 230 K: (a) methyl formate formation rate (m/z = 60) and (b) *in situ* IRAS measurements during the oxygen pulse (blue) and in the delay times (red) across the pulse sequence (from top to bottom).

formate formation rate, the initial methyl formate formation rate amounts to approx. 4×10^{11} s^{-1} cm^{-2} corresponding to a selectivity of approx. 20% with respect to the supplied oxygen atoms. Fragmentation signals of methanol and methyl formate hampered the quantification of formaldehyde formation which is expected to compete effectively with the coupling reaction to methyl formate at 230 K under single collision conditions. Similarly, quantification of the total oxidation product CO_2 was hindered by fragmentation signals of methyl formate and also by signals due to background reactions in the chamber. Across the pulse sequence, the methyl formate formation rate decreases roughly linearly indicating a surface deactivation for this reaction. *In situ* IRAS measurements (duration approx. 3 min) were conducted both during the oxygen pulse (start approx. 5–10 s after beginning of the oxygen pulse) and during the delay times (start after approx. 10–20 s after end of the oxygen pulse, when the methyl formate formation rate was roughly decreased to background level). These *in situ* IRAS measurements shown in Fig. 1b demonstrate the appearance of a strong signal centered at 1332 cm^{-1} and weaker signals around 2832 cm^{-1} and 2907 cm^{-1}. The intensity of the peaks grows across the pulse sequence, while their positions remain largely constant and no clear additional peaks occur. While the observed IRAS signals are shifted with respect to signals attributed by Xu *et al.* to formate species on Au(111),[15] the positions are overall comparable to signals reported by Senanayake *et al.* at 1332 cm^{-1}, 2824 cm^{-1} and 2896 cm^{-1} assigned to formate prepared by adsorption of formic acid on O pre-covered Au(111) and attributed to the ν_s(OCO) stretching, ν_aCH and a combination of the ν_s(OCO) and ν_aCH modes of bidentate formate species, respectively.[30] The signals attributed to formate species remain stable on the surface after the pulsed isothermal MB experiment conducted at 230 K, in agreement with previous literature reports for Au surfaces.[15,18,30] Thus, despite the about 10 fold excess of methanol flux, an overoxidation of methanol, as compared to the desired product methyl formate (or formaldehyde), occurs under the applied conditions.

Considering the transient behavior of the methyl formate formation rate in more detail (Fig. 1a), it can be seen that the rate upon oxygen exposure rapidly increases and subsequently approaches a (quasi) steady state value for each oxygen pulse. It should be noted that no clear rate decrease during the pulse duration is detected which may be expected, if the surface deactivates during the pulse *e.g.* due to the formation of formate. After switching off the oxygen supply, the methyl formate formation rate decreases initially very fast and levels back to baseline within about 100 s. For the first pulse, the corresponding amount of methyl formate desorbing during the delay time is about 5% of the amount produced during the pulse. This suggests that a fraction of the deposited oxygen atoms is still present at the end of the oxygen pulse. The methyl formate formation rate for the subsequent oxygen pulse is, however, significantly decreased indicating the progressing deactivation for methyl formate formation to occur rather in the delay time between the oxygen pulses. Concomitantly, the IRAS signal intensity of the formate related peaks (Fig. 1b) is found to increase mostly during the delay times between the oxygen pulses. The increase in formate concentration during the delay times clearly shows that some of the oxygen present at the end of the pulse results in the formation of the unwanted overoxidation product.

The observation of a higher effective formation rate of formate species under rather oxygen-deficient conditions, *i.e.* between oxygen pulses, is unexpected at first glance, as the formation of overoxidation products, such as formate in the absence of an oxygen supply, *i.e.* conditions of low oxygen availability, is counterintuitive. It can be understood assuming that formate is not a spectator species, *i.e.* the formate cannot only be formed but also removed, in particular during the oxygen pulses, which allows their concentration to stay almost constant during the pulse. The increase of the formate concentration in the delay times thus points to a significant reduction of the decomposition channel under rather oxygen-deficient conditions. To verify that formate can be further oxidized already at 230 K during conditions of the oxygen pulses, a formate covered Au(332) surface, as obtained after a pulsed isothermal methanol oxidation experiment discussed above, was exposed to atomic oxygen (same flux without additional

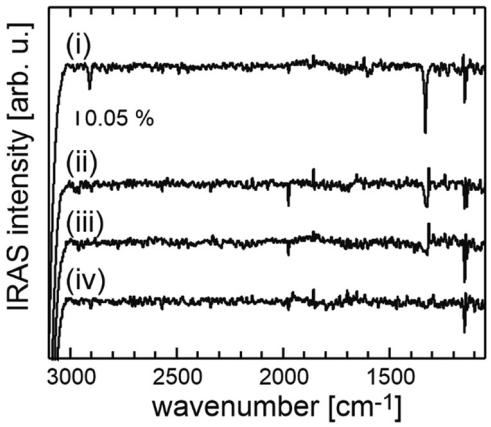

Fig. 2 *In situ* IRAS measurements of a formate pre-covered Au(332) surface obtained after isothermal methanol oxidation experiment (i) directly after formate formation and after exposure with atomic oxygen (0.4×10^{13} s^{-1} cm^{-2}) at 230 K for (ii) 230 s, (iii) 410 s and (iv) 610 s.

methanol exposure) and IRAS measurements were conducted to follow the evolution of the formate signals. The IRAS measurements, displayed in Fig. 2, clearly show that the IRAS intensity of the formate signals (*e.g.* the band around 1332 cm^{-1}) decreases and even vanishes for a prolonged exposure to atomic oxygen. As some of the oxygen is expected to be consumed in the oxidative decomposition of formate, an oxygen TPD (Fig. S2, ESI†) was conducted after the experiment displayed in Fig. 2. Desorption of residual oxygen shows that not all oxygen is consumed by the oxidative decomposition of formate species. However, the amount of desorbing oxygen is lower than expected for a clean Au(332) surface (Fig. S2, ESI†). Moreover, for a formate surface coverage, for which the IRAS signal intensity is saturated, the reduction in oxygen desorption is consistent with an overall high surface coverage of the formate species. A further quantification by monitoring the presumable product CO_2 of the formate decomposition is prevented by fragmentation signals of methyl formate as well as non-negligible background reactions in the chamber.

The analysis of an isothermal experiment with 15 oxygen pulses shows that the formation of formate species as quantified by the IRAS signal intensity of the formate species at 1332 cm^{-1} is clearly correlated with the decrease in the methyl formate formation rate (Fig. 3a, see also Fig. S3, ESI†). After the 10th pulse of the pulse sequence, the methyl formate formation rate levels below 10% of the initial rate and the IRAS intensity saturates. This suggests that the accumulating formate species block surface sites required for the coupling reaction and thereby deactivate the surface for methyl formate formation.

While the methyl formate formation is strongly reduced across the pulse sequence, the surface remains active for other reaction channels as indicated by the evolution of the signal intensity of m/z = 30 (formaldehyde) and m/z = 18 (water) during the pulse sequence (Fig. 3b). Even though a quantification of these products is not possible, the data show a clear increase of the signal intensity of m/z = 30 (red triangles) during the first 6 pulses which exhibits only a slight decrease towards the end of the experiment. This indicates a shift in selectivity from the coupling reaction yielding methyl formate towards desorption of formaldehyde, as the surface becomes covered with formate species. The H_2O formation (m/z = 18, black squares) remains, after an initial drop, constant until the m/z = 30 signal reaches its maximum. Afterwards, the m/z = 18 signal decreases to a constant, but slightly lower intensity for the last pulses in this series.

How to reconcile this behavior? To this end, it is important to recall that partial oxidation of methanol to formaldehyde and methyl formate results in the same amount of water per oxygen atom, while the formation of higher oxidation products such as formate or CO_2 produces less water.

$$2CH_3OH + 2O_{act} \rightarrow H_3COCHO + 2H_2O \quad (R1)$$

$$2CH_3OH + 2O_{act} \rightarrow 2CH_2O + 2H_2O \quad (R2)$$

$$CH_3OH + 3O_{act} \rightarrow CO_2 + 2H_2O \quad (R3)$$

$$2CH_3OH + 5O_{act} \rightarrow 2HCOO + 3H_2O \quad (R4)$$

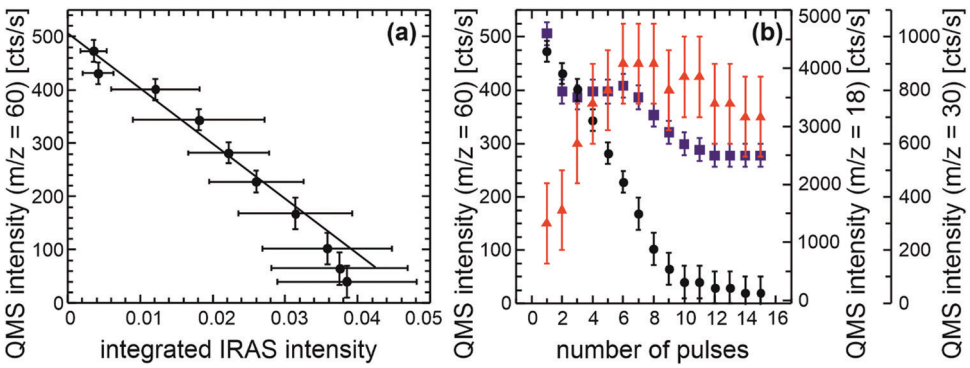

Fig. 3 Results of a pulsed isothermal experiment on the methanol partial oxidation on Au(332) at 230 K using conditions identical to Fig. 1. (a) Methyl formate formation rate (m/z = 60) (see also Fig. S3, ESI†) as function of the integrated IRAS intensity of the formate signal centered at 1332 cm^{-1} obtained from measurements during the first 10 oxygen pulses and (b) intensity of the QMS signals m/z = 60 (black circles), m/z = 18 (blue squares) and m/z = 30 (red triangles) as a function of the number of O pulses.

Thus, the almost constant water formation after the initial drop may result from a compensation of the decreasing methyl formate formation with the increasing formaldehyde production. However, towards the end of the experiment, the water formation drops to a reduced level which is accompanied by a slight reduction of formaldehyde formation. This is consistent with a selectivity shift to overoxidation where the fraction of oxygen that is incorporated into C-containing products, *e.g.* formate, increases, resulting in a decrease of the amount of water that can be produced per oxygen atom. The observation is thus consistent with a formation and subsequent oxidative decomposition of formate during the oxygen pulses (see Fig. 2) which competes with methanol oxidation to methyl formate and formaldehyde under the applied conditions.

While the formal reaction eqn (R1)–(R4) can explain the observed changes of the different reaction products throughout the pulse series, they do not allow to gain insight into the mechanistic reason for this behavior. With respect to this, it is important to consider the activated oxygen species, globally denoted O_{act} in the equations, in more detail.

Xu *et al.* reported TPR experiments of methanol oxidation on O pre-covered Au(111) and observed a decreasing selectivity towards methyl formate formation with increasing oxygen precoverage.[15] This is in line with reports on np-Au showing that in the presence of oxidic phases as *e.g.* prepared by an ozone treatment of the sample exposure to methanol at 150 °C leads to total oxidation,[12,13,32] while partial oxidation to methyl formate or formaldehyde on ozone-treated np-Au is detected rather in the absence of the oxidic phases and in the presence of different "selective" oxygen species.[12] However, a detailed microscopic understanding of the correlation between the different oxygen species (atom, oxygen islands, preferred decoration of step edges, or oxides as indicated by the high saturation coverage *etc.*) and their activity for the different reaction pathways is not yet available.[12,13,17,31–33] The experiments presented above allow to shed some light on this question. To this end Fig. 4 provides a simplified reaction network based on the mechanism proposed in literature also indicating contributions of the different oxygen species to reaction channels.[15,18,20]

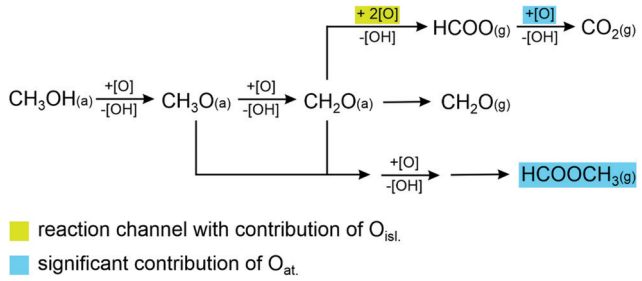

Fig. 4 Simplified reaction network for the partial oxidation of methanol on Au and competing reaction pathways *i.e.* desorption formaldehyde and overoxidation of formaldehyde to formate and subsequently CO_2. Subscript (a) denotes adsorbed species; subscript (g) gas phase products. Methyl formate is highlighted because the importance of oxygen atoms for the kinetics of the different reaction steps is unknown.

We basically observe constant methyl formate formation rates during the oxygen pulse (Fig. 1a) despite the fact that oxygen accumulates on the surface in this period. This strongly suggests that accumulated oxygen does not alter the activity of the surface for this reaction channel during the pulse, *e.g.* by blocking sites for methyl formate formation. In contrast to that, increasing amounts of adsorbed formate species correlate with a decreasing formation rate of methyl formate which points to the fact that adsorbed formate species can block sites active for the coupling reaction to methyl formate. As previously shown, oxygen atoms tend to form AuO_x islands/phases whose reactivity and selectivity depend *e.g.* on the size of the islands,[17,31,34] and is expected to be different than that of atomic oxygen supplied by the thermal cracker. From the results presented here it is possible to deduce that formate cannot only be formed but is also removed during the oxygen pulses presumably by the formation of CO_2 which desorbs at the temperature chosen here. Hence, the final oxidation of formate to CO_2 is at least significantly suppressed in the absence of oxygen atoms, while formate formation is readily possible by AuO_x islands/phases. This is in line with TPR-like experiments in which CO_2 and H_2O desorption due to formate decomposition from Au(111) was reported around 280 K and on Au(110) around 340 K, *i.e.* at higher temperatures, despite the presence of residual oxygen.[15,35] In case the reaction network sketched in Fig. 4 resembles the reaction mechanism, one can conclude that the formation of formaldehyde has to be feasible on AuO_x islands/phases as well, because of the formation of formate in the delay times between the oxygen pulses.[36]

Previously, it has been shown that at least small AuO_x islands/phases (low oxygen coverage) allow to form methyl formate with high selectivity on Au(111). As we accumulate oxygen on the surface and thus increase the number of possible reaction sites on such AuO_x islands/phases, one would expect a change in the methyl formate formation rate in case this reaction channel would contribute considerably to the rate of methyl formate formation. This is not observed in the experiment. This suggests that atomic oxygen species are kinetically more important in the isothermal experiments performed here, however, their precise role for the different reaction steps is not known.

Conclusions

Pulsed isothermal molecular beam experiments were conducted to investigate the partial oxidation of methanol to methyl formate on the stepped Au(332) surface at 230 K. While methyl formate formation was observed under the applied single collision conditions, the formation rate was found to decrease across the pulse sequence due to the build-up of formate species as evidenced by *in situ* IRAS measurements. The concentration of the formate species was found to effectively increase in the delay times between the oxygen pulses, thus, under rather oxygen-deficient conditions during which methyl formate formation is rather limited. The lack of formate

build-up during the pulses is due to a faster oxidative decomposition of formate species occurring even at the low surface temperature of 230 K during the exposure with atomic oxygen *i.e.* under more strongly oxidizing conditions. In contrast to formate species, accumulating oxygen expected to form AuO_x-phases was not found to deactivate the methyl formate formation during the pulses. Hence, its presence does not change the selectivity of the reaction strongly towards total oxidation products, which is in contrast to TPR studies suggesting a strong dependence of the selectivity on the oxygen coverage. These results further suggest a lower reactivity of accumulated oxygen for the methyl formate formation and the oxidative decomposition of formate, while residual oxygen forms formate species effectively. Even though the ability to form methyl formate is rapidly lost under these conditions, the results indicate that the surface remains active for the formation of formaldehyde throughout the sequence, suggesting that the Au surface capability to do partial oxidation of methanol is at least transiently present during the oxygen pulses. However, the local concentration of methoxy species required for a coupling to methyl formate is reduced such that the formaldehyde desorption becomes the dominant channel.

Author contributions

The manuscript was written through contributions of all authors. All authors have given approval to the final version of the manuscript.

Conflicts of interest

The authors declare no competing financial interest.

Acknowledgements

We acknowledge the financial support from the German Research Foundation (DFG) within the framework of research unit 2231 "NAGOCAT" Project No. RI 1025/3-1(2). C. D. F. thanks the International Max-Planck Research School "Functional Interfaces in Physics and Chemistry" for support and the IMPRS for Elementary Processes in Physical Chemistry. R. M. thanks to the DAAD for support (Project No.: 290149/2014-2 DAAD/CNPq).

References

1 M. Haruta, T. Kobayashi, H. Sano and N. Yamada, *Chem. Lett.*, 1987, 405–408.
2 R. Meyer, C. Lemire, S. K. Shaikhutdinov and H. Freund, *Gold Bull.*, 2004, **37**, 72–124.
3 A. S. K. Hashmi and G. J. Hutchings, *Angew. Chem., Int. Ed.*, 2006, **45**, 7896–7936.
4 V. Zielasek, B. Jürgens, C. Schulz, J. Biener, M. M. Biener, A. V. Hamza and M. Bäumer, *Angew. Chem., Int. Ed.*, 2006, **45**, 8241–8244.
5 C. X. Xu, J. X. Su, X. H. Xu, P. P. Liu, H. J. Zhao, F. Tian and Y. Ding, *J. Am. Chem. Soc.*, 2007, **129**, 42–43.
6 A. Wittstock, V. Zielasek, J. Biener, C. M. Friend and M. Bäumer, *Science*, 2010, **327**, 319–322.
7 B. S. Takale, X. J. Feng, Y. Lu, M. Bao, T. A. Jin, T. Minato and Y. Yamamoto, *J. Am. Chem. Soc.*, 2016, **138**, 10356–10364.
8 G. C. Bond, *Catal. Today*, 2002, **72**, 5–9.
9 M. Sankar, Q. He, R. V. Engel, M. A. Sainna, A. J. Logsdail, A. Roldan, D. J. Willock, N. Agarwal, C. J. Kiely and G. J. Hutchings, *Chem. Rev.*, 2020, **120**, 3890–3938.
10 T. Fujita, P. F. Guan, K. McKenna, X. Y. Lang, A. Hirata, L. Zhang, T. Tokunaga, S. Arai, Y. Yamamoto, N. Tanaka, Y. Ishikawa, N. Asao, Y. Yamamoto, J. Erlebacher and M. W. Chen, *Nat. Mater.*, 2012, **11**, 775–780.
11 L. C. Wang, M. L. Personick, S. Karakalos, R. Fushimi, C. M. Friend and R. J. Madix, *J. Catal.*, 2016, **344**, 778–783.
12 B. Zugic, L. C. Wang, C. Heine, D. N. Zakharov, B. A. J. Lechner, E. A. Stach, J. Biener, M. Salmeron, R. J. Madix and C. M. Friend, *Nat. Mater.*, 2017, **16**, 558–564.
13 B. Zugic, M. A. van Spronsen, C. Heine, M. M. Montemore, Y. Y. Li, D. N. Zakharov, S. Karakalos, B. A. J. Lechner, E. Crumlin, M. M. Biener, A. I. Frenkel, J. Biener, E. A. Stach, M. B. Salmeron, E. Kaxiras, R. J. Madix and C. M. Friend, *J. Catal.*, 2019, **380**, 366–374.
14 L. C. Wang, C. M. Friend, R. Fushimi and R. J. Madix, *Faraday Discuss.*, 2016, **188**, 57–67.
15 B. J. Xu, X. Y. Liu, J. Haubrich, R. J. Madix and C. M. Friend, *Angew. Chem., Int. Ed.*, 2009, **48**, 4206–4209.
16 B. J. Xu, C. G. F. Siler, R. J. Madix and C. M. Friend, *Chem. – Eur. J.*, 2014, **20**, 4646–4652.
17 F. Hiebel, S. Karakalos, Y. F. Xu, C. M. Friend and R. J. Madix, *Top. Catal.*, 2018, **61**, 299–307.
18 D. A. Outka and R. J. Madix, *J. Am. Chem. Soc.*, 1987, **109**, 1708–1714.
19 J. Gong, D. W. Flaherty, R. A. Ojifinni, J. M. White and C. B. Mullins, *J. Phys. Chem. C*, 2008, **112**, 5501–5509.
20 B. J. Xu, J. Haubrich, T. A. Baker, E. Kaxiras and C. M. Friend, *J. Phys. Chem. C*, 2011, **115**, 3703–3708.
21 S. P. Liu, P. Jin, D. H. Zhang, C. Hao and X. M. Yang, *Appl. Surf. Sci.*, 2013, **265**, 443–451.
22 W. L. Yim, T. Nowitzki, M. Necke, H. Schnars, P. Nickut, J. Biener, M. M. Biener, V. Zielasek, K. Al-Shamery, T. Klüner and M. Bäumer, *J. Phys. Chem. C*, 2007, **111**, 445–451.
23 G. Tomaschun, W. Dononelli, Y. Li, M. Bäumer, T. Klüner and L. V. Moskaleva, *J. Catal.*, 2018, **364**, 216–227.
24 M. J. Prieto, E. A. Carbonio, S. Fatayer, R. Landers and A. de Siervo, *Phys. Chem. Chem. Phys.*, 2014, **16**, 13329–13339.
25 R. Moreira, PhD thesis, Freie Universtität Berlin, 2018.
26 J. Libuda, I. Meusel, J. Hartmann and H. J. Freund, *Rev. Sci. Instrum.*, 2000, **71**, 4395–4408.
27 M. J. Prieto, E. A. Carbonio, R. Landers and A. de Siervo, *Surf. Sci.*, 2013, **617**, 87–93.
28 K. Mortensen, C. Klink, F. Jensen, F. Besenbacher and I. Stensgaard, *Surf. Sci.*, 1989, **220**, L701–L708.
29 P. R. Norton, J. A. Davies and T. E. Jackman, *Surf. Sci.*, 1982, **122**, L593–L600.

30 S. D. Senanayake, D. Stacchiola, P. Liu, C. B. Mullins, J. Hrbek and J. A. Rodriguez, *J. Phys. Chem. C*, 2009, **113**, 19536–19544.
31 B. K. Min and C. M. Friend, *Chem. Rev.*, 2007, **107**, 2709–2724.
32 M. L. Personick, B. Zugic, M. M. Biener, J. Biener, R. J. Madix and C. M. Friend, *ACS Catal.*, 2015, **5**, 4237–4241.
33 Y. Li, W. Dononelli, R. Moreira, T. Risse, M. Bäumer, T. Klüner and L. V. Moskaleva, *J. Phys. Chem. C*, 2018, **122**, 5349–5357.
34 B. K. Min, A. R. Alemozafar, D. Pinnaduwage, X. Deng and C. M. Friend, *J. Phys. Chem. B*, 2006, **110**, 19833–19838.
35 D. A. Outka and R. J. Madix, *Surf. Sci.*, 1987, **179** 361–376.
36 B. C. Krüger, G. B. Park, S. Meyer, R. J. V. Wagner, A. M. Wodtke and T. Schäfer, *Phys. Chem. Chem. Phys.*, 2017, **19**, 19896–19903.

Supporting Information

Methanol oxidation on Au(332): An isothermal pulsed molecular beam study

Christoph D. Feldt[1], Thorren Gimm[1,2], Raphaell Moreira[1], Wiebke Riedel[1], Thomas Risse[1]

[1]Institut für Chemie und Biochemie, Freie Universität Berlin, Arnimallee 22, 14195 Berlin, Germany

[2]Helmholtz-Zentrum Berlin für Materialien und Energie, Hahn-Meitner-Platz 1, 14109 Berlin, Germany

Corresponding Authors

*E-Mail: risse@chemie.fu-berlin.de; wiebke.riedel@fu-berlin.de

Supplementary Figures

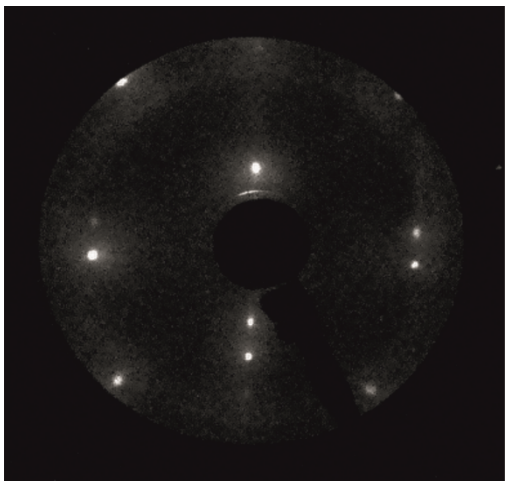

Figure S1. LEED measurement of clean Au(332) surface.

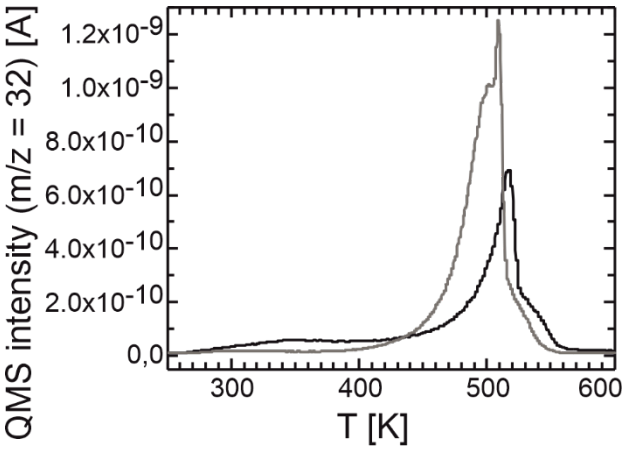

Figure S2. O_2 desorption from Au(332) after exposure to activated oxygen (0.4×10^{13} $s^{-1}cm^{-2}$) for 3000 s of the clean Au(332) surface (grey) corresponding to saturation coverage and for 725 s of the surface covered with formate after a pulsed isothermal methanol oxidation molecular beam experiment (black). Based on a calibration series, which was conducted with a slightly modified experimental setup preventing direct comparison of the absolute intensities, (80-85) % of the saturation coverage are expected to be reached after 700 s of oxygen exposure onto the clean Au(332) surface.

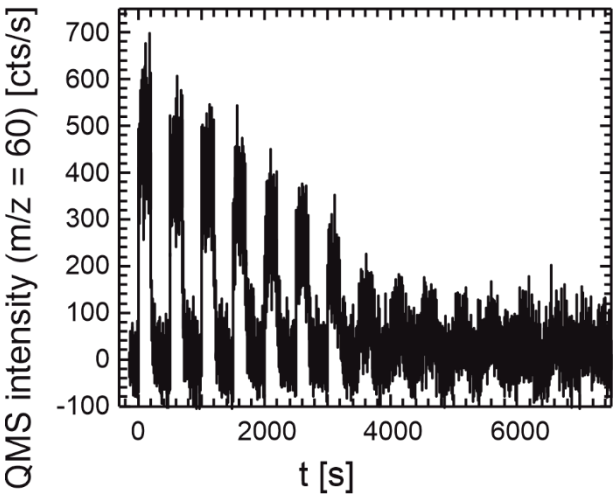

Figure S3. Methyl formate formation rate (m/z = 60) of pulsed, isothermal MB experiment on the methanol oxidation at 230 K on Au(332) for a prolonged pulse sequence (15 pulses) by applying a constant flux of methanol (1.6×10^{-7} mbar, 4.2×10^{13} $s^{-1}cm^{-2}$) and pulsing (200 s on, 300 s off) atomic oxygen (2.6×10^{-3} ML/s, 0.4×10^{13} $s^{-1}cm^{-2}$, approx. 0.5 ML per pulse) onto the surface.

Paper III

Methanol oxidation on Au(332): Methyl formate selectivity and surface deactivation under isothermal conditions

Christoph D. Feldt, Thorren Kirschbaum Jian Liang Low, Wiebke Riedel and Thomas Risse, submitted to Catalysis Science & Technology.

Contributions

I conducted all measurements on the the flux depencence with methanol-^{12}C and for methanol-^{13}C together with Jian Liang Low. Thorren Kirschbaum neé Gimm conducted the measurements on the temperature depencence, which are a part of his bachelor thesis. The scientific model was developed by me, Wiebke Riedel and Thomas Risse. The writing of the paper was coordinated by Wiebke Riedel with contributions by all co-authors.

Methanol oxidation on Au(332): Methyl formate selectivity and surface deactivation under isothermal conditions

Christoph D. Feldt[a], Thorren Kirschbaum[a,b], Jian Liang Low[a], Wiebke Riedel*[,a], Thomas Risse[a]

[a] *Institut für Chemie und Biochemie, Freie Universität Berlin, Arnimallee 22, 14195 Berlin*

[b] *Helmholtz-Zentrum Berlin für Materialien und Energie, Hahn-Meitner-Platz 1, 14109 Berlin, Germany*

* Email: wiebke.riedel@fu-berlin.de

Abstract

Methanol oxidation on the stepped Au(332) surface was investigated by pulsed isothermal molecular beam (MB) experiments. The effect of the surface temperature as well as the influence of changes in the methanol and atomic oxygen flux on the partial oxidation to methyl formate was studied. A maximum in methyl formate formation is observed at 250 K under the applied single collision conditions. Increasing the methanol to oxygen ratio was found to increase the selectivity to methyl formate and decrease unwanted overoxidation to surface deactivating formate detected by in situ infrared reflection absorption spectroscopy (IRAS). The results show evidence for the importance of an additional deactivation mechanism for methyl formate formation connected to methanol which is active under oxygen-deficient conditions at low temperatures. Moreover, the measurements suggest a small number of sites to be highly reactive for methyl formate formation which are preferentially blocked under oxygen-deficient conditions.

Introduction

Gold based catalysts have been the subject of numerous investigations since the first publication by Haruta.[1] The development of nanoporous gold (np-Au) renewed the interest, as these fully metallic catalysts also exhibit high activity in oxidation reactions[2-5] despite the lack of an oxidic support and ligament sizes being about an order of magnitude larger than the size of supported Au nanoparticles of active supported gold catalysts.[1, 6-7] Np-Au catalysts are typically obtained by etching the less noble metal, such as silver or copper, from an alloy with gold. The resulting material has a porous structure and contains mainly gold, but also residuals of the less noble metal. This residual metal plays an important role in the activation of molecular oxygen, which is the rate limiting step for aerobic oxidation catalysis.[2, 8-11] In the partial oxidation of methanol, np-Au shows high selectivity to methyl formate at high conversion.[2] Reduced contact times, however, enhance formaldehyde formation,[11] while increased oxygen or Ag contents favor total

oxidation.[2, 11-13] Moreover, the selectivity is affected by the presence of different oxygen species, including oxidic phases.[12, 14] Under typical reaction conditions, however, the oxygen surface concentration is assumed to be rather low.[11, 13] Recently, also carbonaceous deposits, presumably located on residual Ag, were reported for non-steady state conditions at low temperatures.[14]

To gain more insights into the underlying microscopic mechanisms, model studies on single crystal surfaces under well-defined ultra-high vacuum (UHV) conditions as well as theoretical investigations have been conducted. Based on Temperature Programmed Reaction (TPR) studies with Au surfaces pre-covered with activated oxygen, a reaction mechanism has been proposed:[15-17] Initially formed methoxy species yield formaldehyde upon hydrogen abstraction, which is the rate limiting step in the formation of methyl formate in case activated oxygen is present. The formally abstracted hydrogen may leave the gold surface as water or methanol, while formaldehyde may either desorb, react with methoxy and oxygen to methyl formate or gets further oxidized finally yielding the total oxidation product CO_2. In agreement with studies on np-Au,[2-3] an increased oxygen pre-coverage was reported to enhance total oxidation in TPR measurements.[15, 18-19] Similarly, kinetic modelling suggested reduced methanol to oxygen ratios to favor total oxidation, while lowering the oxygen pressure (at rather high methanol to oxygen pressure ratios) in np-Au catalysts is predicted to enhance formaldehyde formation.[20-21]

The TPR investigations have mainly been conducted on low-index surfaces, while np-Au catalysts contain a significant number of low-coordinated Au sites which presumably alter the reactivity.[22-24] Moreover, Au surfaces pre-covered with activated oxygen exhibit even at low coverage oxygen islands or oxidic phases next to oxygen atoms and thus, at least locally high oxygen concentrations.[19] Recent pulsed isothermal molecular beam experiments using an atomic oxygen beam provided by a thermal cracker suggested a different reactivity of AuO_x phases, i.e. accumulated, residual oxygen, as compared to atomic oxygen provided during the oxygen pulses.[25] Formate species formed in the presence of AuO_x phases were found to poison the stepped Au(332) surface with respect to the formation of methyl formate.[25] Furthermore, methoxy and formaldehyde formation occur in the presence of AuO_x phases, while methyl formate formation as well as (oxidative) decomposition of formate species proceed preferentially in the presence of atomic oxygen.

In this study, the influence of the surface temperature as well as the oxygen and methanol fluxes on the (partial) oxidation of methanol is investigated by pulsed isothermal MB experiments using the stepped Au(332) surface as a model system for np-Au. In particular, the effects of

rather oxygen-deficient conditions and increased surface temperature on the undesired surface deactivation are examined, in addition to their influence on the (initial) selectivity to methyl formate.

Experimental Details

The measurements were performed in a UHV setup with two chambers that has been described before.[26] One chamber is equipped with a sputter gun (IQE 11/35, SPECS), a low-energy electron diffraction (LEED) system (Omicron MCP LEED), an Auger spectrometer (PHI 11–010, Perkin Elmer), and a quadrupole mass spectrometer (Prisma, Pfeiffer) for temperature programmed desorption (TPD) measurements using a Feulner cup to enhance the sensitivity. In the second chamber, two effusive molecular beams[27] and a thermal atomic oxygen source (Dr. Eberl MBE-Komponenten GmbH) being operated as an effusive beam are installed that can be modulated by automated valves and shutters. A stagnation flow monitor with a high precision ion gauge (360 Stabil-Ion, Granville-Phillips) is used to measure the pressure at the sample position. During pulsed isothermal MB experiments gas phase species are detected by a quadrupole mass spectrometer (MAX–500HT, Extrel), while surface adsorbates are monitored by in situ IRAS measurements in grazing reflection geometry employing an IR spectrometer (IFS 66v, Bruker, 256 scans, nominal resolution of 4 cm^{-1}, zero filling factor of 16). Using Mo clamps, the Au(332) single crystal (10 mm diameter, 2 mm thick, Mateck) is pressed onto a boron nitride heater (HT–01, Momentive) mounted to a home-made Mo-holder which is connected to a liquid nitrogen cooled Cu bock allowing for sample cooling down to approx. 100 K. The crystal temperature is measured applying a Type K thermocouple inserted in a 0.2 mm hole in the Au crystal edge. A commercial PID controller (3508, Eurotherm) is used to monitor the thermocouple voltage and to control the sample temperature in TPD and isothermal experiments.

Repeated cycles of Ar^+ ion sputtering (1000 V, 7-10 μA, 15 min) and subsequent annealing to 1000 K i. vac. for 10 min were employed to clean the Au(332) surface until a sharp LEED image expected for the (332) surface was observed.[25, 28] Methanol (Roth, ≥99.98 % or ^{13}C-methanol, 99 atom % ^{13}C, Sigma Aldrich; both dried over molecular sieve 3 Å) and methyl formate (Sigma Aldrich, ≥ 99.8 %) were further purified by repeated freeze-pump-thaw cycles and dosed onto the sample surface by an effusive molecular beam. Oxygen (Air Liquide, 99.998 %) was used as received. For removal of carbonyl species from the CO (Linde, 99.997 %) feed, a liquid nitrogen cryo-trap was used. By a beam monitor, the pressure at the sample position was calibrated as function of the inlet pressure of the beam using Ar gas. A thermal cracker (T

= 1615 °C, 12.45 V, 12.60 A and for some experiments shown in SI 1700 °C, 15.8 V, 13.85 A) was employed to provide atomic oxygen. TPD measurements were conducted to calibrate the flux of atomic oxygen comparing the integrated signal intensities for O_2 desorption from an Au(332) surface with respect to O_2 desorption from a Pt(111) surface after O_2 exposure at 300 K resulting in a p(2x2) structure with a coverage of 0.25 monolayer (ML).[29-30] The saturation coverage of oxygen on Au(332) achieved by exposure to atomic oxygen from the thermal cracker was 2.1 ML (1 ML corresponding to 1.4×10^{15} cm^{-2}, thus, to one O atom per Au surface atom). Calibration measurements with varying fluxes of methyl formate provided by a well-defined effusive molecular beam source were conducted to quantify the QMS signal intensity for methyl formate formation applying a non-reactive flag at the sample position to ensure comparable scattering conditions. Reference measurements with a well-defined flux of methanol provided by an effusive molecular beam source were conducted after each experiment to calibrate the measured QMS intensity. Moreover, pulsed MB experiments were repeated to ensure the reproducibility of the results.

Results and Discussion

Figure 1 shows results of pulsed isothermal molecular beam experiments of the partial methanol oxidation on Au(332) as a function of the surface temperature. In these experiments, a continuous flux of methanol (52.7×10^{13} $s^{-1}cm^{-2}$, p(MeOH) =19.6×10^{-7} mbar) was dosed onto the surface, while a flux of atomic oxygen (2.6×10^{-3} ML/s ≈ 0.4×10^{13} $s^{-1}cm^{-2}$) provided by a thermal cracker was pulsed onto the surface (5 pulses, 200 s on, 600 s off). In Figure 1a, the initial methyl formate formation rates are displayed relative to the maximum rate observed in this series for temperatures ranging between 220 K and 300 K. While the effective methyl formate formation rate increases when the temperature is raised from 220 K to 250 K, it decreases for higher temperatures. For a surface temperature of 300 K, the methyl formate formation essentially vanishes under the applied conditions. This temperature dependence can be understood considering that an increased surface temperature not only results in a faster coupling reaction to methyl formate, but also accelerates the desorption of molecular species, such as methanol and formaldehyde, essentially removing them from the reaction network under the applied single collision conditions. As formaldehyde needs to couple to surface bound methoxy to yield methyl formate according to the proposed mechanism[15-17] schematically depicted in Figure 2, a reduced residence time at elevated temperature will eventually tip the balance away from the coupling reaction to methyl formate towards formaldehyde desorption.

It should be noted that the position of the rate maximum is expected to depend on the applied fluxes, shifting to higher temperatures for a higher flux, and thus pressure, on the surface.

In a previous study, the methyl formate formation rate was found to decrease across the pulse sequence as formate species accumulate on the surface.[25] It can be speculated that an increase in surface temperature may prevent such a surface deactivation process by accelerating the (oxidative) decomposition of the formate species and thereby freeing up the surface sites. However, it can be seen from Figure 1b that the methyl formate formation rate decreases for all studied surface temperatures across the pulse sequence. The decrease in rate relative to the first pulse is overall similar for temperatures between 220 K and 280 K and clearly does not diminish at higher temperatures. In fact, it appears to be even slightly stronger for the highest surface temperature of 280 K. This is consistent with an enhanced formation of formate at 280 K, as the increased diffusion rate and the reduced transient concentration of molecules is expected to foster the formation of AuO_x phases at the expense of the transient concentration of atomic oxygen. The AuO_x phases are known to favor the formation of formate, while atomic oxygen is beneficial for methyl formate formation and also shown to be active in total oxidation of formate.[25] Thus, it is clear that the deactivation of the Au(332) surface is not lifted under the applied conditions by an increased surface temperature, before methyl formate formation ceases.

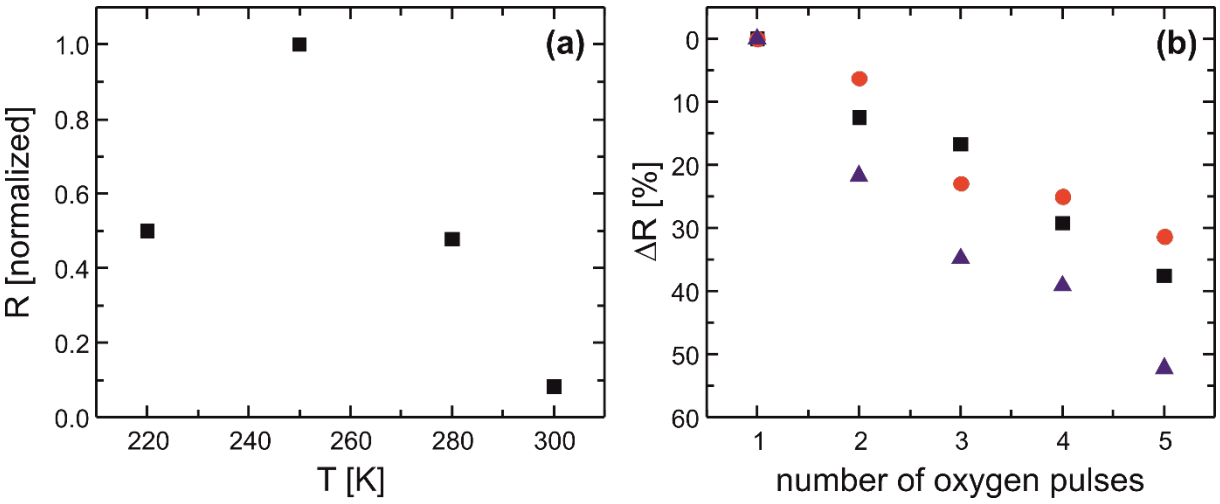

Figure 1 Results of pulsed isothermal MB experiments on methanol oxidation to methyl formate on Au(332) for varying sample temperatures applying a constant flux of methanol (52.7×10^{13} $s^{-1}cm^{-2}$, p(MeOH) $=19.6\times10^{-7}$ mbar) and pulsing (200 s on, 600 s off) atomic oxygen (2.6×10^{-3} ML/s $\approx 0.4\times10^{13}$ $s^{-1}cm^{-2}$). (a) Initial methyl formate formation rates R normalized to the maximum rate detected in this series as a function of the surface temperature. (b) Relative decrease in methyl formate formation rate ΔR across the pulse sequence for different surface temperatures given relative to the initial rate obtained for the respective surface temperature: 220 K (black squares), 250 K (red circles), 280 K (blue triangles).

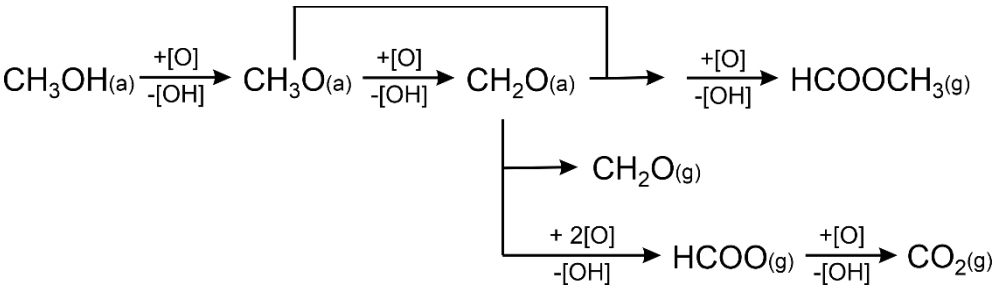

Figure 2 Schematic depiction of reaction mechanism for methanol oxidation on gold as previously proposed.[15-17]

The flux dependence of the methanol oxidation to methyl formate on Au(332) was studied by pulsed isothermal MB experiments at 230 K (Figure 3). In these experiments, atomic oxygen was similarly pulsed (200 s on, 300 s off), while methanol was supplied continuously in excess in the gas phase. Experiments were conducted with a rather high oxygen atom flux (0.4×10^{13} $s^{-1}cm^{-2}$, 2.6×10^{-3} ML/s, approx. 0.5 ML per pulse, Figures 3a and 3b) and with a significantly lower oxygen atom flux (0.08×10^{13} $s^{-1}cm^{-2}$, 0.6×10^{-3} ML/s, approx. 0.12 ML per pulse, Figures 3c and 3d). For each set of oxygen fluxes, measurements with a high (52.7×10^{13} $s^{-1}cm^{-2}$, 19.6×10^{-7} mbar, Figures 3b and 3d) and a low methanol flux (4.3×10^{13} $s^{-1}cm^{-2}$, 1.6×10^{-7} mbar, Figures 3a and 3c) were performed (see also Table 1 for details). Upon increasing the oxygen flux, the initial methyl formate formation rate at the beginning of the pulse sequence increases for both the lower and the higher methanol flux (see also Table 1). This is qualitatively in agreement with the expectation that methyl formate formation is limited by the availability of activated oxygen. However, the increase in the rate of methyl formate formation is considerably lower than the five-fold increase of oxygen flux, a direct consequence of the complex reaction network with competing reaction paths. When increasing the methanol flux, the initial methyl formate formation rate also increases, at least slightly, for both low and high oxygen fluxes, despite the applied excess of methanol flux (factor of ≥10, see also Table 1). To this end, it is important to note that oxygen does not desorb from Au(332) at 230 K,[25] while there is no stable methanol adsorption on gold at 230 K (methanol desorption temperature: 155 K on Au(111),[31] 200 K on clean Au(110),[16] 220 K on 0.2 ML O pre-covered Au(111)[15]). Hence, the methanol to oxygen ratio on the surface is significantly reduced as compared to the gas phase. It should be noted that the increase of the initial rate for high methanol and high oxygen fluxes is less pronounced than for the lower fluxes. In all measurements of this series, the methyl formate formation rate decreases across the pulse sequence. The rate reduction at the end of the pulse sequence relative to the initial rate is overall very similar (approx. 40 %) for the different applied

conditions, except for the measurement with a low oxygen and a relatively low methanol flux (Figure 3c) where the relative rate decrease is smaller (approx. 10 %). For the high oxygen fluxes used here, the rate decrease across the pulse sequence was previously found to be correlated to the accumulation of formate species blocking the active surface sites for methyl formate formation.[25]

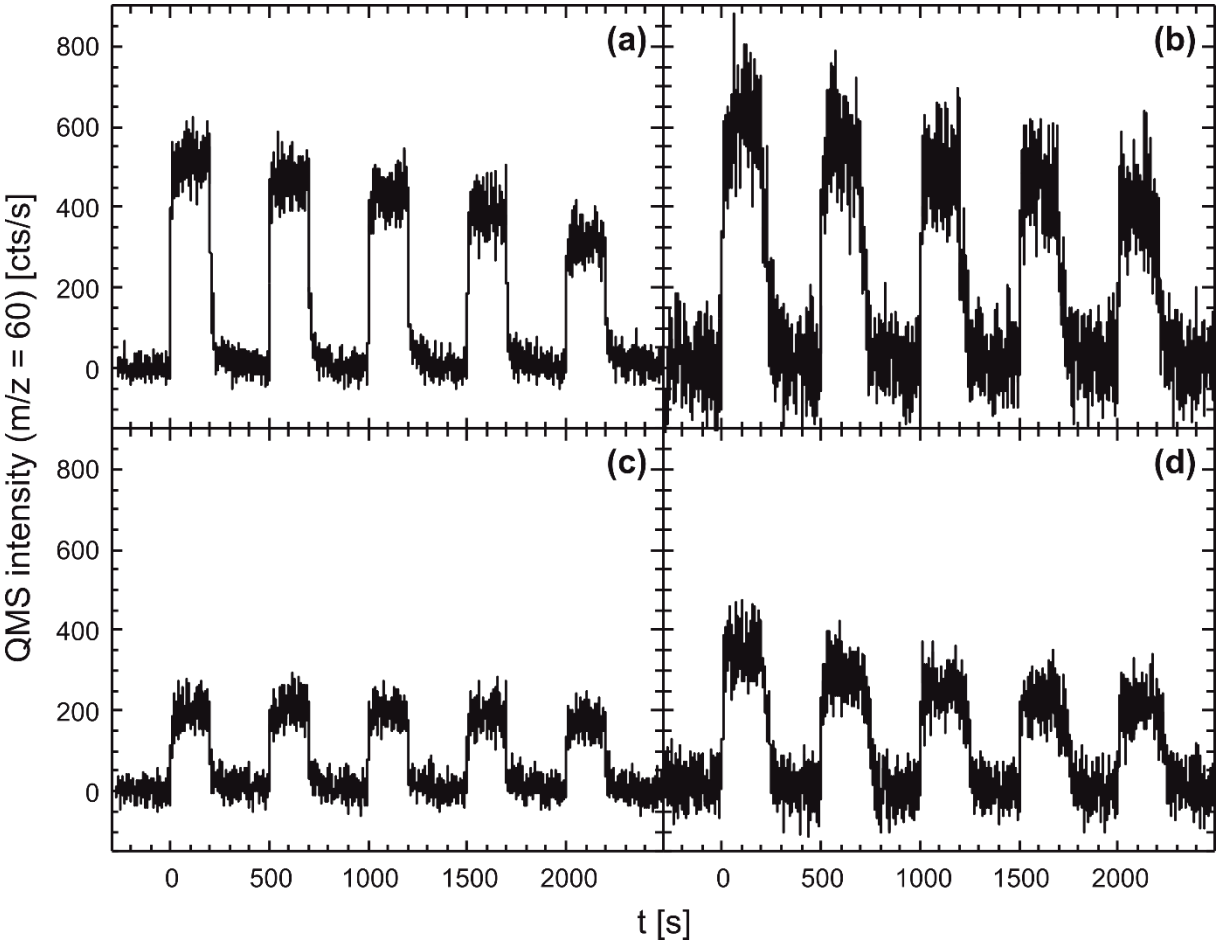

Figure 3 Pulsed isothermal MB experiments of the partial methanol oxidation on Au(332) to methyl formate (molecular peak: m/z = 60) at 230 K under a continuous methanol flux, while applying pulses of atomic oxygen (200 s, delay 300 s). An atomic oxygen flux of 2.6×10^{-3} ML/s $\simeq 0.4\times10^{13}$ $s^{-1}cm^{-2}$ is applied in (a) and (b), while in (c) and (d) a flux of 0.6×10^{-3} ML/s $\approx 0.08\times10^{13}$ $s^{-1}cm^{-2}$ was used. The methanol flux applied in (a) and (c) was 4.3×10^{13} $s^{-1}cm^{-2}$ (p(MeOH) = 1.6×10^{-7} mbar), while in (b) and (d) a methanol flux of 52.7×10^{13} $s^{-1}cm^{-2}$ (p(MeOH) =19.6×10^{-7} mbar) was used.

In situ IRAS measurements conducted during the oxygen pulse as well as during the delay times of the pulsed isothermal MB experiments are displayed in Figure 4. For the measurement with the low methanol and the high oxygen flux (Figure 4a), a strong signal around 1332 cm^{-1} as well as weaker signals around 2832 cm^{-1} and 2907 cm^{-1} are clearly detectable which were assigned to the ν_s(OCO) stretching, ν_aCH and a combination of the ν_s(OCO) and ν_aCH modes of bidentate formate species based on results by Senanayake et al. for Au(111).[25, 32] As

previously reported,[25] the formate intensity effectively increases mainly during the delay times between the oxygen pulses, demonstrating the accumulation of residual oxygen during the pulse for the measurement with a high oxygen and a low methanol flux. The nearly constant intensity during the oxygen pulses was explained by an increased (oxidative) decomposition of formate due to a higher concentration of (atomic) oxygen.[25] These formate signals exhibit a lower intensity, when a lower oxygen flux (Figures 4c and 4d) or higher methanol flux (Figures 4b and 4d) is applied. For the experiment with the combination of a high methanol and a low oxygen flux (Figure 4d), the signals are basically absent. These observations agree with the expectation that overoxidation to formate, as compared to methyl formate formation, should be reduced for lower oxygen contents (relative to methanol).

Table 1. Atomic oxygen flux f(O), methanol flux f(CH_3OH), their gas phase ratio f(CH_3OH):f(O) for the pulsed isothermal MB experiments on the methanol oxidation at 230 K on Au(332) (Figures 3 and 4) as well as the initial methyl formate formation rate v_0(MF).

	f(O) [10^{13} s^{-1} cm^{-2}]	**f(CH_3OH) [10^{13} s^{-1} cm^{-2}]**	**approx. flux ratio f(CH_3OH):f(O)**	**approx. v_0(MF) [10^{11} s^{-1} cm^{-2}]**
a	0.4	4.3	10	4
b	0.4	52.7	130	4.8
c	0.08	4.3	55	1.6
d	0.08	52.7	660	2.8

In the measurements with a high methanol flux, additional broad signals around 2948 cm^{-1}, 2918 cm^{-1}, 2816 cm^{-1} and a sharper one around 1015 cm^{-1} are observed during the oxygen pulse, while being absent in the delay times. The intensity of these species is somewhat lower for the experiment with a low oxygen flux (Figure 4d) as compared to the experiment with a high oxygen flux (Figure 4b). These results point to the presence of methoxy species, which is corroborated by the good agreement with the value reported for the $\nu_{C\text{-}O}$ mode of methoxy in EELS measurements on Cu(110) with the signal around 1015 cm^{-1}.[33] The signal of the $\nu_{C\text{-}O}$ mode is, however, red-shifted compared to previous HREELS results for Au(111) displaying at 160 K a signal at 1060 cm^{-1}.[15] Yet, it should be noted that these HREELS measurements exhibit a signal at 1020 cm^{-1} for a surface temperature of 225 K which is in fair agreement with the position observed here for Au(332). The signals around 2948 cm^{-1}, 2918 cm^{-1} and 2816 cm^{-1} can be assigned to C-H stretching modes of methoxy. While the C-H stretching signals differ in shape and are red-shifted as compared to previous reports for HREEL spectra on Au(111),[15] ^{13}C-methanol adsorbed at low temperature on clean Au(332) yielded IRAS signals in the C-H stretching region which are similar in shape, but are shifted (Figure S1). A signal shift is expected (at least) due to the use of a different isotopologue of methanol, the spectral shape of

the C-H stretching region, however, is expected to be similar for methanol and methoxy supporting the assignment to methoxy. Across the pulse sequence, the intensity of these methoxy signals during the oxygen pulse decreases for the measurement with a high methanol and a high oxygen flux, while the signal intensity of formate related lines increases (Figure 4b) which is consistent with a poisoning of adsorption sites for methoxy by formate species. For the experiment with a low oxygen flux (and a high methanol flux, Figure 4d) where no clear formate accumulation is detected, in contrast, the intensity of the methoxy signals appears to even increase at the beginning of the pulse sequence, exhibiting only a slight intensity decrease towards the end of the pulse sequence.

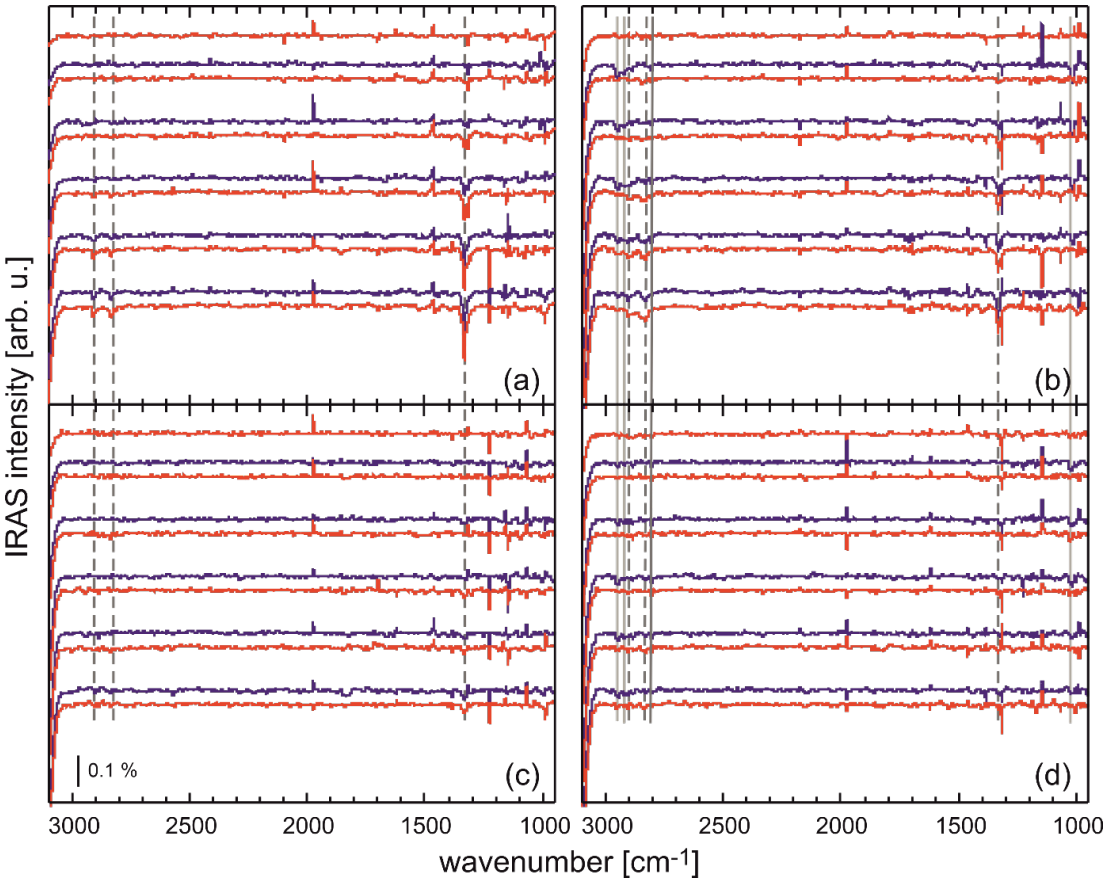

Figure 4 In situ IRAS measurements conducted during the pulsed isothermal MB experiments of the methanol oxidation on Au(332) at 230 K (see also Figure 3) under a continuous methanol flow, while applying pulses of atomic oxygen (200 s, delay 300 s). An atomic oxygen flux of 2.6×10^{-3} ML/s ≈ 0.4×10^{13} $s^{-1}cm^{-2}$ is applied in (a) and (b), while in (c) and (d) a flux of 0.6×10^{-3} ML/s ≈ 0.08×10^{13} $s^{-1}cm^{-2}$ was used. The methanol flux applied in (a) and (c) was 4.3×10^{13} $s^{-1}cm^{-2}$ (p(MeOH) = 1.6×10^{-7} mbar), while in (b) and (d) a methanol flux of 52.7×10^{13} $s^{-1}cm^{-2}$ (p(MeOH) =19.6×10^{-7} mbar) was used. IRAS measurements (duration approx. 3 min) were conducted during the oxygen pulses (blue, start approx. 5-10 s after beginning of oxygen pulse) and also in the delay times (red, start after approx. 10-20 s after end of oxygen pulse, when the methyl formate formation rate was roughly decreased to background level) across the pulse sequence (from top to bottom).

Thus, in agreement with expectations, in situ IRAS shows a lower accumulation of formate species for lower oxygen and higher methanol fluxes. Yet, the relative surface deactivation for methyl formate formation does not differ accordingly, especially for the measurements with a low oxygen flux: The measurement with a rather low methanol flux displays only a slight surface deactivation, despite significant formate accumulation (Figure 3c and 4c), while the measurement with a high methanol flux exhibits a pronounced surface deactivation for methyl formate, even though no clear evidence for formate accumulation is detected (Figures 3d and 4d). Thus, formate (alone) cannot account for the loss in reactivity towards partial oxidation to methyl formate, instead an additional mechanism appears to contribute to the observed surface deactivation for methyl formate which is not clearly detectable by IRAS measurements. Please note that the formally abstracted hydrogen atoms were previously reported to react to water or methanol[15] which both desorb rapidly from Au(332) at 230 K and thus, cannot cause the surface deactivation. Moreover, it should be emphasized that accumulation of oxygen on the surface is neither the origin of this additional deactivation: (i) Accumulating residual oxygen was connected to formate formation[25] which is not clearly detected for the measurement shown in Figures 3d and 4d. From the measurement with a low oxygen and a rather low methanol flux (Figures 3c and 4c), it can be estimated that less than 0.25 ML of residual oxygen are sufficient to clearly observe formation of formate species (after the third pulse). The (maximum) amount of oxygen which may accumulate on the surface was estimated based on the absolute methyl formate formation rate and the applied oxygen flux, neglecting any oxygen consumption due to formaldehyde desorption or CO_2 formation. For the experiment with a high methanol and a low oxygen flux (Figures 3d and 4d), a maximum of 0.3 ML oxygen at the end of the measurement may have accumulated, potentially sufficient for formate formation which is however not detected, suggesting the oxygen accumulation to be negligible under these conditions. (ii) For the measurement with a high oxygen and low methanol flux where formate formation in the delay times attests to the presence of residual oxygen, the transient pulse shape does not show decreasing methyl formate formation rates across the pulse duration, suggesting no significant deactivating effect of accumulating oxygen on the methyl formate formation under these conditions. (iii) The additional deactivation is clearly observed for the measurement conducted with a low oxygen and a high methanol flux corresponding to the highest applied methanol excess in the gas phase in this series, suggesting a sufficiently high methanol surface concentration for a fast consumption of rather low amounts of oxygen (an upper bound of 0.04 ML - 0.07 ML of unreacted oxygen per pulse can be estimated based on the methyl formate formation).

To further understand the surface deactivation mechanisms, the relative reduction of the methyl formate formation rate (with respect to the initial rate) is displayed as a function of the oxygen and the methanol exposure (after the first oxygen pulse) in Figures 5a and 5b, respectively. For the (three) experiments in which significant formate accumulation on the surface is observed (Figures 4a-c), the relative decrease of the rate exhibits a similar correlation with the oxygen exposure, further validating the role of formate in the deactivation under these conditions. In contrast, the measurement with a high methanol and a low oxygen flux (green symbols, Figure 5a), for which essentially no formate was detected, exhibits a significantly faster deactivation, indicating the contribution of other deactivation mechanism(s). Additional indication for the importance of an additional mechanism can be found comparing the experiments with a high oxygen flux (red and black symbols in Figure 5a): The relative rate decrease as a function of the oxygen exposure is the same, but the amount of formate observed by IRAS is significantly different (see Figures 4a and 4b) which is inconsistent with formate being the only cause for the observed deactivation.

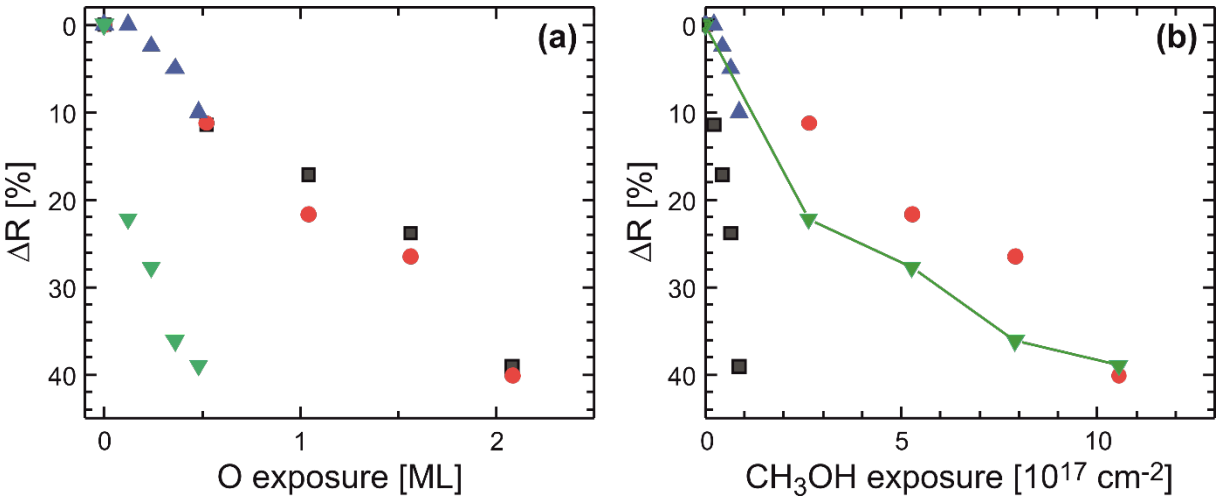

Figure 5 Methyl formate rate decrease ΔR relative to the initially observed rate at the beginning of the pulse sequence for the different pulsed isothermal MB experiments conducted at 230 K on Au(332) (see also Figures 3 and 4) as a function of (a) the oxygen exposure and (b) the methanol exposure (after the first oxygen pulse): low methanol and high oxygen flux (black squares, Figure 3a), high methanol and high oxygen flux (red circles, Figure 3b), low methanol and low oxygen flux (blue triangles, Figure 3c), and high methanol and low oxygen flux (green triangles, Figure 3d). The connecting lines are a guide to the eye.

Considering next the relative rate reduction as a function of the methanol exposure (Figure 5b), the correlation varies significantly between the different experiments. For the experiment with a high oxygen and a rather low methanol flux, thus the lowest applied methanol to oxygen flux ratio (black symbols, Figure 5b), the relative rate reduction is steeper than for the other

measurements attributed to the highest formate accumulation. In contrast, for the highest methanol to oxygen flux ratio where no clear formate accumulation was detected, a kind of bimodal behavior is observed, i.e. the initially steep decrease flattens towards the end of the pulse sequence (green symbols/line, Figure 5b). The initial steep decrease is similar to that observed for the measurement with a low oxygen and a low methanol flux (blue symbols, Figure 5b), while the flatter slope is similar to that observed for the measurement with a high oxygen and a high methanol flux (red symbols, Figure 5b). While a slightly steeper slope of the measurement with low oxygen and low methanol flux (blue symbols, Figure 5b), as compared to the initial slope for the highest methanol to oxygen flux ratio (green symbols, Figure 5b), may be (partially) attributed to formate accumulation blocking active surface sites, the rather shallow initial relative rate decrease for a high oxygen and high methanol flux (red symbols, Figure 5b), where also significant formate signals are detected, cannot be explained in a similar manner, but points to the importance of a different deactivation mechanism under oxygen-deficient conditions which causes an even faster, methanol dependent deactivation than the formate accumulation under the investigated conditions.

Additional pulsed isothermal MB experiments (with a different methanol batch) were conducted to test this hypothesis: Extending the delay time between the oxygen pulses and thus, increasing the methanol exposure, while keeping the methanol to oxygen ratio during the oxygen pulse constant, resulted in a stronger methyl formate rate reduction for a constant oxygen exposure (Figure S2). In addition, prolonging the methanol exposure before the first oxygen pulse resulted in an even reduced initial rate (Figure S3). Both results are consistent with the (proposed) blocking of surface sites for methyl formate formation by species related to the exposure of methanol. This deactivation pathway is further justified by the rate decrease during each oxygen pulse, as expected for a decreasing number of available surface sites reactive for methyl formate formation. With this batch of methanol, in situ IRAS across the pulse sequence evidenced the accumulation of species containing C-H bonds, however lacking clear signals attributable to CO modes (Figure S2). These species block the surface for CO adsorption (Figure S4) and were found to be oxidizable by atomic oxygen at 230 K, as previously shown for formate species.[25] Furthermore, a short annealing i. vac. to 310 K and 450 K results in the reduction and even disappearance of IRAS signals that characterize these species restoring the ability of the surface to adsorb CO and re-establishing the surface activity for methyl formate formation (Figures S4 and S5). These results suggest the C-H bond containing species to be a molecular species bound moderately strongly on the Au(332) surface, presumably an impurity present in the methanol. It should be noted that high purity methanol

was used also in these experiments which did not display, however, clear evidence for impurities in QMS measurements implying that even very small concentrations may be detrimental to the surface reactivity towards methyl formate. For the measurements with a high methanol flux shown in Figures 3 and 4, a similar effect may have caused the observed deactivation as indicated by a comparable correlation to a high methanol flux and rather oxygen-deficient conditions as well as by decreasing methyl formate formation rates across the pulse duration for methanol-rich conditions. Presumably, a different type of species accumulates which may escape IRAS detection due to very low concentrations or the metal surface selection rule preventing detection of vibrational modes parallel to the surface. The more pronounced deactivation observed at low oxygen flux indicates that these species can possibly be oxidized by atomic oxygen at 230 K on the Au(332) surface, as was shown for the contaminations having an IR spectrum discussed above.

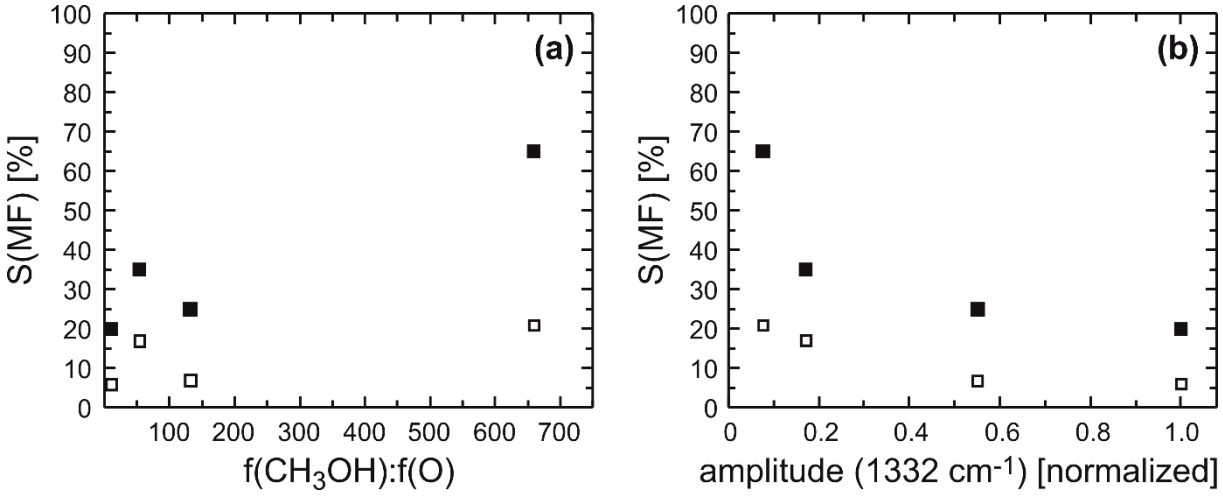

Figure 6 Selectivity to methyl formate S(MF) with respect to the number of supplied oxygen atoms for the pulsed isothermal MB experiments of the methanol oxidation on Au(332) at 230 K shown in Figure 3 displayed as a function of (a) the methanol to atomic oxygen flux ratio $f(CH_3OH):f(O)$ and (b) the relative IRAS signal intensity as indicated by the amplitude of the formate band at 1332 cm^{-1} at the end of the pulse sequence relative to the maximum observed in this series. The initial selectivity (pulse 1, solid symbols) and the selectivity at the end of the pulse sequence (pulse 5, open symbols) are shown.

The selectivity towards methyl formate with respect to the number of supplied oxygen atoms is given in Figure 6a as a function of the methanol to oxygen flux ratio. Significant fragmentation in the QMS of methanol and methyl formate hampers quantification of formaldehyde desorption which is expected to compete effectively with methyl formate formation under the applied single collision conditions. Similarly, the quantification of the CO_2 formation rate

resulting from the total oxidation of methanol on Au(332) is not possible because of background reactions of the chamber also exposed to atomic oxygen. Please note that methyl formate is exclusively formed on the Au surface. Thus, the selectivity towards methyl formate *S(MF)* is based on quantitative calibrations of the atomic oxygen flux *f(O)* and the methyl formate flux *f(MF)* based on the QMS signal (m/z = 60) considering that two oxygen atoms are required for methyl formate formation from methanol:

$$S(MF) = \frac{2 \cdot f(MF)}{f(O)} \quad (1)$$

The selectivity is given for all experiments of this series for both the beginning (pulse 1, solid symbols) and the end (pulse 5, open symbols) of the pulse sequence. Overall, the selectivity towards methyl formate increases for a higher methanol to oxygen flux ratio reaching an initial value of approx. 65 % for the highest applied methanol to oxygen flux ratio (factor of approx. 660). Moreover, the selectivity is larger for the experiments where a low oxygen flux was applied. This is in qualitative agreement with results for np-Au catalysts, TPR experiments and kinetic simulations.[2-3, 15, 18-21] The absolute values remain, however, clearly below those reported for np-Au catalysts. This is expected because of the competition between coupling and desorption of formaldehyde (desorption temperature from clean Au(110) is 160 K[34]) which limits the selectivity under single collision conditions, whereas desorbed formaldehyde can undergo multiple collisions with the surface of np-Au catalysts allowing for a subsequent coupling reaction to methyl formate and, thus, an enhanced selectivity.[2-3]

A discussion of the observed selectivity in a simplified kinetic model assuming low coverage, constant availability of reactive sites etc. is hampered by the complexity of the reaction network, e.g. the presence of deactivation processes discussed above. The effect of the latter is readily seen for the experiments done at low oxygen flux, for which a high methanol pressure exhibits a significantly higher initial selectivity than observed for the experiment using the low methanol pressure, while the selectivity is significantly lower and more importantly similar for both methanol pressures at the end of the pulse series.

Based on the proposed reaction mechanism, a high methanol to oxygen ratio on the surface is expected to be beneficial for methyl formate formation, while lowering this ratio should favor overoxidation.[2, 15, 18-21] In addition, the competition of formaldehyde desorption with subsequent coupling to methyl formate is expected to lower the selectivity towards methyl formate for lower surface concentrations, in specific also of methoxy, in case of single scattering conditions. While these considerations allow to reconcile the changes in the initial

selectivity found for the two pairs of experiments using high and low oxygen flux, respectively, the higher selectivity towards methyl formate found for a methanol to oxygen ratio of 55 (low methanol, low oxygen) as compared to the high oxygen/high methanol flux experiment with a ratio of 130 cannot be understood based on these simplified considerations. The IRAS results presented above clearly show that the high oxygen/high methanol flux condition leads to a significant transient concentration of methoxy on the surface as well as a sizeable amount of unreacted oxygen at the end of the pulse which gives rise to the formation of formate species in the delay periods.[25] In contrast to that, the IRAS experiments for low methanol and low oxygen flow show no indication for a significant transient methoxy concentration and a considerably reduced formation of formate. Hence, the transient concentration of 'excess' activated oxygen, i.e. oxygen which does not contribute to methyl formate formation, but tends to form AuO_x phases and is known to shift the selectivity towards overoxidation products, has to be considered one factor determining the selectivity of the surface. This interpretation is further corroborated by the fact that the selectivity drops monotonously with increasing amounts of excess oxygen atoms at the end of the pulse as estimated from the relative IR intensity of formate (Figure 6b). It is important to note that overoxidation is rather efficient for high methanol and oxygen fluxes even though there is a significant transient concentration of methoxy, whose surface concentration is critical for methyl formate selectivity as it needs to react with transiently formed formaldehyde before the latter gets overoxidized or desorbs. This implies that the methanol supply from the gas phase is not sufficient to react with the oxygen atoms deposited on the surface predominantly to methyl formate, corroborating the expectation that the ratio of methanol to oxygen on the surface is significantly smaller than expected based on the impinging fluxes. The blocking of surface sites by oxygen as well as methoxy found for high oxygen and high methanol flux also allows to explain the less pronounced increase of the initial rates for high oxygen and high methanol fluxes as compared to the low fluxes (Figure 3).

Given the significant role of methoxy species on the reaction network, it is interesting to discuss the intensity of the methoxy species observed for the experiments with high methanol flux in more detail. Based on the previously suggested reaction mechanism[15-17] (see also Figure 2), the steady state concentration of methoxy $[H_3CO]_{stst}$ should be obtained by equating the rate of its formation (reaction of methanol with activated oxygen) to the rate(s) of its consumption (reactions to formaldehyde or methyl formate):

$$[H_3CO]_{stst} = \frac{k_{H_3CO}[CH_3OH][O_{act}]}{k_{CH_2O}[O_{act}]+k_{H_3COCHO}[CH_2O][O_{act}]} \quad (2)$$

with [CH_3OH], [CH_2O] and [O_{act}] denoting the steady state surface concentrations of methanol, formaldehyde and activated oxygen, respectively, and k_{H_3CO}, k_{CH_2O} and k_{H_3OCHO} denoting the rate constants for methoxy, formaldehyde and methyl formate formation, respectively. Assuming only one type of activated oxygen species and the steady state concentration of formaldehyde to be independent of the activated oxygen concentration, for simplicity, the steady state concentration of methoxy should increase with the methanol concentration, but should be independent of oxygen flux. While the methoxy concentration increases with methanol concentration (Figures 4b and 4d as compared to Figures 4a and 4c) in agreement with this simplified model, the model clearly fails to predict the observed increase of the initial methoxy concentration by a factor of approx. 2.5, when the oxygen flux is increased by a factor of 5 (Figure 4b as compared to Figure 4d). The observed reduction in selectivity towards methyl formate associated with the increase in oxygen flux indicates that the second consumption reaction in Eq. 2 is significantly suppressed, which would result in a higher steady state concentration of the methoxy species. It should be noted that this simple model neglects the effects of the various types of activated oxygen species, such as atomic oxygen, oxidic AuO_x phases of different island size, or O-Au-O chains on step edges[12, 14, 19, 35-37] here summarized as O_{act}, on the formation and consumption reactions of methoxy as well as the influence of competing reaction channels, such as formaldehyde desorption or overoxidation of formaldehyde whose relative importance also depends on the relative concentration of the various types of activated oxygen species. The loss of the methoxy signal at the end of the pulse sequence using high methanol and high oxygen flux is correlated with the increase of the formate concentration on the surface. Previous experiments suggested that formate concentration on the surface is sizable[25] under these conditions rendering site blocking by formate a viable explanation for the observed loss in methoxy concentration. However, the surface is still active towards methyl formate formation, which clearly shows that although a significant number of sites for adsorbed methoxy is blocked, the surface can still accommodate a sufficiently high transient concentration of methoxy to produce methyl formate. This also shows that the adsorption of methanol required for subsequent methoxy formation still proceeds under these conditions. Based on the previously suggested reaction mechanism[15-17] (see also Figure 2), it is expected that the rate of methyl formate formation $\left(\frac{d[H_3COCHO]}{dt}\right)$ is proportional to the surface concentration of methoxy:

$$\frac{d[H_3COCHO]}{dt} = k_{H_3COCHO}[H_3CO][CH_2O][O_{act}] \quad (3)$$

Experimentally, the reduction in methyl formate formation is considerably smaller than the loss of methoxy concentration on the surface. This is in line with the expectation that formaldehyde formation and not the methoxy concentration or the preceding methanol adsorption is rate limiting.

For the experiment using a high methanol and a low oxygen flux, an increase of the methoxy concentration is observed if comparing the first and the second pulse. This can be understood along the same lines as the discussion above, as this increase in methoxy intensity is associated with a significant drop in methyl formate selectivity (Figure 5b, green symbols), hence a reduction in one of the depletion channels for methoxy (Eq. 2). However, this reduction in selectivity between the first two pulses is not associated with a significant site blocking for methoxy. In contrast, the methanol related deactivation dominates under oxygen-deficient conditions. This observation can be understood assuming a preferential blocking of a small number of sites which are, however, highly reactive for methyl formate formation. While the exact nature of these reactive sites towards methyl formate formation cannot be determined from these measurements, viable candidates for minority sites on the stepped Au(332) surface which bind the methanol related deactivating species strongly are low-coordinated sites, such as steps or kinks (present due to a miscut with respect to the ideal (332) orientation[28]).

As compared to np-Au catalysts, the methyl formate formation decreases in the isothermal MB experiments on Au(332) already at rather low temperatures, where methanol conversion with molecular oxygen on np-Au is still small, but increases significantly for higher temperatures.[2-3] This can be attributed to formaldehyde (and methanol) desorption competing with the coupling reaction to methyl formate due to the inability to re-adsorb formaldehyde (or methanol) on Au(332) under the applied single collision conditions, whereas on np-Au desorbing formaldehyde may contribute to methyl formate formation for long contact times due to multiple collisions with the np-Au surface before exiting the catalyst bed.[11] At lower temperatures, the isothermal MB experiments show under all applied conditions a deactivation of the Au(332) surface for methyl formate formation. The deactivation due to formate accumulation observed for oxygen-rich conditions is expected to be less relevant for np-Au studies with rather low oxygen concentrations under typically applied conditions. However, for increased oxygen or Ag contents, this channel may become more important resulting in unwanted overoxidation products, such as CO_2, for higher temperatures.[2, 11-13] Under oxygen-deficient conditions, a different deactivation related to methanol or an impurity in methanol was found to be important on Au(332). While surface deactivation by impurities may appear to be

a trivial issue, this methanol related deactivation is very effective at low temperatures under oxygen-deficient conditions, thereby blocking the active sites on the Au(332) surface for methyl formate formation, even for high purity methanol. Thus, in np-Au studies with molecular oxygen where the surface concentration of activated oxygen is typically rather low,[11, 13] a similar mechanism may be relevant. Specifically, it may be important for achieving steady state conditions at low temperatures. So far, steady state reactivity in the methanol oxidation to methyl formate on np-Au has been reported for temperatures ≥20 °C,[2] while oxygen activation on np-Au catalysts proceeds already at temperatures significantly below 0 °C as evidenced by CO oxidation.[4, 38] Moreover, carbonaceous deposits were recently reported to be present on np-Au catalysts under non-steady state conditions with decreasing amounts as the temperature increases to 323 K and further to 423 K, which is the steady-state reaction temperature applied in the np-Au study.[14] While the authors suggested the carbonaceous deposits to be adsorbed on residual Ag in the np-Au catalyst, our results indicate that even Au sites may be blocked at low temperatures after high exposures of methanol, even when high purity methanol is used.

Conclusion

The influence of surface temperature and variation of the flux on the (partial) methanol oxidation over the stepped Au(332) surface was investigated by pulsed isothermal molecular beam experiments. In these measurements, atomic oxygen provided by a thermal cracker was pulsed, while methanol was provided continuously, at an excess in the gas phase.

With increasing surface temperature, the methyl formate formation rate exhibits a maximum at 250 K under the applied (single collision) conditions, as the desorption of methanol and formaldehyde limit the coupling reaction to methyl formate. The surface deactivation observed across the pulse sequence is not lifted by an increased surface temperature in the investigated temperature range, but even slightly increases.

Variation of the methanol and oxygen fluxes demonstrated a reduced surface deactivation across the pulse sequence, when both the methanol and the atomic oxygen flux were chosen to be rather small. For oxygen-rich conditions, i.e. low methanol to oxygen flux ratios, in situ IRAS measurements evidence increased formation of formate species blocking the surface for methoxy and methyl formate formation. At high methanol fluxes and under rather oxygen-deficient conditions, an additional deactivation mechanism is effective in reducing methyl formate formation at low surface temperatures which may also be important for achieving steady state conditions on np-Au catalysts at low temperatures. In contrast to deactivation by formate species, the results indicate that this methanol related deactivation preferentially blocks

a small number of highly reactive sites for methyl formate formation, while methoxy formation is (initially) not reduced by this deactivation.

In agreement with expectations, the selectivity to methyl formate increased for higher methanol to oxygen ratios. Deviations from this trend were observed, however, for conditions where the number of available surface sites is expected to be limited. A maximum selectivity to methyl formate of 65 % was achieved for the highest applied methanol to atomic oxygen flux ratio of approx. 660.

These results demonstrate the importance of deviations from the idealized methanol oxidation mechanism on gold arising from different deactivation pathways and thus, provide additional insights into the processes under isothermal conditions at low temperatures.

Supporting Information

IRAS measurements of ^{13}C methanol on Au(332). Pulsed isothermal MB experiments with in situ IRAS measurements on methanol oxidation on Au(332) with ^{13}C methanol for varying delay times between oxygen pulses as well as extended methanol exposure prior to the first oxygen pulse. CO IRAS measurements of Au(332) surface after pulsed isothermal MB experiment and subsequent annealing. Pulsed isothermal MB experiments with in situ IRAS measurements on methanol oxidation on Au(332) for annealed surface after prior pulsed isothermal MB experiment.

Author Information

Corresponding Author

Wiebke Riedel - *Institut für Chemie und Biochemie, Freie Universität Berlin, Arnimallee 22, 14195 Berlin, Germany;* orcid.org/0000-0001-6561-2305; E-Mail: wiebke.riedel@fu-berlin.de

Authors

Christoph D. Feldt - *Institut für Chemie und Biochemie, Freie Universität Berlin, Arnimallee 22, 14195 Berlin, Germany;* orcid.org/0000-0002-0464-0780

Thorren Kirschbaum - *Institut für Chemie und Biochemie, Freie Universität Berlin, Arnimallee 22, 14195 Berlin, Germany, Helmholtz-Zentrum Berlin für Materialien und Energie, Hahn-Meitner-Platz 1, 14109 Berlin, Germany*

Jian Low - *Institut für Chemie und Biochemie, Freie Universität Berlin, Arnimallee 22, 14195 Berlin, Germany*

Thomas Risse - *Institut für Chemie und Biochemie, Freie Universität Berlin, Arnimallee 22, 14195 Berlin, Germany;* orcid.org/0000-0003-0228-9189; E-Mail: risse@chemie.fu-berlin.de

Author Contribution

The manuscript was written through contributions of all authors. All authors have given approval to the final version of the manuscript.

Conflicts of Interest

There are no conflicts to declare.

Acknowledgement

We acknowledge the financial support from the German Research Foundation (DFG) within the framework of research unit 2231 "NAGOCAT" Project No. RI 1025/3-1(2). We thank S. Eltayeb and K. Tang for technical support. C. D. F. thanks the International Max-Planck Research School "Functional Interfaces in Physics and Chemistry" for support and the IMPRS for Elementary Processes in Physical Chemistry.

References

1. Haruta, M.; Kobayashi, T.; Sano, H.; Yamada, N., Novel Gold Catalysts for the Oxidation of Carbon-Monoxide at a Temperature Far Below 0 °C *Chem. Lett.* **1987**, 405-408.
2. Wittstock, A.; Zielasek, V.; Biener, J.; Friend, C. M.; Bäumer, M., Nanoporous Gold Catalysts for Selective Gas-Phase Oxidative Coupling of Methanol at Low Temperature. *Science* **2010**, *327*, 319-322.
3. Wittstock, A.; Biener, J.; Bäumer, M., Nanoporous Gold: A New Material for Catalytic and Sensor Applications. *Phys. Chem. Chem. Phys.* **2010**, *12*, 12919-12930.
4. Xu, C. X.; Su, J. X.; Xu, X. H.; Liu, P. P.; Zhao, H. J.; Tian, F.; Ding, Y., Low Temperature CO Oxidation over Unsupported Nanoporous Gold. *J. Am. Chem. Soc.* **2007**, *129*, 42-43.
5. Yin, H. M.; Zhou, C. Q.; Xu, C. X.; Liu, P. P.; Xu, X. H.; Ding, Y., Aerobic Oxidation of D-Glucose on Support-Free Nanoporous Gold. *J. Phys. Chem. C* **2008**, *112*, 9673-9678.

6. Meyer, R.; Lemire, C.; Shaikhutdinov, S. K.; Freund, H., Surface Chemistry of Catalysis by Gold. *Gold Bull.* **2004**, *37*, 72-124.
7. Bond, G. C., Gold: A Relatively New Catalyst. *Catal.Today* **2002**, *72*, 5-9.
8. Erlebacher, J.; Aziz, M. J.; Karma, A.; Dimitrov, N.; Sieradzki, K., Evolution of Nanoporosity in Dealloying. *Nature* **2001**, *410*, 450-453.
9. Wang, L. C.; Zhong, Y.; Widmann, D.; Weissmüller, J.; Behm, R. J., On the Role of Residual Ag in Nanoporous Au Catalysts for CO Oxidation: A Combined Microreactor and Tap Reactor Study. *ChemCatChem* **2012**, *4*, 251-259.
10. Wang, L. C.; Zhong, Y.; Jin, H. J.; Widmann, D.; Weissmüller, J.; Behm, R. J., Catalytic Activity of Nanostructured Au: Scale Effects Versus Bimetallic/Bifunctional Effects in Low-Temperature CO Oxidation on Nanoporous Au. *Beilstein J. Nanotechnol.* **2013**, *4*, 111-128.
11. Wang, L. C.; Personick, M. L.; Karakalos, S.; Fushimi, R.; Friend, C. M.; Madix, R. J., Active Sites for Methanol Partial Oxidation on Nanoporous Gold Catalysts. *J. Catal.* **2016**, *344*, 778-783.
12. Zugic, B.; Wang, L. C.; Heine, C.; Zakharov, D. N.; Lechner, B. A. J.; Stach, E. A.; Biener, J.; Salmeron, M.; Madix, R. J.; Friend, C. M., Dynamic Restructuring Drives Catalytic Activity on Nanoporous Gold-Silver Alloy Catalysts. *Nat. Mater.* **2017**, *16*, 558-564.
13. Wang, L. C.; Friend, C. M.; Fushimi, R.; Madix, R. J., Active Site Densities, Oxygen Activation and Adsorbed Reactive Oxygen in Alcohol Activation on NpAu Catalysts. *Faraday Discuss.* **2016**, *188*, 57-67.
14. Zugic, B., et al., Evolution of Steady-State Material Properties During Catalysis: Oxidative Coupling of Methanol over Nanoporous $Ag_{0.03}Au_{0.97}$. *J. Catal.* **2019**, *380*, 366-374.
15. Xu, B. J.; Liu, X. Y.; Haubrich, J.; Madix, R. J.; Friend, C. M., Selectivity Control in Gold-Mediated Esterification of Methanol. *Angew. Chem. Int. Ed.* **2009**, *48*, 4206-4209.
16. Outka, D. A.; Madix, R. J., Bronsted Basicity of Atomic Oxygen on the Au(110) Surface - Reactions with Methanol, Acetylene, Water and Ethylene. *J. Am. Chem. Soc.* **1987**, *109*, 1708-1714.
17. Xu, B. J.; Haubrich, J.; Baker, T. A.; Kaxiras, E.; Friend, C. M., Theoretical Study of O-Assisted Selective Coupling of Methanol on Au(111). *J. Phys. Chem. C* **2011**, *115*, 3703-3708.
18. Xu, B. J.; Siler, C. G. F.; Madix, R. J.; Friend, C. M., Ag/Au Mixed Sites Promote Oxidative Coupling of Methanol on the Alloy Surface. *Chem. Eur. J.* **2014**, *20*, 4646-4652.
19. Hiebel, F.; Karakalos, S.; Xu, Y. F.; Friend, C. M.; Madix, R. J., Structural Differentiation of the Reactivity of Alcohols with Active Oxygen on Au(110). *Top. Catal.* **2018**, *61*, 299-307.
20. Reece, C.; Luneau, M.; Madix, R. J., Dissecting the Performance of Nanoporous Gold Catalysts for Oxygen-Assisted Coupling of Methanol with Fundamental Mechanistic and Kinetic Information. *ACS Catal.* **2019**, *9*, 4477-4487.
21. Reece, C.; Luneau, M.; Friend, C. M.; Madix, R. J., Predicting a Sharp Decline in Selectivity for Catalytic Esterification of Alcohols from Van Der Waals Interactions. *Angew. Chem. Int. Ed.* **2020**, *59*, 10864-10867.
22. Yim, W. L., et al., Universal Phenomena of CO Adsorption on Gold Surfaces with Low-Coordinated Sites. *J. Phys. Chem. C* **2007**, *111*, 445-451.
23. Tomaschun, G.; Dononelli, W.; Li, Y.; Bäumer, M.; Klüner, T.; Moskaleva, L. V., Methanol Oxidation on the Au(310) Surface: A Theoretical Study. *J. Catal.* **2018**, *364*, 216-227.
24. Fujita, T., et al., Atomic Origins of the High Catalytic Activity of Nanoporous Gold. *Nat. Mater.* **2012**, *11*, 775-780.
25. Feldt, C. D.; Gimm, T.; Moreira, R.; Riedel, W.; Risse, T., Methanol Oxidation on Au(332): An Isothermal Pulsed Molecular Beam Study. *Phys. Chem. Chem. Phys.* **2021**, *23*, 21599 - 21605.
26. Moreira, R. Setup of a Molecular Beam Apparatus to Study the Reactivity of Single Crystal Surfaces and Its Application to CO Oxidation on Au(332). Freie Universtität Berlin, Berlin, 2018.
27. Libuda, J.; Meusel, I.; Hartmann, J.; Freund, H. J., A Molecular Beam/Surface Spectroscopy Apparatus for the Study of Reactions on Complex Model Catalysts. *Rev. Sci. Instrum.* **2000**, *71*, 4395-4408.
28. Prieto, M. J.; Carbonio, E. A.; Landers, R.; de Siervo, A., Structural and Electronic Characterization of Co Nanostructures on Au(332). *Surf. Sci.* **2013**, *617*, 87-93.

29. Mortensen, K.; Klink, C.; Jensen, F.; Besenbacher, F.; Stensgaard, I., Adsorption Position of Oxygen on the Pt(111) Surface. *Surf. Sci.* **1989**, *220*, L701-L708.
30. Norton, P. R.; Davies, J. A.; Jackman, T. E., Absolute Coverages of CO and O on Pt(111) - Comparison of Saturation Co Coverages on Pt(100), (110) and (111) Surfaces *Surf. Sci.* **1982**, *122*, L593-L600.
31. Gong, J.; Flaherty, D. W.; Ojifinni, R. A.; White, J. M.; Mullins, C. B., Surface Chemistry of Methanol on Clean and Atomic Oxygen Pre-Covered Au(111). *J. Phys. Chem. C* **2008**, *112*, 5501-5509.
32. Senanayake, S. D.; Stacchiola, D.; Liu, P.; Mullins, C. B.; Hrbek, J.; Rodriguez, J. A., Interaction of CO with OH on Au(111): HCOO, CO_3, and HOCO as Key Intermediates in the Water-Gas Shift Reaction. *J. Phys. Chem. C* **2009**, *113*, 19536-19544.
33. Sexton, B. A.; Hughes, A. E.; Avery, N. R., Surface Intermediates in the Reaction of Methanol, Formaldehyde and Methyl Formate on Cu(110). *Appl. Surf. Sci.* **1985**, *22-3*, 404-414.
34. Outka, D. A.; Madix, R. J., Acid-Base and Nucleophilic Chemistry of Atmoic Oxygen on the Au(110) Surface - Reactions with Formic Acid and Formaldehyde *Surf. Sci.* **1987**, *179*, 361-376.
35. Min, B. K.; Friend, C. M., Heterogeneous Gold-Based Catalysis for Green Chemistry: Low-Temperature CO Oxidation and Propene Oxidation. *Chem. Rev.* **2007**, *107*, 2709-2724.
36. Personick, M. L.; Zugic, B.; Biener, M. M.; Biener, J.; Madix, R. J.; Friend, C. M., Ozone-Activated Nanoporous Gold: A Stable and Storable Material for Catalytic Oxidation. *ACS Catal.* **2015**, *5*, 4237-4241.
37. Li, Y.; Dononelli, W.; Moreira, R.; Risse, T.; Bäumer, M.; Klüner, T.; Moskaleva, L. V., Oxygen-Driven Surface Evolution of Nanoporous Gold: Insights from Ab Initio Molecular Dynamics and Auger Electron Spectroscopy. *J. Phys. Chem. C* **2018**, *122*, 5349-5357.
38. Zielasek, V.; Jürgens, B.; Schulz, C.; Biener, J.; Biener, M. M.; Hamza, A. V.; Bäumer, M., Gold Catalysts: Nanoporous Gold Foams. *Angew. Chem. Int. Ed.* **2006**, *45*, 8241-8244.

Table of Content

Surface deactivation of partial methanol oxidation to methyl formate on Au(332) under oxygen-deficient conditions at low temperatures suggests a small number of highly active sites for methyl formate formation.

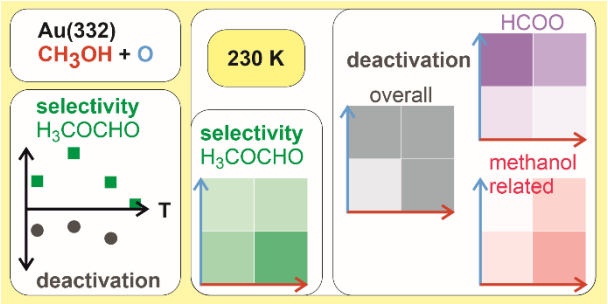

Supporting Information

Methanol oxidation on Au(332): Methyl formate selectivity and surface deactivation under isothermal conditions

Christoph D. Feldt[a], Thorren Kirschbaum[a,b], Jian Liang Low[a], Wiebke Riedel*[,a], Thomas Risse[a]

[a] *Institut für Chemie und Biochemie, Freie Universität Berlin, Arnimallee 22, 14195 Berlin*

[b] *Helmholtz-Zentrum Berlin für Materialien und Energie, Hahn-Meitner-Platz 1, 14109 Berlin, Germany*

* Email: wiebke.riedel@fu-berlin.de

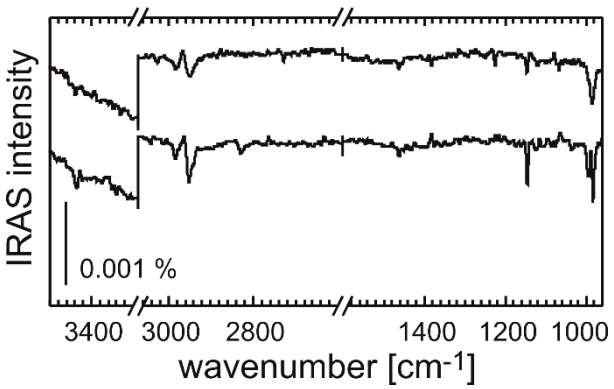

Figure S1 IRAS measurements of 0.1 L (top) and 0.3 L (bottom) ^{13}C-methanol (99 atom % ^{13}C, Sigma Aldrich) adsorbed on clean Au(332) at 120 K.

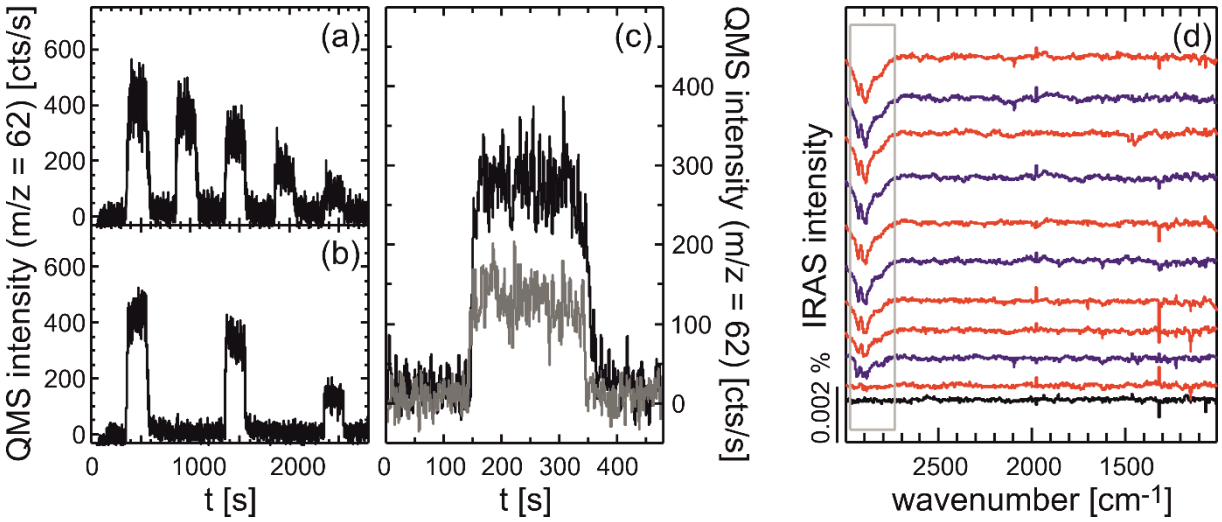

Figure S2 Pulsed isothermal MB experiments of methanol oxidation on Au(332) at 230 K to methyl formate using a different batch of methanol (^{13}C-methanol, 99 atom % ^{13}C, Sigma Aldrich) applying a methanol flux of 52×10^{13} $s^{-1}cm^{-2}$ (p(MeOH) =19.6×10^{-7} mbar) and an atomic oxygen flux of $1.25\cdot10^{-3}$ ML/s ≈ $1.9\cdot10^{12}$ $s^{-1}cm^{-2}$ employing a delay time of (a) 300 s and (b) 800 s between oxygen pulses (methyl formate molecular peak: m/z = 62). In (c) a direct comparison of the third pulses of the measurements with 300 s (black) and 800 s (grey) delay time displayed in (a) and (b) is shown. (d) In situ IRAS measurements conducted for the MB experiment shown in (a) during (blue) and in between (red) the oxygen pulses of the sequence (from bottom to top). The grey box highlights the signals in the CH stretching region attributed to C-H bond containing species accumulation on the surface.

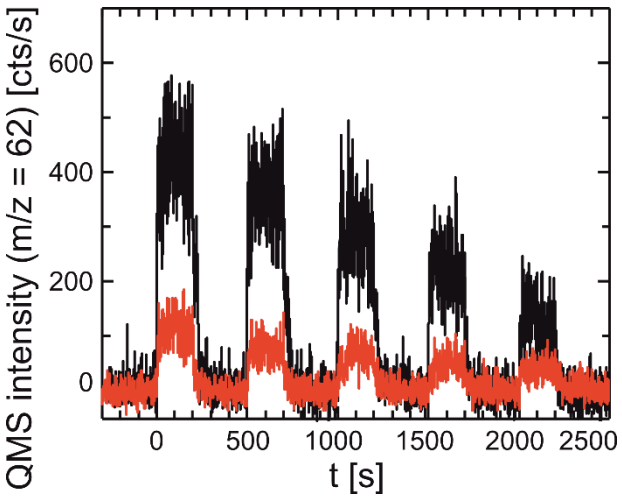

Figure S3 Pulsed isothermal MB experiment on the methanol oxidation to methyl formate on Au(332) at 230 K using a different batch of methanol (^{13}C-methanol, 99 atom % ^{13}C, Sigma Aldrich) applying a methanol flux of 52×10^{13} $s^{-1}cm^{-2}$ (p(MeOH) =19.6×10^{-7} mbar) and an atomic oxygen flux of $1.25\cdot10^{-3}$ ML/s ≈ $1.9\cdot10^{12}$ $s^{-1}cm^{-2}$ for 300 s (black) and 3000 s (red) methanol exposure before the first oxygen pulse. The initial methyl formate formation rate is clearly reduced for the prolonged methanol exposure, even below the rate observed at the end of the experiment with a shorter pre-exposure attesting to the surface deactivation due to methanol or some impurity in methanol.

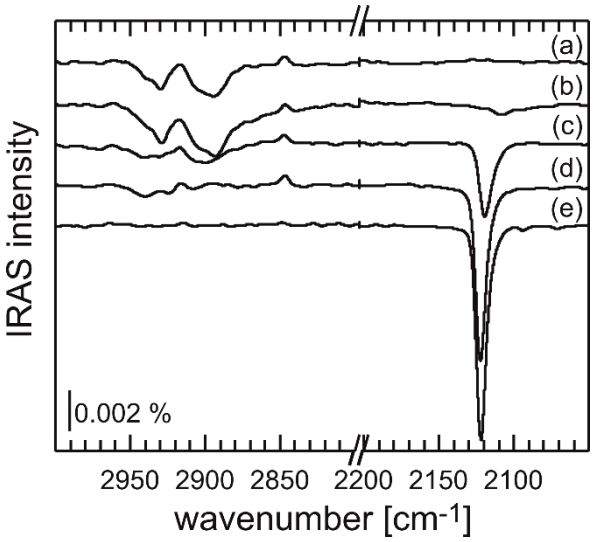

Figure S4 IRAS measurements (a) after a pulsed isothermal MB experiment on the partial oxidation of methanol (different batch: ^{13}C-methanol, 99 atom % ^{13}C, Sigma Aldrich) on Au(332) at 230 K (methanol flux of 52×10^{13} $s^{-1}cm^{-2}$ (p(MeOH) =19.6×10^{-7} mbar), flux of atomic oxygen $0.46\cdot10^{-3}$ ML/s), (b) during subsequent CO exposure (p(CO) = $8.2\cdot10^{-6}$ mbar) at 190 K, and after heating the sample shown in (b) i. vac. to (c) 310 K and (d) 450 K during CO exposure (p(CO) = $8.2\cdot10^{-6}$ mbar) at 190 K, (e) during CO exposure (p(CO) = $8.2\cdot10^{-6}$ mbar) at 190 K for a clean Au(332) surface.

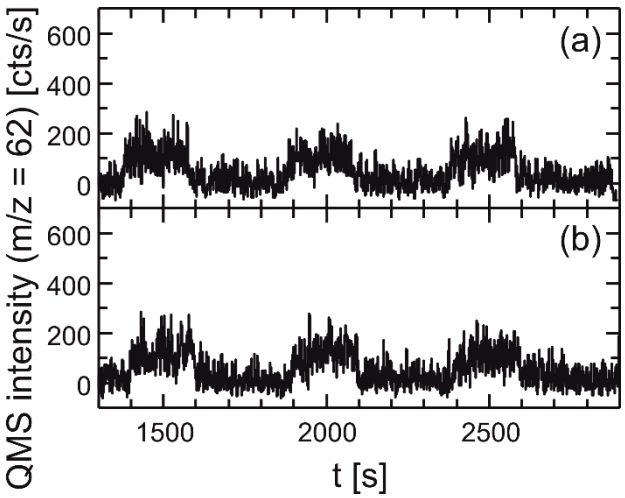

Figure S5 Pulsed isothermal MB experiments of methanol oxidation on Au(332) to methyl formate (molecular peak: m/z = 62) at 230 K using a different batch of methanol (^{13}C-methanol, 99 atom % ^{13}C, Sigma Aldrich) applying a methanol flux of 4×10^{13} $s^{-1}cm^{-2}$ (p(MeOH) = $1.6\cdot10^{-7}$ mbar) and an oxygen flux of $0.46\cdot10^{-3}$ ML/s displaying the last three pulses of the measurement. (a) Experiment conducted on a clean Au(332) surface. (b) The Au(332) surface was initially deactivated for methyl formate formation by a pulsed isothermal MB experiment at 230 K applying a high methanol flux of 52×10^{13} $s^{-1}cm^{-2}$ (CO IRAS after sequence shown in Fig. S3) and subsequently heated i. vac. to 450 K, before conducting the displayed experiment at 230 K applying the same fluxes of methanol and atomic oxygen as in a). The methyl formate formation rates are comparable demonstrating a lifting of the surface deactivation by the thermal treatment.

Paper IV

Low Temperature Oxidation of Methyl Formate on Au(332)

Christoph D. Feldt, Jian Liang Low, Paul Albrecht, Keyun Tang, Wiebke Riedel and Thomas Risse, The Journal of Physical Chemistry C, **2021**, 125, 26522-26529. DOI: https://doi.org/10.1021/acs.jpcc.1c08531

Contributions

The experiments are a part of the bachelor thesis of Paul Albrecht who performed the experiments together with Jian Liang Low under my supervision. I wrote the paper which was revised by Wiebke Riedel and Thomas Risse.

Page 128 - 138 are not displayed due to copyright protection of the article

Paper V

Heterogeneity of oxygen reactivity is crucial for selectivity of partial oxidation of methanol on gold surfaces

Christoph D. Feldt, Paul A. Albrecht, Salma Eltayeb, Wiebke Riedel and Thomas Risse, submitted to Chemical Communications.

Contributions

I conducted the experiments evaluated the data and developed the scientific model together with Wiebke Riedel and Thomas Risse. The writing of the paper was coordinated by Wiebke Riedel with contributions by all co-authors.

COMMUNICATION

Heterogeneity of oxygen reactivity is crucial for selectivity of partial oxidation of methanol on gold surfaces

Received 00th January 20xx,
Accepted 00th January 20xx

DOI: 10.1039/x0xx00000x

Christoph D. Feldt,[a] Paul A. Albrecht,[a] Salma Eltayeb,[a] Wiebke Riedel,*[a] and Thomas Risse*,[a]

Recent evidence for low-temperature oxidation of methyl formate on Au(332) may affect the selectivity of gold catalysts during partial oxidation of methanol. Under isothermal conditions, overoxidation of methyl formate is significantly slower than methanol oxidation which can be attributed to special oxygen species required for overoxidation.

Methyl formate is an important intermediate for a variety of bulk chemicals, such as formic acid, formamide or dimethyl formamide, and more recently was also tested as a possible alternative fuel (additive).[1-4] Apart from the currently applied industrial synthesis (reaction of CO with methanol over sodium or potassium methoxide requiring dry and CO_2-free feeds), [2, 4, 5] dehydrogenation and the thermodynamically more favourable partial oxidation of methanol are pursued as alternative routes.[1, 2] On nanoporous gold (np-Au), aerobic partial oxidation of methanol to methyl formate shows a temporally stable, high selectivity at high conversion for temperatures below 100 °C.[6] Np-Au is a fully metallic catalyst which is prepared by dealloying a gold alloy containing a less noble metal, mostly Ag, resulting in a porosity on the nanometer scale characterized by ligaments exhibiting a large fraction of low coordinated sites as well as low index facets.[7-9] Residual Ag in np-Au was found to be key for aerobic oxidation catalysis. The activation of molecular oxygen is typically the rate limiting step[8, 10] rendering the transient concentration of activated oxygen on np-Au low under typical reaction conditions.[11, 12] Increasing the reactive oxygen concentration either by increasing the Ag content or the oxygen pressure resulted in a reduced selectivity towards methyl formate formation.[6, 11, 13] In agreement, temperature programmed reaction (TPR) studies on Au(111) showed preferred formation of methyl formate at low coverage of activated oxygen, while high coverages of activated oxygen favour total oxidation of methanol.[14] Please note, that molecular oxygen does not dissociate on Au surfaces under ultrahigh vacuum (UHV) conditions which requires supply of activated oxygen (O-atoms, ozone etc.) in UHV experiments.[15, 16] A recent TPR study on Au(332), a surface with 6 atom-wide (111)-terraces separated by monoatomic steps as well as a smaller number of kink sites depending on the miscut of the crystal,[17] showed oxidation of methyl formate already at 135 K for low-oxygen coverage previously reported to result in high selectivity to methyl formate formation from methanol on Au(111).[18] For catalysis on np-Au, where molecules will exhibit multiple collisions with the catalyst surface along the catalyst bed, low-temperature overoxidation channels of the desired product may impact the selectivity of the system. While temperature programmed experiments allow to identify such reaction channels and elucidate conditions required for them to be active, conclusions on their impact on the kinetics of the reaction network, hence, selectivity of a catalyst can typically not be drawn. Therefore, a combination of temperature programmed and isothermal experiments will be presented here.

TPR measurements of methyl formate on oxygen pre-covered Au(332) (see Fig. 1a) reveal the formation of CO_2 at 135 K, 185 K and 320 K, based on the lack of CO_2 related signals in reference measurements. Using isotopic labelling, CO_2 formation at these temperatures was attributed to three distinct reaction pathways consistent with an attack of oxygen on the carbonyl carbon, the methyl carbon and through a cyclic transition state, respectively.[18] Accordingly, a different and rather specific geometry of the transition state is expected to be required for all three pathways.[18] Moreover, the CO_2 desorption at 320 K resulted from dehydrogenation of formate species located on special sites, presumably kinks.[18] It should be noted that the observed desorption of unreacted methyl formate is consistent with a sufficiently high coverage to prevent restricted CO_2 formation by low temperature availability of methyl formate (see also Fig. S1). For high pre-coverages of activated oxygen, however, the CO_2 desorption features at 135 K and 320 K vanish (see Figure 1b). Less CO_2 is desorbing at 185 K compared to 135

[a] Institut für Chemie und Biochemie, Freie Universität Berlin, Arnimallee 22, 14195 Berlin, Germany, Email: wiebke.riedel@fu-berlin.de, risse@chemie.fu-berlin.de

Electronic Supplementary Information (ESI) available: Experimental details and supporting Figures. See DOI: 10.1039/x0xx00000x

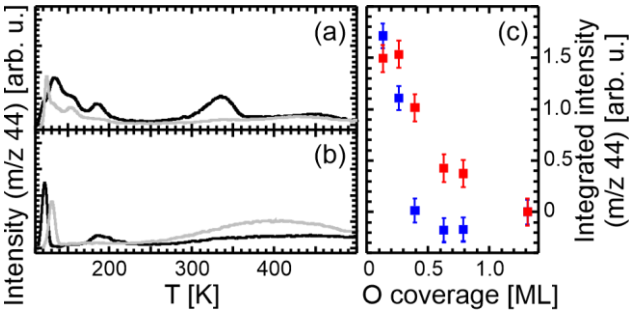

Fig. 1 $C^{16}O_2$ desorption of TPR experiments with 0.11 L methyl formate (black) on Au(332), pre-covered with (a) 0.13 ML and (b) 1.3 ML ^{16}O. For comparison, also results of reference measurements of the O pre-covered Au(332) surface are shown (grey). (c) Integrated intensity of CO_2 evolution at 135 K (blue) and 320 K (red) in TPR experiments of 0.11 L methyl formate on oxygen pre-covered Au(332) with O pre-coverages ranging between 0.13 ML and 1.3 ML. Error bars are estimated from the area variation obtained for different integration approaches (see ESI for details).

K and 320 K for low oxygen coverage, however, a quantitative analysis of the CO_2 amount for this pathway is hampered by the interference with signals from coinciding methyl formate desorption. Figure 1c evidences a steep drop in the amount of CO_2 desorbing at 135 K and 320 K for increasing oxygen pre-coverages indicative of a blocking of corresponding sites by excess oxygen. Thus, methyl formate oxidation requires a small surface coverage of activated oxygen, as expected for typical reaction conditions on np-Au catalysts. It should be noted that the decrease in CO_2 formation on Au(332) occurs when the oxygen pre-coverage exceeds the number of step sites on Au(332) (approx. 17 %). As theoretical calculations indicate a preferential decoration of low-coordinated sites (steps, kinks, etc.) by oxygen atoms,[19] it is concluded that oxygen species active in methyl formate oxidation are predominantly found at low coordinated sites. It is estimated for the lowest oxygen pre-coverage (0.13 ML) that approx. one CO_2 molecule is formed per reacted methyl formate molecule (see ESI for details), in agreement with previous isotopic labelling results.[18] For the oxygen pre-coverage of 0.13 ML associated with the highest observed CO_2 formation, less than 10 % of the oxygen is used to form CO_2 in all three reaction pathways combined (see ESI for details). This is significantly lower than the number of step sites on the Au(332) surface (approx. 17 %). The estimation is consistent with desorption of unreacted oxygen (and methyl formate) observed for all TPR measurements. These results evidence that all three reaction pathways resulting in methyl formate oxidation require special oxygen species on low coordinated sites which exhibit a low apparent activation barrier as indicated by the CO_2 (or formate) formation already at temperatures below 200 K (see Fig. 1 and Ref. [18]).

To elucidate the importance of these reaction channels for the reaction kinetics, isothermal pulsed molecular beam (MB) experiments were performed on Au(332) using oxygen-lean conditions. In the experiment shown in Figure 2a, the surface was continuously exposed to methyl formate, while oxygen atoms (^{18}O) were pulsed at a low flux (approx. 0.015 ML per pulse; flux $6.9 \cdot 10^{11} cm^{-2}s^{-1}$) onto the surface. The applied surface temperature of 310 K was chosen to be similar to those reported in np-Au studies[6] and sufficiently high to prevent surface deactivation by formate accumulation, i.e. above the onset of the high-temperature CO_2 desorption exhibiting a maximum at 320 K (see Fig. 1a). Formation of water ($H_2{}^{18}O$) during the oxygen pulse demonstrates methyl formate oxidation to proceed on Au(332) also under isothermal conditions. It should be noted that detection of other (potential) products including CO_2 is impeded by strong fragmentation signals of methyl formate or non-negligible reactions in the chamber exposed to atomic oxygen, as detected by reference measurements applying a non-reactive quartz flag. Upon atomic oxygen exposure (dashed line at 0 s), the $H_2{}^{18}O$ rate increases within approx. 10 s before levelling to a constant rate (approx. 30 counts per second (cps)). After the end of the oxygen pulse (dashed line at 30 s), the rate remains constant for at least 20 s before decaying back to the level prior to the oxygen pulse. This behaviour is consistent with accumulation of some of the oxygen during the pulse which is quantitatively consumed in the delay time. This is further supported by the absence of $^{18}O_2$ desorption in a temperature programmed desorption (TPD) measurement after the pulsed MB experiment (see Fig. S2). The oxygen accumulation during the oxygen pulse indicates a rather slow reaction of oxygen with methyl formate on Au(332) considering the large excess of

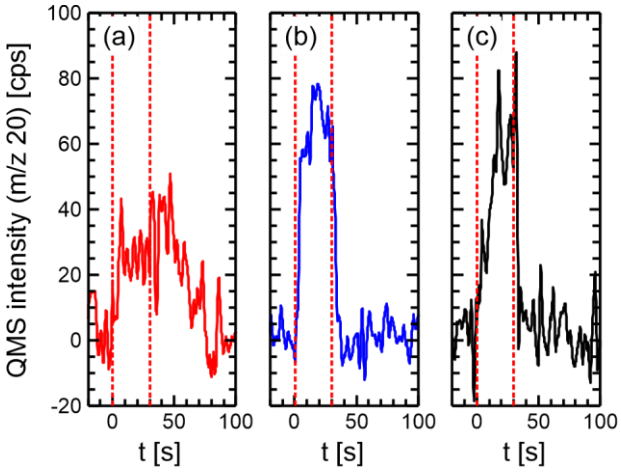

Fig. 2 Isothermal pulsed molecular beam experiments on Au(332) at 310 K pulsing atomic oxygen ($6.9 \cdot 10^{11} cm^{-2}s^{-1}$, 30 s on, 100 s off), while continuously supplying (a) methyl formate ($1.2 \cdot 10^{15}$ $cm^{-2}s^{-1}$), (b) methanol-^{13}C ($4.2 \cdot 10^{13}$ $cm^{-2}s^{-1}$) and (c) both methanol-^{13}C ($4.2 \cdot 10^{13}$ $cm^{-2}s^{-1}$) and methyl formate ($1.2 \cdot 10^{15} cm^{-2} \cdot s^{-1}$) at a large excess in the gas phase. The graphs show the difference of the $H_2{}^{18}O$ (m/z = 20) production rate (averaged over 31 pulses) between exposed Au(332) and a reference measurement with a non-reactive quartz flag. The length of one single oxygen pulse is indicated by the red dashed lines.

methyl formate in the gas phase (factor of approx. 1700) and the small amount of oxygen (0.015 ML) supplied per pulse.

In comparison to that, oxidation of methanol-^{13}C (60-fold excess of flux compared to oxygen) shows a steep increase in the $H_2{}^{18}O$ formation upon oxygen exposure (same condition as above; approx. 0.015 ML per pulse) levelling off at about twice the rate and returning back to baseline shortly after the end of the oxygen pulse indicating almost quantitative consumption of oxygen during the pulse (see Figure 2b; for $^{18}O_2$-TPD after the reaction see Fig. S2). It should be noted that no methyl formate formation is detected under the applied conditions for temperatures above 270 K,[20, 21] while detection of small amounts of formaldehyde, which is expected to be the main product in the partial methanol oxidation at high temperatures under single collision conditions, is hampered by large (fragmentation) signals due to methanol. These results suggest a significantly faster reaction of methanol with oxygen on Au(332) as compared to the methyl formate oxidation, despite the 30-fold reduced flux of methanol as compared to that of methyl formate.

For a direct comparison, a pulsed MB experiment with a co-feed of methanol and methyl formate using the fluxes of the individual experiments presented above (30-fold excess of methyl formate) was conducted (Figure 2c). In this measurement, the quasi-steady-state $H_2{}^{18}O$ formation rate is only slightly lower than that observed for methanol oxidation, in agreement with a significantly faster methanol than methyl formate oxidation on Au(332) despite the higher flux of methyl formate. However, the slight reduction in the quasi steady state rate as well as a slower increase and decrease after start and end of the oxygen exposure, respectively, show a kinetically relevant contribution of methyl formate to the observed water formation. The reaction probability of oxygen towards water can be estimated to be lower by a factor of approx. 60 for methyl formate than for methanol considering the quasi-steady-state rate during the pulse is halved (Fig. 2a and 2b) and the flux is increased by a factor of approx. 30 for methyl formate (combined with quantitative oxygen consumption by the end of the delay time). This strong reactivity difference suggests gold surfaces allowing for high methanol conversions, before overoxidation of the partial oxidation product methyl formate significantly contributes to a selectivity loss, as desired for an ideal partial oxidation catalyst.

But how can the reduced reactivity of oxygen towards methyl formate be understood given the fact that oxidation was observed as low as 125 K[18] indicative of a low activation barrier? As the desorption temperatures of methyl formate and methanol from bare Au(332) are very similar (see Fig. S3 and Ref.[18]), it is expected that the ratio of their surface concentrations is similar to the ratio of the applied fluxes in the gas phase. Thus, the lower reactivity cannot be explained by a significantly reduced availability of methyl formate on the surface. In this regard, it is important to recall that methyl formate oxidation takes place with a small number of highly reactive oxygen species only. Additionally, the different reaction mechanisms for the three reaction channels as deduced from the isotopic distribution of CO_2 suggest rather specific transition state geometries.[18] Under isothermal conditions at low oxygen flux, the availability of these specific oxygen species is small. Accordingly, the probability for transiently adsorbed methyl formate to encounter one of these specific oxygen species in a suitable adsorption geometry for a successful reaction will be small. During the pulse, unreacted oxygen accumulates on the surface and will preferentially accommodate at low coordinated sites. Some of these were shown to allow for methyl formate oxidation resulting in an increase of the rate during the oxygen pulse and leading to a constant water formation rate as soon as the reactive surface sites are populated with oxygen and subsequently oxidize methyl formate at a specific rate. The reactivity is, however, too low to react all oxygen atoms impinging on the surface, which leads to further accumulation of oxygen to be removed in the delay times between the pulses.

In contrast to that, partial oxidation of methanol is fast and the transient kinetics shows that oxygen accumulation during the pulses is very small. This is in line with a previous MB study on the partial oxidation of methanol which indicates an effective reaction of methanol with different types of oxygen species, i.e. without specific requirements for oxygen to be located on specific surface sites.[20]

As methanol was found to react so much faster than methyl formate, it is at first glance surprising that co-feeding methyl formate together with methanol has a significant impact on the reactivity of the system. The rate of water formation rises considerably slower in case of the co-feed than observed for pure methanol, while the rate at the end of the pulse is considerably higher than the one observed for pure methyl formate. This indicates that methyl formate can alter the availability of oxygen for the reaction with methanol at least at the beginning of the pulse. This behaviour can be understood by methyl formate interaction with activated oxygen on the surface reducing the probability of a reactive encounter with transiently adsorbed methanol. However, these methyl formate oxygen species are transient and will dissociate without reaction in most of the cases. In this respect, it is also important to recall that the methyl formate flux is about 30 times that of methanol which is also the ratio for collisions between oxygen and the molecules in case of similar residence times (s. a.). The ability of methyl formate to interact with activated oxygen was already demonstrated by TPD showing an increase of the desorption temperature of molecular methyl formate desorption by about 15 K, if comparing oxygen pre-covered with the pristine Au(332) surface.[18] A reduction of the reaction rate will result in an accumulation of oxygen on the surface allowing for an increase of methanol oxidation at later times during the pulse which will surpass the reaction rate of methyl formate because of the reduced requirements of methanol with respect to the nature of the oxygen species.

To assess the implications of these results for partial methanol oxidation on np-Au catalysts, it is important to recall that these exhibit a high density of low-coordinated sites, such as steps and kinks, in curved regions of the ligaments, but also [111] and [100]-facets in flat regions[9] and that the oxygen coverages under typical conditions applied in the partial methanol

oxidation are even lower (saturation coverage of approx. 0.004 ML[11, 12]) than those employed in the pulsed isothermal MB experiments (0.015 ML per pulse). The presence of low-coordinated sites and low oxygen coverages allow for methyl formate oxidation to occur on np-Au. However, as the oxygen coverage is very low (saturation coverage of approx. 0.004 ML[11, 12]) and as the specific sites, which are only a part of all low-coordinated sites, are also on np-Au catalysts a minority species, the number of specific oxygen species required for the methyl formate oxidation and, thus, its contribution to a selectivity loss under isothermal conditions is expected to be lower than in the pulsed MB experiments, even for high conversions. Moreover, reactive collisions of methanol with activated oxygen and thus, its reaction rate are expected to be (slightly) reduced by high methyl formate excess concentrations, as found for high conversions at the end of the catalyst bed. Please, note that the applied flux ratio of methyl formate and methanol in the isothermal MB experiments corresponds to a methanol conversion of > 95 %.

In conclusion, the results show that under isothermal conditions the oxidation of methyl formate is significantly slower than the oxidation of methanol, despite of reaction pathways with low activation barriers. The low reaction rate for overoxidation of methyl formate is due to fact that special oxygen species being minority species on the surface are required for this reaction whereas methanol reacts with various oxygen species. Hence, the heterogeneous reactivity of different oxygen species on gold surfaces is critical for the high selectivity in the aerobic partial oxidation of methanol towards methyl formate. These results not only emphasise the potential of np-Au catalysts, but importantly provides an improved microscopic understanding required for a rational improvement of these catalysts.

Conflicts of interest

There are no conflicts to declare.

Notes and references

1. D. Kaiser, L. Beckmann, J. Walter and M. Bertau, *Catal.*, 2021, **11**.
2. L. Rong, Z. Xu, J. Sun and G. Guo, *J. Ener. Chem.*, 2018, **27**, 238-242.
3. *EU Pat.,* 91890292.5, 1995.
4. J. S. Lee, J. C. Kim and Y. G. Kim, *Appl. Catal.*, 1990, **57**, 1-30.
5. S. Jali, H. B. Friedrich and G. R. Jullius, *J. Mol. Catal. A Chem.*, 2011, **348**, 63-69.
6. A. Wittstock, V. Zielasek, J. Biener, C. M. Friend and M. Bäumer, *Science*, 2010, **327**, 319-322.
7. J. Erlebacher, M. J. Aziz, A. Karma, N. Dimitrov and K. Sieradzki, *Nature*, 2001, **410**, 450-453.
8. L. C. Wang, Y. Zhong, D. Widmann, J. Weissmüller and R. J. Behm, *ChemCatChem*, 2012, **4**, 251-259.
9. T. Fujita, P. F. Guan, K. McKenna, X. Y. Lang, A. Hirata, L. Zhang, T. Tokunaga, S. Arai, Y. Yamamoto, N. Tanaka, Y. Ishikawa, N. Asao, Y. Yamamoto, J. Erlebacher and M. W. Chen, *Nat. Mater.*, 2012, **11**, 775-780.
10. L. C. Wang, Y. Zhong, H. J. Jin, D. Widmann, J. Weissmüller and R. J. Behm, *Beilstein J. Nanotechnol.*, 2013, **4**, 111-128.
11. L. C. Wang, M. L. Personick, S. Karakalos, R. Fushimi, C. M. Friend and R. J. Madix, *J. Catal.*, 2016, **344**, 778-783.
12. L. C. Wang, C. M. Friend, R. Fushimi and R. J. Madix, *Faraday Discuss.*, 2016, **188**, 57-67.
13. B. Zugic, L. C. Wang, C. Heine, D. N. Zakharov, B. A. J. Lechner, E. A. Stach, J. Biener, M. Salmeron, R. J. Madix and C. M. Friend, *Nat. Mater.*, 2017, **16**, 558-564.
14. B. J. Xu, X. Y. Liu, J. Haubrich, R. J. Madix and C. M. Friend, *Angew. Chem. Int. Ed.*, 2009, **48**, 4206-4209.
15. J. J. Pireaux, M. Chtaib, J. P. Delrue, P. A. Thiry, M. Liehr and R. Caudano, *Surf. Sci.*, 1984, **141**, 211-220.
16. A. G. Sault, R. J. Madix and C. T. Campbell, *Surf. Sci.*, 1986, **169**, 347-356.
17. M. J. Prieto, E. A. Carbonio, R. Landers and A. de Siervo, *Surf. Sci.*, 2013, **617**, 87-93.
18. C. D. Feldt, J. L. Low, P. A. Albrecht, K. Tang, W. Riedel and T. Risse, *J. Phys. Chem. C*, 2021, DOI: https://doi.org/10.1021/acs.jpcc.1c08531, accepted.
19. Y. Li, W. Dononelli, R. Moreira, T. Risse, M. Bäumer, T. Kluner and L. V. Moskaleva, *J. Phys. Chem. C*, 2018, **122**, 5349-5357.
20. C. D. Feldt, T. Gimm, R. Moreira, W. Riedel and T. Risse, *Phys. Chem. Chem. Phys.*, 2021, **23**, 21599 - 21605.
21. C. D. Feldt, T. Kirschbaum, J. L. Low, W. Riedel and T. Risse, *Catal. Sci. Technol.*, 2021, **submitted**.

Oxygen on gold preferentially reacts with methanol than its partial oxidation product methyl formate due to different oxygen species requirements.

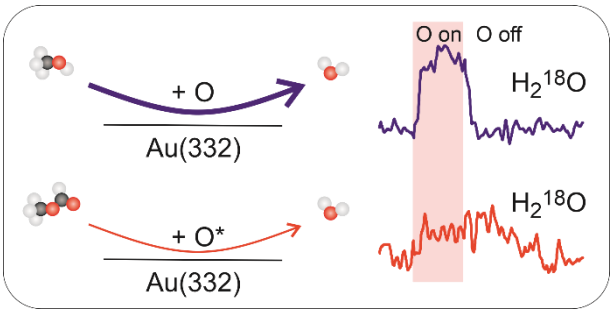

Supporting Information

Heterogeneity of oxygen reactivity is crucial for selectivity of partial oxidation of methanol on gold surfaces

Christoph D. Feldt,[a] Paul A. Albrecht,[a] Salma Eltayeb,[a] Wiebke Riedel,*[a] and Thomas Risse*[,a]

Experimental Details

All experiments were conducted in an ultrahigh vacuum apparatus which is described in detail elsewhere.[1] In brief, the apparatus consists of two chambers which can be separated by a mechanical gate valve. One chamber is equipped with a sputter gun (IQE 11/35, SPECS), a MCP LEED system (Omicron), an Auger spectrometer (PHI 11-010, PerkinElmer) and a quadrupole mass spectrometer (Prisma, Pfeiffer) with a self-made Feulner cup,[2] mounted onto the mass spectrometer to increase sensitivity for temperature-programmed reaction (TPR) experiments. The second chamber contains two effusive molecular beams (MB)[3] and a thermal oxygen atom source (Dr. Eberl MBE-Komponenten GmbH) which can be modulated by automated valves and shutters. A stagnation flow monitor, equipped with a high precision ion gauge (360 Stabil-Ion, Granville-Phillips) is mounted for pressure detection at the sample position. A quadrupole mass spectrometer (MAX-500HT, Extrel) is used for time resolved measurements of gas phase species ($H_2{}^{18}O^+$ at 20 a.m.u, $C^{16}O^{18}O^+$ at 46 a.m.u, $^{13}C^{16}O^{18}O$ at 47 a.m.u and $^{13}C^{18}O_2$ at 49 a.m.u.) during pulsed, isothermal MB experiments. A movable flag consisting of stainless-steel lever connected to a non-reactive quartz plate was used to block direct exposure of the sample in reference MB experiments. The round Au(332) single crystal (10 mm diameter, 2 mm thick, MaTecK) is fixed onto a BN heater (HT-01, Momentive) by means of Mo clamps. A 0.2 mm hole in the crystal edge is used to connect a type K thermocouple. The sample temperature is measured and controlled by a commercial PID controller (Eurotherm). The BN heater is attached to a Mo holder connected to a liquid nitrogen cooled copper block, which enables sample cooling to 100 K. The Au(332) single crystal was cleaned by repeated cycles of Ar^+ ion sputtering (1keV, 5 – 6 µA, 15 min) and subsequent annealing to 1000 K for 10 min.[4-6]

For TPR experiments, ^{16}O ($^{16}O_2$, Air Liquide, 99.998 %) atoms were supplied by the thermal atomic oxygen source (T = 1630 °C, 1.35 mbar $^{16}O_2$ backing pressure) with an atom flux of $4.0\cdot10^{12}$ s^{-1} cm^{-2}. The oxygen flux was determined by TPD measurements assuming a saturation coverage of $2.9\cdot10^{15}$ atoms cm^{-2} (corresponding to 2.1 monolayers (ML) defining 1 ML as one oxygen atom per Au surface atom $1.4\cdot10^{15}$ atoms/cm^2). This number was evaluated by referencing the integrated $^{16}O_2$ (m/z = 32) peak intensity of a fully covered Au(332) to the desorption of O_2 from a 2x2 O superstructure on Pt(111), which amounts to 0.25 ML.[7, 8] Oxygen was adsorbed onto the Au(332) at 250 K and subsequently, methyl formate (Sigma Aldrich, ≥ 99.8 %), cleaned by repeated freeze-pump-thaw cycles, was exposed onto the ^{16}O pre-covered Au(332) at 110 K using a manual leaking valve. The methyl formate exposure was quantified by the pressure difference during exposure as compared to the base pressure, measured by an ion gauge calibrated to N_2 pressure. Deviations in the indicated pressure for methyl formate and N_2 due to differences in ionization probability were accounted for by measurements of methyl formate and argon individually dosed into the chamber by a molecular beam using the same backing pressure. For the difference in indicated pressure and considering the correction factor between argon and N_2 given by the manufacturer's manual, a correction factor for methyl formate was deduced. The TPR experiments were conducted by programmed temperature ramps (110 K – 800 K, 2 $K\cdot s^{-1}$) and simultaneously time-resolved monitoring m/z = 18 ($H_2{}^{16}O^+$), m/z = 32 ($^{16}O_2{}^+$), m/z = 44 ($C^{16}O_2{}^+$) and m/z = 60 ($HC^{16}O^{16}OCH_3{}^+$) with a quadrupole mass spectrometer (-100 eV, 0.1 s). The analog output signals were converted into a digital signal with a polling rate of 10 ms and matched to the sample

temperature by a self-written computer software. Next to the TPR measurement of Au(332) exposed to both activated oxygen and methyl formate, also for each applied exposure reference measurements with Au(332) exposure to merely oxygen or methyl formate were conducted to gauge on one hand the amount of reacted methyl formate and to determine on the other hand signals due to desorption from the sample holder as well as due to fragmentation in the mass spectrometer. The integrated intensities of the CO_2 desorption in the TPR experiments as measured on m/z = 44 were determined by different approaches. On one hand, the off-set corrected spectra were directly integrated in the corresponding temperature range and subsequently subtracting the integrated intensity of the oxygen or methyl formate measurements in the corresponding temperature range. While this approach is well-suited for the CO_2 desorption at 320 K, where no strong signals are observed for the reference measurements, the low temperature CO_2 desorption peaks required a different method. Therefore, all CO_2 desorption features were also fitted to reproduce the experimental spectra taking also in this approach the difference between the TPR measurement and the corresponding reference. The error bars shown in Fig. 2c were estimated from the difference in area obtained by the different integration approaches. The amount of reacted methyl formate in the TPR experiment was estimated from the integrated intensity on m/z = 60 with respect to the reference measurement with merely methyl formate, i.e. without oxygen. Assuming a sticking coefficient of unity for methyl formate at 110 K, it was found that 24 % of the initially provided 0.11 L methyl formate reacted in the TPR with the Au(332) surface pre-exposed to 0.13 L atomic oxygen. Considering the separately measured fragmentation pattern of methyl formate on m/z = 60 and m/z = 44, the number of desorbing methyl formate molecules and the fragmentation pattern of CO_2 on m/z = 44, the absolute number of CO_2 molecules formed in the TPR measurements on the methyl formate oxidation on Au(332) was estimated from the integrated intensities of the desorption peaks corrected for the reference measurements. For the feature at 185 K, methyl formate desorption coincides with CO_2 formation. Therefore, the integrated intensity measured on m/z = 60 was rescaled according to the measured fragmentation pattern of methyl formate and subtracted from that of the TPR experiment. It should be noted that also other (partial) oxidation products may contribute to the intensity at 185 K on m/z = 44, as other m/z traces show this feature.[9]

For the isothermal oxidation of methanol and methyl formate, the atomic oxygen source was modified. An additional quartz tube connected to a differential pumping stage was mounted. The source was operated at 1700 °C at an $^{18}O_2$ (97.39 %, Eurisotop) backing pressure of 3 mbar corresponding to an atom flux of $6.9 \cdot 10^{11}$ $cm^{-2}s^{-1}$. Within one experiment, 31 oxygen pulses with a length of 30 s were dosed onto the Au(332) followed by a delay time of 100 s without oxygen exposure. Methanol-^{13}C (99 atom % ^{13}C, Sigma Aldrich) and methyl formate (≥ 99.8 %, Sigma Aldrich), were cleaned by repeated freeze-pump-thaw cycles and dosed onto the Au(332) surface by means of effusive molecular beams. The molecular fluxes of methyl formate ($1.2 \cdot 10^{15}$ cm^{-2} s^{-1}) and methanol ($4.2 \cdot 10^{13}$ cm^{-2} s^{-1}) were calculated according to calibrations with the beam monitor using Ar. Time resolved mass spectra (1 mA, - 70 eV) were recorded simultaneously with a time constant of 2 s using a pulse counting amplifier. Reference measurements placing a non-reactive quartz flag in front of the sample were conducted to account for background reactions in the chamber. TPD spectra after isothermal MB experiments were recorded in a temperature range of 310 to 800 K with a heating rate of 2 $K \cdot s^{-1}$ simultaneously recording m/z = 32 ($^{16}O_2^+$), m/z = 34 ($^{16}O^{18}O^+$), m/z = 36 ($^{18}O_2^+$) and m/z = 46 ($C^{16}O^{18}O^+$). $^{18}O_2$ and methanol-^{13}C were used to discriminate the produced water and CO_2 in the oxidation reaction from naturally abundant $H_2{}^{16}O$ and $^{12}CO_2$.

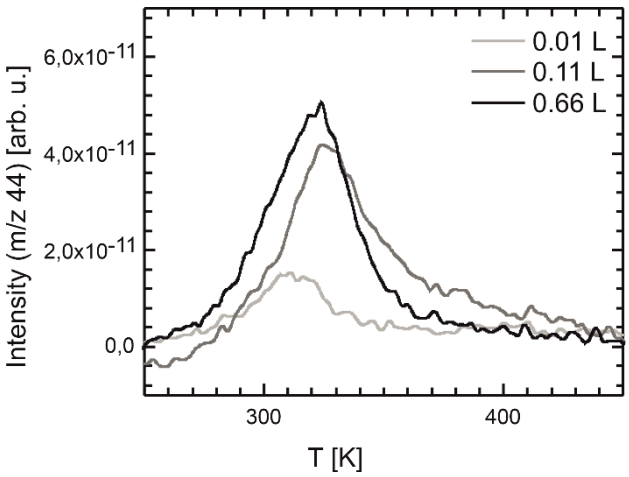

Figure S1 CO_2 desorption at 320 K from Au(332) pre-covered with 0.13 ML activated oxygen and varying exposures of methyl formate. While CO_2 desorption increases for raising the methyl formate exposure from 0.01 L to 0.11 L, it remains nearly constant for a further increase to 0.66 L.

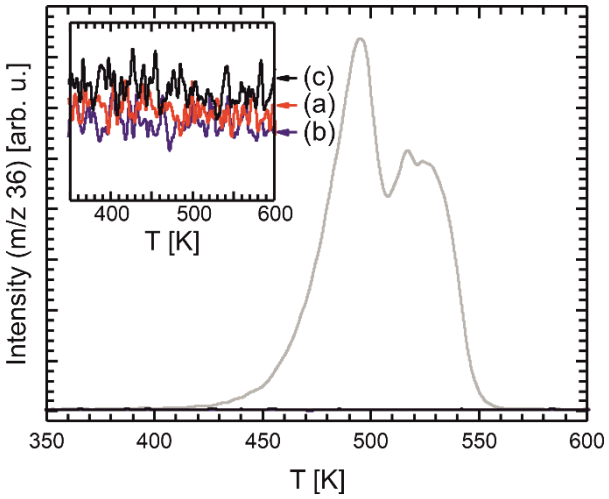

Figure S2 TPD spectra of $^{18}O_2$ (m/z = 36) after the pulsed isothermal molecular beam experiments shown in Fig. 2. The inset shows the $^{18}O_2$ TPD after pulsed MB oxidation experiments of (a) methyl formate (red), (b) methanol (blue) and (c) a co-feed of methanol and methyl formate (black). Next to the oxidation experiments, also a reference (grey) is shown where the experiment was conducted without applying methanol or methyl formate.

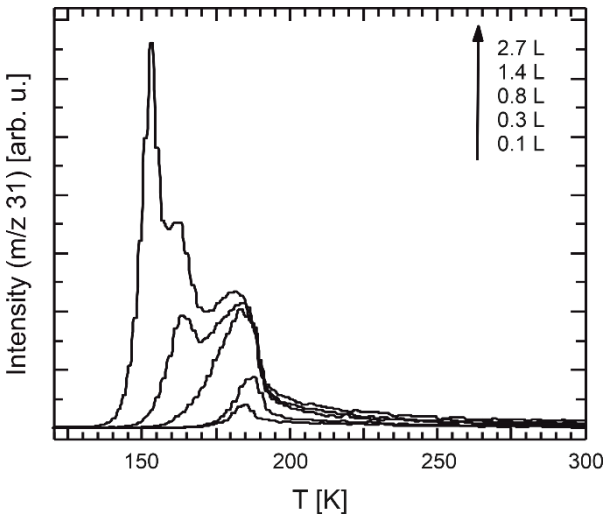

Figure S3 Methanol desorption from Au(332) for varying exposures of methanol.

References

1. R. Moreira, Ph.D., Freie Universtität Berlin, 2018.
2. P. Feulner and D. Menzel, *J. Vac. Sci. Technol.*, 1980, **17**, 662-663.
3. J. Libuda, I. Meusel, J. Hartmann and H. J. Freund, *Rev. Sci. Instrum.*, 2000, **71**, 4395-4408.
4. M. J. Prieto, E. A. Carbonio, R. Landers and A. de Siervo, *Surf. Sci.*, 2013, **617**, 87-93.
5. C. D. Feldt, R. Moreira, E. Meyer, P. Clawin, W. Riedel, T. Risse, L. Moskaleva, W. Dononelli and T. Klüner, *J. Phys. Chem. C*, 2019, **123**, 8187-8197.
6. C. D. Feldt, T. Gimm, R. Moreira, W. Riedel and T. Risse, *Phys. Chem. Chem. Phys.*, 2021, **23**, 21599 - 21605.
7. K. Mortensen, C. Klink, F. Jensen, F. Besenbacher and I. Stensgaard, *Surf. Sci.*, 1989, **220**, L701-L708.
8. P. R. Norton, J. A. Davies and T. E. Jackman, *Surf. Sci.*, 1982, **122**, L593-L600.
9. C. D. Feldt, J. L. Low, P. A. Albrecht, K. Tang, W. Riedel and T. Risse, *J. Phys. Chem. C*, 2021, DOI: https://doi.org/10.1021/acs.jpcc.1c08531, accepted.

List of Abbreviations

AD converter	Analog to digital converter
AIMD	*Ab initio* molecular dynamics
AO	Atomic orbital
AuO_x phase	Gold oxygen phase
DFT	Density functional theory
FTIR	Fourier transformation infrared
GCA	Glass capillary array
HAADF-STEM	High-angle annular dark-field scanning transmission electron microscopy
HOMO	Highest occupied molecular orbital
IRAS	Infrared reflection adsorption spectroscopy
LEED	Low energy electron diffraction
LUMO	Lowest unoccupied molecular orbital
MB	Molecular beam
ML	Monolayer
MO	Molecular orbital
MS	Mass spectrometry
np-Au	Nanoporous gold
PID controller	Proportional-integral-derivative controller
SEM	Scanning electron microscopy
STEM	Scanning transmission electron microscopy
TEM	Transmission electron microscopy
TPD	Temperature programmed desorption
TPR	Temperature programmed reaction
UHV	Ultrahigh vacuum

List of Figures